Experimental Investigation of Frictional Properties of the Human Fingerpad

by

Jung-Chi Liao

B.S. Mechanical Engineering
National Taiwan University, 1993

Submitted to the Department of Mechanical Engineering
in partial fulfillment of the requirements for the degree of

Master of Science in Mechanical Engineering

at the

MASSACHUSETTS INSTITUTE OF TECHNOLOGY

January 1998

Author .....
Department of Mechanical Engineering
Jan 16, 1998

Certified by .....
Dr. Mandayam A. Srinivasan
Principal Research Scientist, Dept. of Mechanical Engineering
Thesis Supervisor

Accepted by .....
Dr. Ain A. Sonin
Professor of Mechanical Engineering
Chairman, Department Graduate Committee

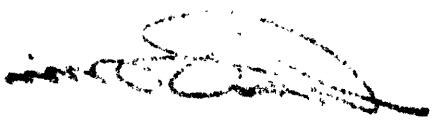

Experimental Investigation of Frictional Properties of the Human Fingerpad

by

Jung-Chi Liao

Submitted to the Department of Mechanical Engineering on
Jan 16, 1998, in partial fulfillment of the requirements for the
degree of Master of Science in Mechanical Engineering

Abstract

A 2-DOF robot was modified to serve as a high precision tactile stimulator, controlled to indent and stroke the fingerpad of human subjects. It was configured to deliver various dynamic stimuli, such as different indentation depths, stroke velocities, and stroke directions. Three kinds of transparent indentors were used in the experiments: glass, polycarbonate, and acrylic planar surfaces. During stroking, the normal and shear forces were recorded by a 2-axis force sensor. A videomicroscopy system was set up to capture the image sequences of the contact region between the fingerpad and the indentor surface while stroking. The stimulator and the videomicroscopy system were synchronized to match the images with corresponding force data. Five subjects participated in this experiment.

The data show distinct frictional behaviors for different indentors. For the glass surface, the curves of normal as well as shear forces increased smoothly to steady state values. When the indentation depth was higher, the normal and shear forces were larger, but the friction coefficient was smaller. When the stroke velocity increased, the normal force was about the same for a given indentation depth, while the shear force and the friction coefficient increased. The stroke direction did not significantly influence the results. The image sequence shows that the relative motion, or slip, between the fingerpad and the glass plate indentor began at the periphery of the contact region and propagated towards the center. Under all the stroke conditions, the glass plate slipped smoothly across the fingerpad. In contrast, both polycarbonate and acrylic surfaces exhibited stick-slip phenomenon consistently. An analysis of the stick-slip frequency and the stick-slip shear force was conducted with respect to various indentation depths and various stroke velocities.

A hypothesis about junction forming rate and junction breaking rate was proposed based on adhesion theory and the observation of images as well as force measurements. This was used to explain the different results from the glass plate indentor and the polycarbonate plate indentor. The frictional properties of the fingerpad is shown to be similar to those exhibited by rubber-like materials.

Thesis Supervisor: Mandayam A. Srinivasan
Title: Principal Research Scientist, Dept. of Mechanical Engineering

Acknowledgment

I would like to take this chance to thank several people whose support made this thesis possible. First, I would like to thank my advisor Dr. Srinivasan for his guidance and support during this work. Many cautious discussions through every critical thinking and idea will always bear in my mind.

I would also like to thank Flora for helping me setting up the experiment, running lots of boring preliminary experiments, and assisting me to build up the digital filter. I would like to thank Mahesh for the collaboration on developing image processing tools. I would like to thank Jyh-Shing for giving me guidance on the videomicroscopy system and the synchronization process. Also thank Chun-Yi, Chung-Yao, Wandy, and Yee-Sue. Without their help the experiment could not be done.

I would like to show my appreciation to all my colleagues in our laboratory. I always got the valuable help from them when I needed. Especially Chih-Hao gave me a lot of encouragement in the lab. Thank Suvranu, Kim, Alex, Cagatay, Raju, Lee, and Mandy.

I would like to thank my dear friends, Jiun-Yu, Yu-Hsuan, Ginger, Ching-Te, for their support on my project and their constant encouragement. Also thank Jane, Cynthia, Kuo-Shen, Ching-Yu, Jung-Sheng and Pei-Wen for their great helpfulness.

Thank Flora again, my best friend, for giving me support, help, and concern. I will always be grateful.

Finally, I would like to thank my parents for their invaluable encouragement and love through half of the earth. Their love supported me to finish this work and conquer obstacles in life. This thesis is dedicated to them.

Table of Contents

Chapter 1

Introduction

1.1 Motivation

Human haptic systems, composed of biomechanical, sensory, motor, and cognitive subsystems, enable us to perform complex manual tasks in the real world. Almost all these tasks performed with our hands can be classified as exploration and manipulation. Exploration is essentially concerned with perception of object properties, such as surface texture, softness, and shape; therefore it is a sensory dominant task. Manipulation is mostly concerned with motion and/or force control of hands in moving or holding objects, so it is a motor dominant task. An important distinction between the human haptic system and other sensory systems such as vision and hearing is that it can both sense and act on the environment.

In order to understand the components of the human haptic system that enable manual tasks to be successfully performed, a quantitative determination of the mechanical properties of the fingerpad is of importance to both the scientist trying to understand how the human haptic system works and to the engineer who is trying to design the hardware and software of haptic interfaces to computers and other machines. Previously, we have conducted research to determine some of the properties of the fingerpad, such as the nature of surface deflection of the primate fingerpad (Srinivasan, 1989), the

compressibility of the human fingerpad (Srinivasan, *et al.,* 1992), and the mechanical impedance properties of the human fingerpad (Gulati and Srinivasan, 1995). The purpose of the present study is to investigate the frictional properties of the human fingerpad, namely, the force response under loads tangential to the skin surface.

The frictional properties of the human fingerpad play an important role in both manual exploration and manipulation of objects. In the case of exploration, such as stroking the fingerpad upon objects, the mechanoreceptors inside the fingerpad first transduce associated mechanical signals and send sensory information to the brain via the afferent nerve fibers in the peripheral nervous system. During this kind of exploration, such as during tactile detection of slip and micro-texture, skin stretch influences peripheral neural codes (Srinivasan, *et al.,* 1990). Therefore, the frictional properties of the fingerpad need to be combined with neural data to understand the relationship between biomechanical and neurophysiological mechanisms. In addition, while exploring the surface texture of objects, there is relative motion between the fingerpad and objects, which pertains to the case of kinetic friction. The stroke velocity and the stroke direction of the relative motion can be possible factors and have been investigated in our experiment. In the case of manipulation, such as gripping an object, the magnitude of the frictional force depends on the normal force exerted between the fingerpad and the object, as well as the frictional properties of the skin-object interface. This normal force is directly related to the indentation of the fingerpad, which is treated as an important variable in our experiment.

The applications of this research can be found in many fields. Recently, there has been a surge of interest in the development of haptic interface devices which enable the user to touch and feel either computer-generated simulations in virtual reality applications or

remote objects during teleoperation through a slave robot. In these synthetic environments, to simulate typical tasks performed in real environments, such as holding a cup, gripping a pen, or to have similar skin stretch response while exploring the surface textures of objects, a knowledge of the frictional properties of the fingerpad will be crucial. The frictional data are necessary to develop the associated simulation programs so that human-machine interactions are realistic. Especially today, when virtual environments of visual and auditory systems are well developed, the progress in the virtual reality of touch becomes increasingly important. Besides the field of virtual reality, the results of this research can also be applied to ergonomics. A recent report from Sweden shows that 6% of all occupational injuries are related to the use of hand tools (Malker, 1991). For example, it is usually not easy to hold the work pieces when using the grinding machine. Therefore, high friction is preferred between the hand skin and the tool handles, and the investigation of frictional behaviors between them are critical for improving the handling problems.

1.2 Previous Research

Very few studies on the friction of the human fingerpad exist in the literature. Buchholz, *et al.* (1988) investigated the frictional characteristics for seven materials under moist and dry conditions. The subjects were asked to exert a nearly constant pinch force with two fingers on a dynamometer, and a controlled pneumatic actuator pulled the dynamometer down out of the subject's fingerpads. Only at the moment of slip were recorded to estimate the static friction coefficient when relative motion between the contact surfaces began to occur. Although this experimental results were analyzed quantitatively, the difficulty of exerting constant pinch force by subjects should be noted

and the variation for the measured pinch force is large. Furthermore, because the analysis of the data only focused on the time point when slip occurred, it could only investigate the maximum static friction coefficient, but the frictional properties other than that point were not available.

Bobjer, *et al.* (1993) conducted an experiment to measure the perceived discomfort and kinetic friction coefficient of the human fingerpad. The subject applied three different values of normal forces with his or her finger on grooved polycarbonate substrates. These substrates had grooves milled at various spacings on the surfaces. The fingerpad was tested under several conditions, such as normal, sweaty and contaminated with glycerol, paraffin oil or lard. The data showed that the kinetic friction coefficient frequently exceeded 1.0 when the normal loads were low, and the coefficient decreased as the normal force increased. The results also demonstrated the influence of the surface grooves and the conditions of the fingerpad. In this experiment, the normal forces were again exerted actively by subjects, so this was still an issue whether it was possible to keep a constant force for the whole stroking process. Also, the results only showed the average kinetic friction coefficients during stroking, but more details of frictional behavior were not investigated.

Recently, Han, *et al.* (1996) performed an experiment to investigate the frictional properties by stroking the fingerpad passively, namely by moving the test object while keeping the fingerpad stationary. The experimental setup was equipped to record the friction coefficient once the stimulus object started to move, so that the static friction coefficients for different normal forces were recorded. An inverse relationship between the static friction coefficient and the normal force was found, and the effects of contact

angle and stroke directions of the stimulus object were also explored. The shortcoming of this experiment is also that only maximum static friction coefficient was recorded, but no kinetic friction coefficients and the trends in the frictional properties subsequent to slipping were investigated.

1.3 Goals and Organization of the Thesis

In this thesis, experiments were conducted *in vivo* to understand the frictional behavior of the human fingerpad, both under static and kinetic friction conditions. The variations of forces and positions over time, before and after the starting of the relative motion between the fingerpad and the object surface, were recorded. Also video image sequences during the strokes of the experiment were captured to support the force data and moreover to identify the motions of the fingerpad as well as those of skin surface ridges under shear loads. The fingerpad was held passive, and was indented and stroked by the test objects mounted on a robotic stimulator controlled by a computer. High precision and high sampling frequency was employed for the apparatus in order to observe even the subtle and rapid changes in forces and images that occurred during the experiment. The effects of normal forces, stroke velocities, stroke directions, and materials of indentors were investigated to characterize the frictional properties of human fingerpads under normal skin conditions.

Chapter 2 covers the background for this research. The first section is on the interior biomechanical structure and mechanical behavior of the human fingerpad, the basic understanding of the system we are interested in. The primary frictional behavior is discussed in the second section, which lays a foundation for further discussion of the experimental data.

Chapter 3 introduces the equipment for the experiment. The experimental setup was comprised of two important parts, the tactile stimulator and the videomicroscopy system, which are described in detail in the first two sections. The tactile stimulator had a feedback position control loop and a set of force sensors. There are six subsections in Sec. 3.1 for all the major components in it. The videomicroscopy system, illustrated in Sec. 3.2, consisted of a microscope, CCD camera, and real time digitization frame grabber of image sequences. The third section of this chapter deals with the synchronization of the tactile stimulator and the videomicroscopy system, so that both systems are referenced to the same time.

Chapter 4 describes the experimental procedure. First, the experimental protocol is introduced step by step. Then, some of the important parameters in this experiment, such as experimental stimuli, different kinds of indentors, and human subjects, are presented in more details in the following sections. Then, in Sec. 4.6, the procedure of capturing images using videomicroscopy system is discussed. The last section describes the image processing tools for the further qualitative and quantitative analyses.

Chapter 5 shows the important results of the experiment. The data are classified by the indentors used; thus the three sections deal with glass, polycarbonate, acrylic indentors, respectively. Inside each section the results for both force and image data obtained from different stimuli for the corresponding indentor are presented.

Chapter 6 discusses the results in the previous chapter. In the first section, the friction theory as applied to the human fingerpad is described. In Sec. 6.2, adhesion, an important factor of the friction theory, is used to interpret observed behaviors both for glass and polycarbonate surfaces. The third section discusses the relationship between the image

data and the proposed adhesion theory. The last section compares the frictional properties of the human fingerpad and the rubber-like materials. This indicates whether it is feasible to model the human fingerpad as a rubber-like material.

Appendix shows the additional data under most of the stimuli for all five subjects.

Chapter 2

Background

2.1 Human Fingerpad -- Structure and Mechanical Behavior

In our experiment and data analysis, the human fingerpad is treated as a black box. From the input of indentation depth and stroke velocity, as well as the output of normal and shear forces, we try to identify the frictional properties of the fingerpad. Even though the human fingerpad is treated as a black box, its structure and mechanical behaviors are introduced so that further discussions can make physical sense.

A fingertip, shown in Fig. 2.1, is comprised of the skin, the soft subcutaneous tissues, the bone, and the nail. The nail and the bone are rigid compared to the soft tissues. There are two contrasting types of skin on the fingertip. The skin on the nail side is the dorsal skin and the skin on the fingerpad side is the palmar skin. The dorsal skin is thinner and it

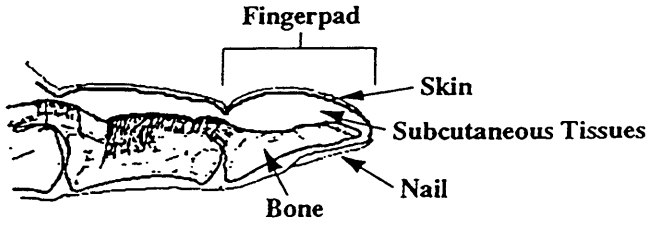

Figure 2. 1 The basic structure of the fingertip.

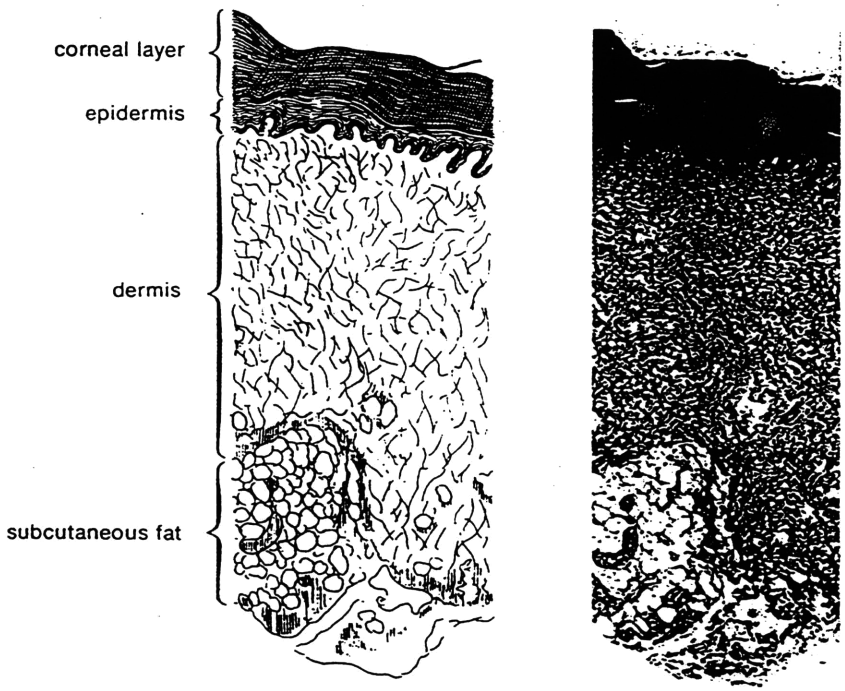

Figure 2. 2 The multi-layer structure of the palmar skin

has only loose connections with the deeper planes. The dorsal skin is also more stretchable than the palmar skin. The palmar skin is thicker and more used to sustain normal pressure and shear loads under stroking. This palmar region, generally called the fingerpad, is the main interest of our research.

The palmar skin is a multi-layered structure, composed of epidermis and dermis, as shown in Fig. 2.2. There are five layers in the epidermis, from outer most layer to inner most layer: the horny layer, stratum lucidum, granular layer, malpighian layer, and basal layer. The horny layer has the thickness ranging from 0.5 to 2 mm, different from 0.02 mm in the skins of other areas of our body (Thomine, 1981). The dermis is composed of connective tissues, intertwining collagen, elastin, and reticular fibers. This thick dermis contributes to the high resistance of the palmar skin. The fat tissue under the dermis works as an energy storage element and protective cushion.

From the point view of the mechanical properties, the palmar skin can be regarded as a multilayered, nonlinear, nonhomogeneous, anisotropic system. Yamada and Evans (1970) reported that the average tensile strength is about 7640 kPa. The "waterbed" model proposed by Srinivasan (1989) predicted skin surface deflection profiles. The skin was modeled as an elastic membrane with incompressible fluid in it. Gulati and Srinivasan (1995) used Kelvin type viscoelastic model to explain the results of indentation experiment, and a lumped parameter model with nonlinear spring in parallel and a spring-dashpot in series is suggested. Dandekar and Srinivasan (1996) used 3D finite element method to model the multi-layer structure of the fingerpad. Pawluk and Howe (1997) proposed the fingerpad model as a combination of two components: the elastic response and the reduced relaxation function.

2.2 Friction Phenomena

Friction has been studied over centuries, and many important theories, including Coulomb's law, the adhesion theory, and the thin film theory of friction, were developed. Results of these studies, both in experimental and theoretical aspects, have been summarized in several monographs (e.g. Bowden and Tabor, 1986; Suh, 1986; Blau, 1995). One of the most important quantities in friction is the friction coefficient, which according to the ASTM standard is defined as "the ratio of the force resisting tangential motion between two bodies to the normal force pressing those bodies together". This definition, which we adopt, implies that the friction coefficient is a measure of the difficulty of moving one object upon the other one, regardless whether there is relative motion between two surfaces or not. Three major contributions on the friction coefficient are summarized as follows (Suh, 1986): μ_d , the friction coefficient due to asperity

deformation, μ_a , the adhesion component of the friction coefficient, and μ_p , the plowing component of the friction coefficient. At a micro scale, surfaces of any objects are full of asperities, which can be demonstrated by using fine surface geometry measuring devices such as profilometers. When one object tends to have relative motion with respect to the other, these asperities start to deform. The deformation of asperities contributes to the resistive force opposite to the direction in which the object is moving or tends to move. This manifests as a friction force at a macro scale. The second cause of friction is adhesion. As two surfaces contact each other, some junctions form between the surfaces (Buckley, 1981). The processes of forming junctions depend on the physical, chemical, or electrical characteristics of both surfaces. These junctions oppose the relative motions of the two surfaces, causing a resistive force against the incipient direction of motion. Even during relative motion, many junctions exist at every instant, and adhesion still contributes to the friction force. The third source of friction occurs in the situation where one surface is harder than the other surface, or there are wear particles between two surfaces, the hard asperities or the wear particles will cut into the soft surface and break it. This is called plowing process. The resistive force generated by the plowing process is another major cause of friction force. Besides these three sources of friction, lubrication is also a primary factor that affects friction. In the experiment of this study, however, the lubrication condition was maintained approximately the same at the skin-object interface across subjects and trials.

According to Coulomb's law, there are two conditions of friction: static friction and kinetic friction. If we treat these two terms in a broad sense, the static friction means the state when no relative motion occurs between two contact surfaces, and the kinetic

friction means the state with relative motion. In general this is the basic frictional phenomenon observed in our daily life. For example, exerting a small horizontal force to an object upon the desk, this object does not move. When the force is exerted larger, the object starts to slip on the desk to some distance. This example is consisted of both static friction and kinetic friction states, but the frictional behavior may not work as Coulomb stated: both static and kinetic friction coefficients are constants. Several different patterns for the static and kinetic coefficients have been found in previous friction experiments. In addition to the two-state movement described above, another interesting phenomenon in friction is stick-slip behavior. During the stick-slip friction, the relative motion of the two contact surfaces is not so smooth, but rather it moves and stops periodically or sometimes randomly. Stick-slip behavior typically occurs when one of the contacting objects is a compliant material, so that it has the degree of freedom to move forward and backward. If the stroke velocity falls in the critical region to cause on instability of the contact system, the stick-slip phenomenon will be induced. In some special conditions, it can be sustained long enough to have periodic oscillations.

Chapter 3

Experimental Setup

The two major equipment systems used in the experiment were the tactile stimulator and the videomicroscopy system. The tactile stimulator handled the position control of the indentor, and also recorded the shear and normal forces. The videomicroscopy system captured and recorded successive frames of visual images in real-time. A communication strategy between these two systems was developed so that the data registered in both systems were synchronized in time.

3.1 Tactile Stimulator

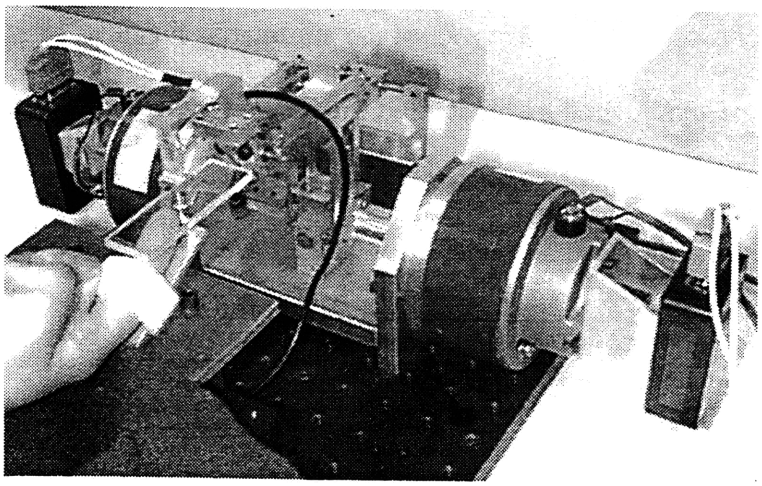

Figure 3. 1 The picture of the tactile stimulator. The stimulator was controlled to indent and stroke the fingerpad.

A two degree of freedom, high precision robot, designed by Howe (1992) and modified to serve as a tactile stimulator (Fig. 3.1), was used to indent and stroke the subject's fingerpad with programmed displacements and velocities controlled by a PC. A 2-axis strain gage based force sensor was attached to the stimulator to measure the normal and shear forces simultaneously. A flat plate indentor (25 mm× 75 mm) was mounted on the force sensor to indent and stroke the fingerpad of the subject's index finger. The back of the finger was fixed to a rigid base by gluing the fingernail to a support plate inclined at 30°, which is the typical contact angle when the fingerpad is used to explore or manipulate objects. The sides of the fingerpad were left free to simulate natural conditions of finger use.

The block diagrams of both the position feedback loop and the force sensor are shown in Fig. 3.2. A 80486 computer controlled the positions and velocities of the tactile stimulator, and synchronously recorded the positions of the linkage as well as the normal and shear forces. From the block diagram of the stimulator, it can be seen that the inputs of this system were the desired positions and the desired velocities at each time instant. These desired inputs, combined with the feedback position signals and a set of difference equations, governed the PID feedback control of this system. The outputs of the control program were then converted to analog voltages through the D/A board. These voltages were filtered, amplified, and then transformed to current signals as the inputs of the two DC servo-motors. A linkage mechanism was connected to these two motors to move the indentor to the desired positions at each moment. The angular positions of the motors were read by two potentiometers. These position data were then filtered, converted to digital signals, and then fedback to the control part of the system.

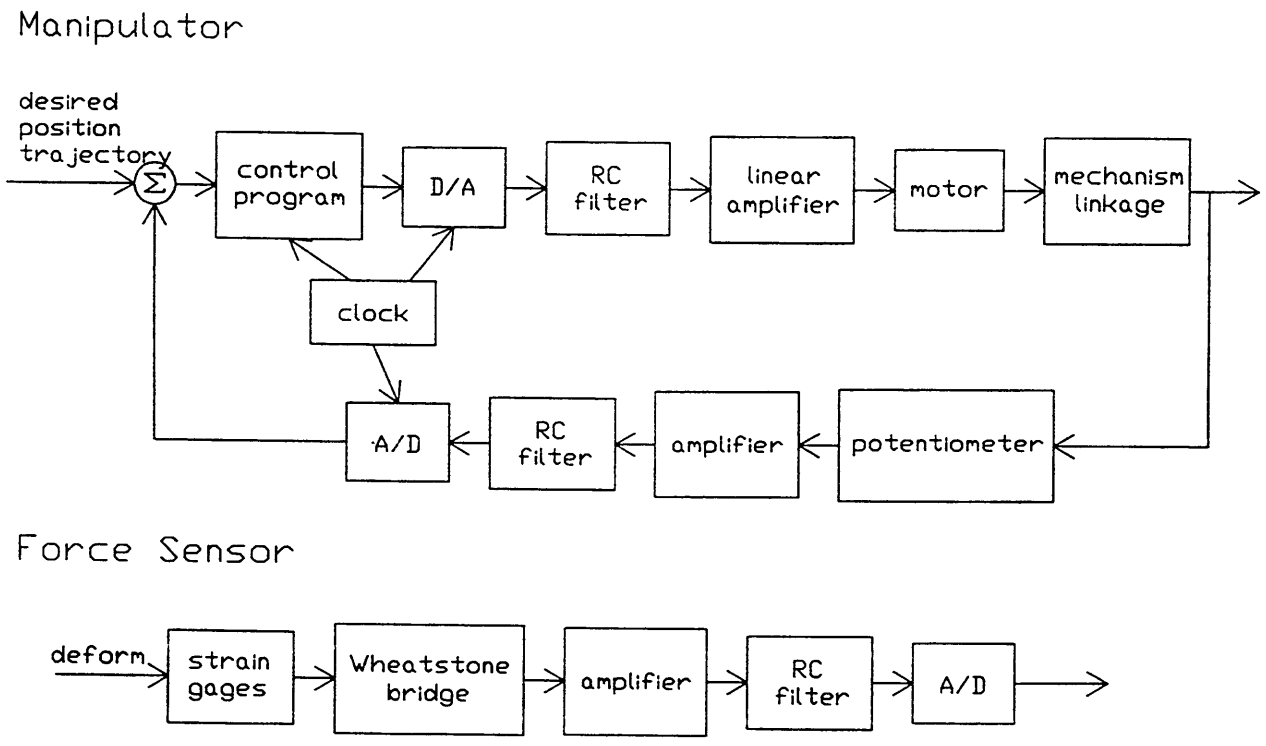

Figure 3. 2 The block diagram of the tactile stimulator, both for the position control part and the force sensor part.

The force sensor part was simpler. The normal and shear forces caused the deformation of the structure of the force sensor, and two sets of Wheatstone bridge strain gages were mounted on the structure to read out the voltage changes through the Wheatstone bridge. The details of the Wheatstone bridge in this setup will be described in a later section. The analog voltages from the output of Wheatstone bridge were then filtered and converted to digital signals, and these signals were recorded in the computer. A timer handled the sampling rate of the force data and the control rate of the stimulator, so that the positions and forces could be synchronized.

The following sections discuss the components in more detail. Because Gulati did a lot of modifications to this setup, some discussions and specifications can be found in his report (Gulati and Srinivasan, 1997).

3.1.1 Motor

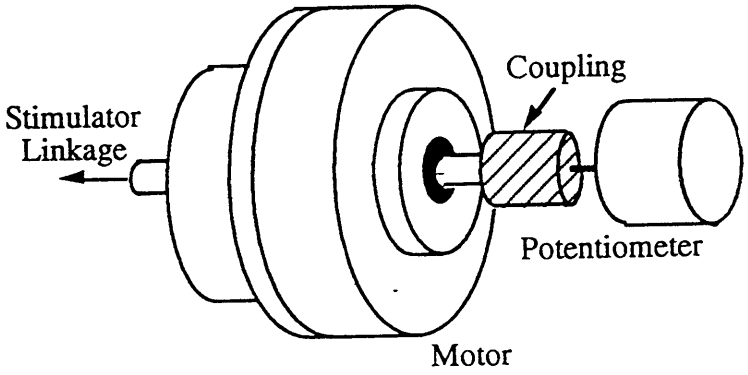

Figure 3. 3 The coupling of the motor shaft. The left side of the motor shaft connects to the stimulator linkage and the right side of the motor shaft connects to the potentiometer.

There were two non-ferrous cup-armature, DC Minertia S02A servomotors to deliver torques to the linkage mechanism. As shown in Fig. 3.3, the shaft of each motor was connected on one side to the linkage mechanism and on the other side to the potentiometer. The linkage mechanism converted the angular positions of the motors to the Cartesian coordinate positions of the endpoint. The potentiometers read the angular positions of the motors and sent them back to the control program for further feedback control. The details of both the linkage mechanism and the potentiometers will be introduced in the following subsections.

The motors were driven by two Eletro-Craft LA-5600 linear amplifiers. These two amplifiers converted the input voltages into current sources for the motors. The input voltages passed through the D/A converters as well as a pair of RC filters. These RC filters reduced high frequency noise from the digital sources. Resistance of the RC filters

was 1500 Ω and capacitance was 0.47 μF. The equation of the cutoff frequency, where the magnitude is -3dB below the 0 frequency, is:

$$f = \frac{1}{2\pi RC}.$$

The cutoff frequency in this case was about 225 Hz. This frequency was selected through frequency spectrum analysis by HP 35660A Dynamic Signal Analyzer to reduce the stability problem in terms of vibration of the linkage mechanism and consequently to improve the accuracy of the position control. Also, to avoid the desired torque and the associated current from exceeding the current limit of the motor, upper and lower bounds of the torque were applied to the program.

3.1.2 Linkage Mechanism

Fig. 3.4 shows the linkage mechanism of the stimulator. This linkage was first designed by Howe (1992) and then modified by Gulati for improving stability and stiffness of the links. The report by Gulati and Srinivasan (1997) shows the main design and assembly details of the components. There were two major functions for this mechanism. One of the function was to convert the angular positions of two motors to the endpoint Cartesian positions of the mechanism. Once the positions of the endpoint was reached, another important function was to preserve the orientation of the flat plate indentor, that is, to always keep the indentor surface horizontal.

First, let us consider the orientation of the indentor. To preserve the orientation, parallel linkage was utilized as shown in Fig. 3.5. In the figure, it can be observed that there were three sets of parallel links in the mechanism. The ground, marked as link 1,

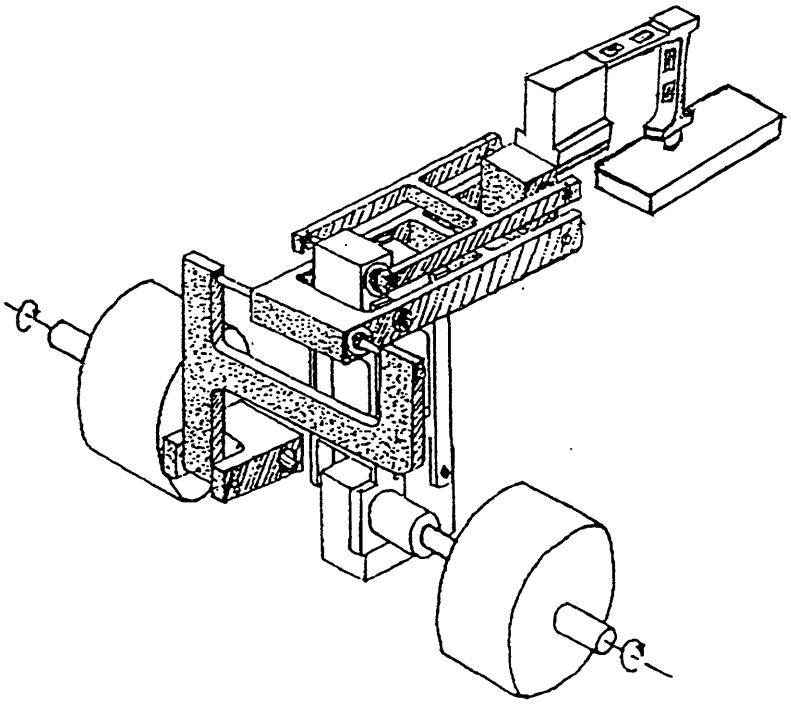

Figure 3. 4 The 2-DOF linkage mechanism of the stimulator.

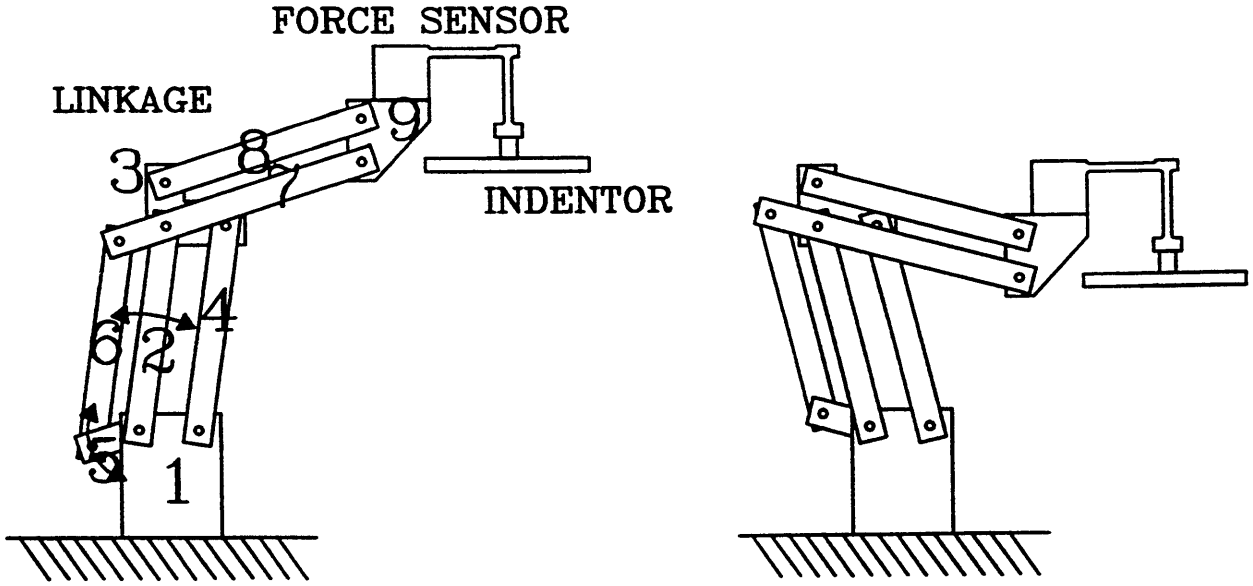

Figure 3. 5 The motion of parallel linkage.

formed a four-link parallel set with links 2, 3, and 4. Also links 2, 5, 6, 7 formed a parallel set, and links 3, 7, 8, 9 formed another one. The set of links 1, 2, 3, 4 ensures the bottom part of the link 3 always parallel to the ground. The design of the link 3, which had the upper part perpendicular to the bottom part, made the upper part always vertical, and thus through the set of links 3, 7, 8, 9 the link 9 was also always vertical. Therefore, the mounted indentor remained horizontal regardless of the motion of the mechanism and motors. The set of parallel links 2, 5, 6, 7 was only to keep the link 5 always parallel to link 7, which made the analysis of the conversion between the angular positions of motors and the endpoint position easier, as shown in the following paragraphs.

Let us define the lower pivot of the link 9 as the endpoint. The horizontal and vertical displacement as well as velocity of the indentor would be exactly the same as this endpoint if the whole force sensor part in front of link 9 is regarded as a rigid body. In fact, this is not perfectly true because of the deformation of the force sensor, but at this point the rigidity was assumed and the verification of this assumption will be discussed in the later section on calibration of potentiometers and positions.

To understand the relationship between the endpoint positions and the angular positions of the motors, we show only some links in Fig. 3.5 where these links were directly related to the kinetics and kinematics of the motion. Four links, link 2, 5, 6, and 7 are replotted in Fig. 3.6 with the ground point as the origin. Link 2 was connected to the right side motor of Fig. 3.4 and link 5 was connected to the left side motor. Thus, the problem reduced to find out the relationship between the angular positions of links 2 and 5, and the Cartesian coordinate positions of endpoint (x,y). Here we set the clockwise angle of link 2 relative to the vertical line above origin as θ and the counterclockwise

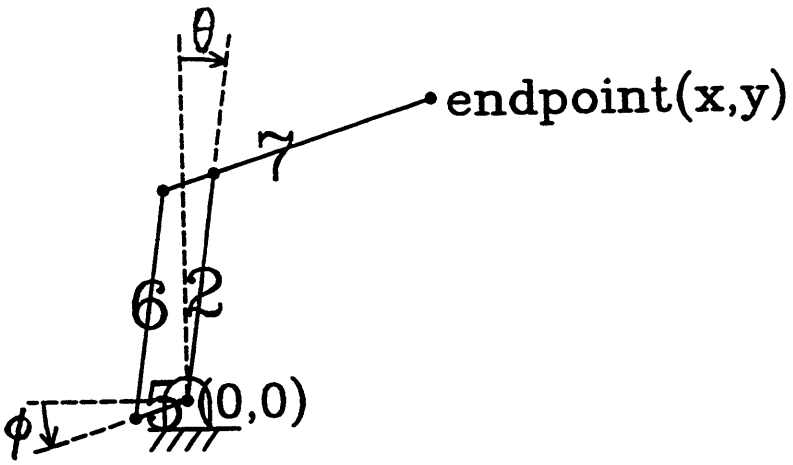

Figure 3. 6 The elementary links for the endpoint position.

angle of link 5 relative to the horizontal line left to origin as ϕ. Due to the design of the set of the parallel links 2, 5, 6, and 7, the angular position of link 7 was the same as that of link 5. All the settings above were selected so that, in the interesting domain of the endpoint motion, an increase of θ implied an increase in x, and an increase of ϕ implied an increase of y, though they were not in proportional scales.

In fact, the only interesting parts of these links for understanding the kinematic relationship were link 2 and the right part of link 7. This mechanism was carefully designed to have the same length, 76.2 mm, for link 2 and right part of link 7, so that the analysis became easier. We use symbol L as the length of both links and replot it in Fig. 3.7. From this figure, it can be easily shown that

$$x = L(\sin\theta + \cos\phi)$$

$$y = L(\cos\theta + \sin\phi).$$

The selection of θ and ϕ makes the relation equations symmetrical. The velocities, that is, the derivatives of these values can be derived and shown in a matrix form:

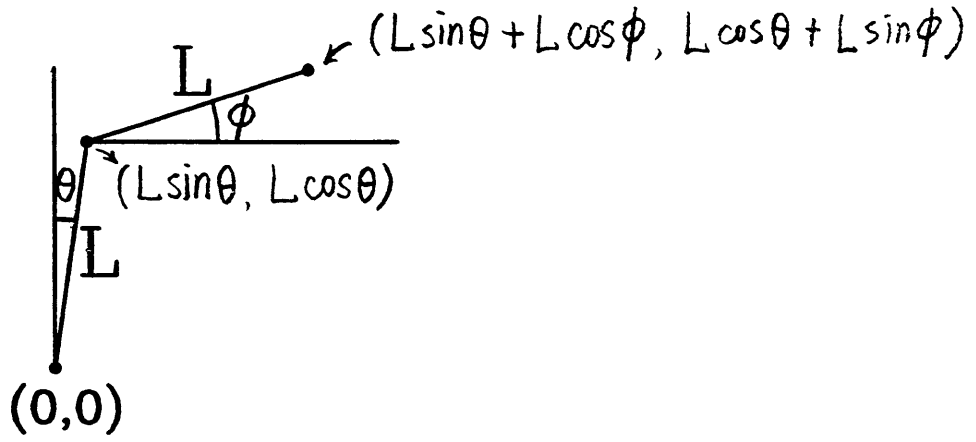

Figure 3. 7 The relationship between the angular positions of the two motors and their endpoint positions.

$$\begin{Bmatrix} \dot{x} \\ \dot{y} \end{Bmatrix} = \begin{bmatrix} L\cos\theta & -L\sin\phi \\ -L\sin\theta & L\cos\phi \end{bmatrix} \begin{Bmatrix} \dot{\theta} \\ \dot{\phi} \end{Bmatrix}.$$

From the above equations, we will know the position and the velocity of the endpoint once the angular positions and velocities of both motors are known.

On the other hand, we should also be able to get the angular positions of motors if we know the endpoint position (x,y). This is known as inverse kinematics and it is important when the Cartesian coordinate positions and velocities are prescribed for some desired trajectories. To derive this, let us use trigonometric relations and plot it in Fig. 3.8. From

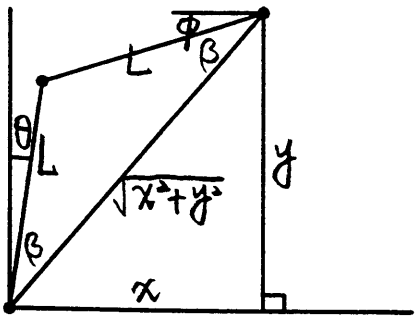

Figure 3. 8 The geometric relations of the linkage.

this plot, it is easily to write down the equations:

$$\tan\alpha = \frac{x}{y}$$

$$\beta = \frac{\pi}{2} - \alpha - \phi = \alpha - \theta$$

$$\theta - \phi = 2\alpha - \frac{\pi}{2} = -\frac{\pi}{2} + 2\tan^{-1}\frac{x}{y}$$

$$\alpha = \frac{\frac{\pi}{2} + \theta - \phi}{2}$$

$$\beta = \alpha - \theta = \frac{\frac{\pi}{2} - \theta - \phi}{2}$$

$$\cos\beta = \frac{\sqrt{x^2 + y^2}}{2L}$$

$$\cos^{-1}\frac{\sqrt{x^2 + y^2}}{2L} = \frac{\frac{\pi}{2} - \theta - \phi}{2}$$

$$\theta + \phi = \frac{\pi}{2} - 2\cos^{-1}\frac{\sqrt{x^2 + y^2}}{2L}$$

$$\Rightarrow \theta = \tan^{-1}\frac{x}{y} - \cos^{-1}\frac{\sqrt{x^2 + y^2}}{2L}$$

$$\Rightarrow \phi = \frac{\pi}{2} - \cos^{-1}\frac{\sqrt{x^2 + y^2}}{2L} - \tan^{-1}\frac{x}{y}.$$

Also, from the relations in equation 2, it can be shown using inverse matrix that

$$\dot{\theta} = \frac{1}{L\cos(\theta + \phi)}(\dot{x}\cos\phi + \dot{y}\sin\phi)$$

$$\dot{\phi} = \frac{1}{L\cos(\theta + \phi)}(\dot{x}\sin\theta + \dot{y}\cos\theta).$$

Using all the equations above, we were able to convert from the angular positions of two motors to the Cartesian positions of the endpoint, and vise versa, so that the linkage mechanism could be used to make the endpoint follow the desired trajectories.

3.1.3 Position Sensor

As shown in Fig. 3.3, one side of each motor was connected with an angular encoder, which was a CP-2UT Midori contactless, precision rotary potentiometer. This kind of potentiometer utilizes a pair of Magneto-Resistive (MR) elements, that is, as the angular position of inside permanent magnet changes, the magnetic flux changes and at the same time the resistance of the MR elements changes. A schematic plot of the circuits of a potentiometer is shown in Fig. 3.9. The potentiometer worked essentially as a voltage divider. Two voltage sources entered the two ends of potentiometers and the middle output voltage was determined by the angular positions of the shafts, which were

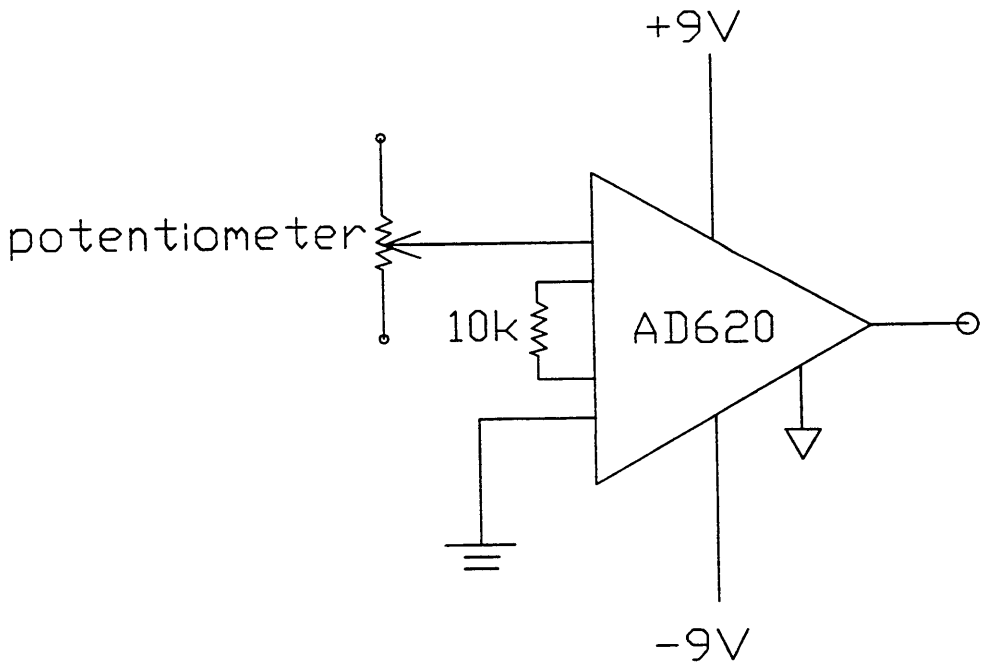

Figure 3. 9 The circuit of the potentiometer.

connected to the motors. The output then went into the instrumental amplifier AD-620 to get a higher resolution. The amplification also introduced an amplified high frequency signal, so the RC low-pass filters were used to reduce it. The capacitance of the filter was 1 μF and the resistance was 21 Ω, and thus the cutoff frequency was about 7500 Hz, which was selected through the spectrum analysis and was enough for reducing the undesired noise.

The calibration of the potentiometers aimed to find out the coefficients between the real angular displacements and the read-out counts from the outputs of the potentiometers. To achieve this, many different angles were measured and the corresponding read-out counts were recorded. The coefficients for both θ and ϕ were then obtained. In our experiment, the most important trajectory included the vertical indentation and horizontal stroke, both of which were straight line motions. To make sure the calibration was correct for these motions, the indentor was controlled to move in the desired straight line length and the LVDT sensor was used to check if the length was correct. The results demonstrated good calibration in both horizontal and vertical motions.

Also important is the deformation of the force sensor. By theoretical calculation, under 0.5 N normal force and 0.5 N shear force together, the bending error in the tip was 0.08 mm in normal direction and 0.1 mm in shear direction. These values were also verified by another measurement using LVDT, with 0.06 mm in normal direction and 0.07 mm in shear direction. The later data will show that the noise level of positions was about ± 0.01 mm when using the glass indentor (smooth friction) and ± 0.05 mm when using the polycarbonate indentor (stick-slip friction).

3.1.4 Force Sensor

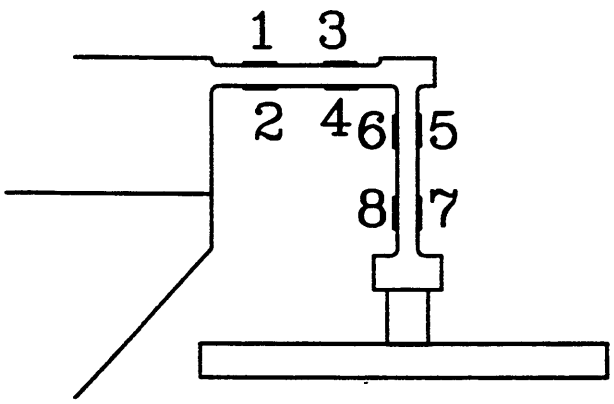

Figure 3. 10 The force sensor with the 8 mounted strain gages.

Fig. 3.10 shows the two-axis force sensor with a flat plate indentor. The force sensor was first designed by Brock and then modified by Gulati. It basically utilized two perpendicular cantilever beams with strain gages mounted on them. As can be seen in Fig. 3.10, four strain gages were on the horizontal beam, with two on the upper surface and two on the bottom surface, and four other strain gages were on the vertical beam, with two on the left and two on the right. The left solid part was mounted to the link 9 of the linkage mechanism in Fig. 3.5, so the left side boundary condition of the horizontal cantilever beam could be treated as a clamp-in boundary condition. The connection between the horizontal and vertical beams had a larger dimension than the thickness of both beams so that the bending effects of both cantilever beams was isolated. A flat plate indentor with a surface dimension of 75 mm by 25 mm was mounted below the vertical beam to indent and stroke the fingerpad.

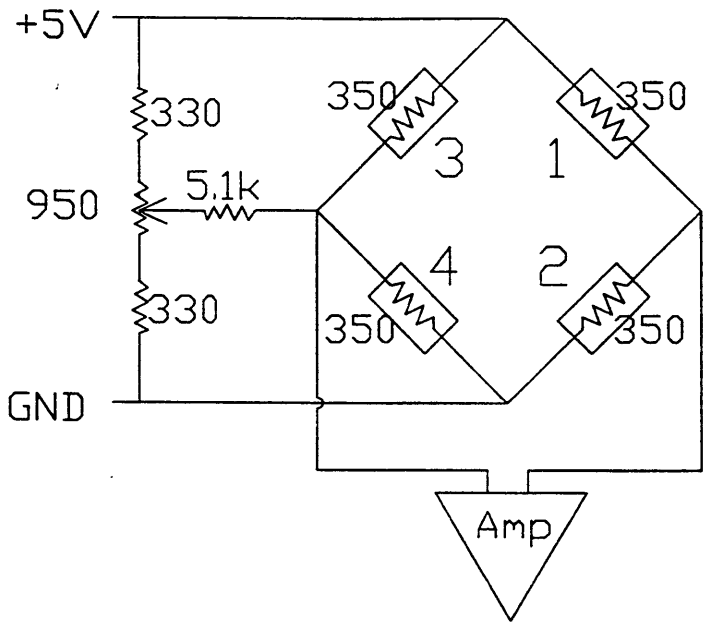

Figure 3. 11 The Wheatstone bridge of the force sensor.

For a more detailed understanding of the force sensor, let us consider the circuits of the strain gages. In Fig. 3.10, each strain gage is marked with a different number. The strain gages 1, 2, 3, and 4 formed one Wheatstone bridge and the strain gages 5, 6, 7, and 8 another one. The circuit of the first Wheatstone bridge is plotted in Fig. 3.11, and the second one will be the same except replacing the number 1, 2, 3, 4 by 5, 6, 7, 8. As seen in Fig. 3.11, each strain gage had a base resistance 350 Ω. The input voltage was 5 V and the Wheatstone bridge worked as a voltage divider. The output depended on the resistances of all strain gages. Because the actual resistance of the strain gages might not be exactly 350 Ω due to residual strains of the adhesive process, a potentiometer and some resistors were used to compensate this effect. This is as shown on the left side of the circuit in Fig. 3.11. In this setup, the output value of this Wheatstone bridge should be zero when no external force was exerted on the cantilever beam. The output then passed

through an operational amplifier to make the read-out value close to the voltage range of the A/D board.

The strain gage is an electronic element whose resistance is proportional to its length. Because the strain gage is bounded to the surface of the cantilever beam, the elongation or compression of the beam at that location is the same as the length change of the strain gage. That is, the local strain of the beam will be the same as the strain of the gage. Furthermore, with the approximation of small deformation, we have $My/I = \sigma$, where M is the bending moment, y is the distance of the neutral axis to the beam surface, I is the cross-section moment of inertia, and σ is the bending stress. It is also known that in one dimensional case, we have $\sigma = E\varepsilon$, the stress is proportional to the strain. Therefore, we have $My/I = \sigma$, $\sigma = E\varepsilon$, $\varepsilon \propto \Delta R$ (change of resistance), we get $\Delta R = kM$, where k also depends on the gage factor.

At this point we know that the bending moment is proportional to the change of resistance of each strain gage. However, if the external force on the indentor moves from one point to another, the bending moment at the location of every strain gage changes, and the external force we are actually interested in cannot be directly estimated from the readout voltage of the strain gage. The placings of the strain gages 1, 2, 3, 4, as well as 5, 6, 7, 8, as shown in Fig. 3.10 were designed to solve this problem. Let us plot the force diagram of the force sensor in Fig. 3.12, with external normal and shear forces acting on the indentor. It can be shown that the bending moments of locations 12 and 34 are as follows:

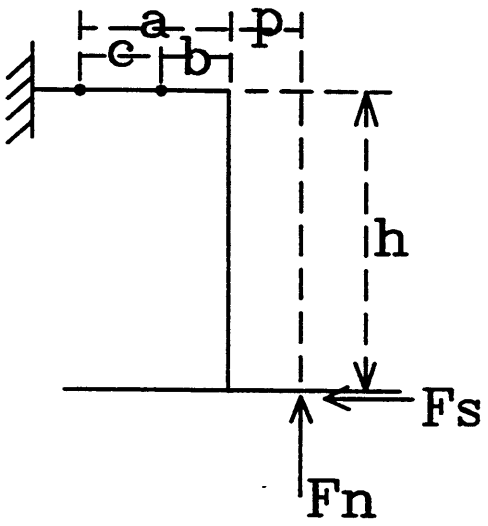

Figure 3. 12 The schematic plot of the force sensor with forces acting on it.

$$M_{12} = F_n(a+p) - F_sh$$
$$M_{34} = F_n(b+p) - F_sh$$

The resistance of each strain gage and the divided voltage of each side are shown in Fig. 3.13. The output voltage is computed as

$$V\frac{S+(F_n(a+p)-F_sh)k}{2S} - V\frac{S+(F_n(b+p)-F_sh)k}{2S} = V\frac{F_nLk}{2S},$$

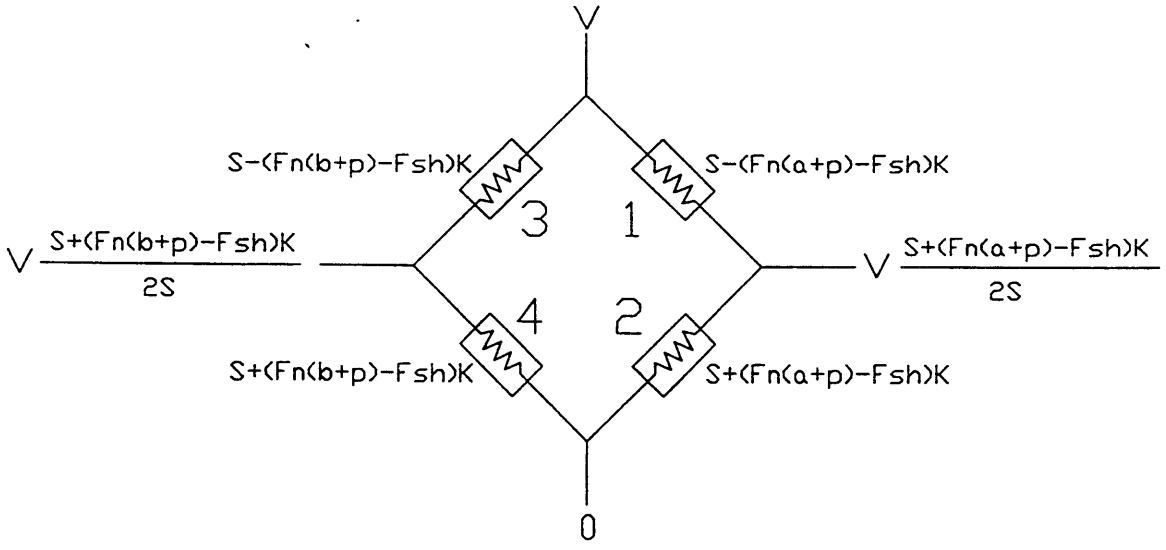

Figure 3. 13 The output of the Wheatstone bridge with loading as in Fig. 3.12.

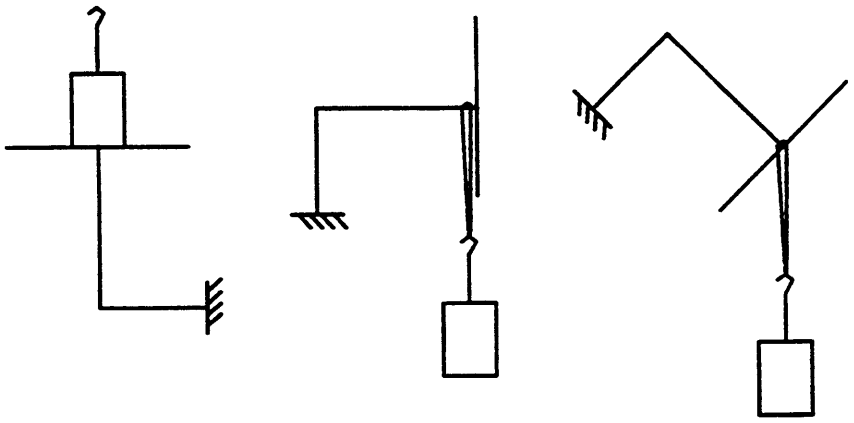

Figure 3. 14 Three different calibration angles of the force sensor.

where S is the original resistance of the strain gages. Therefore, the output voltage of strain gages 1, 2, 3, and 4 is only proportional to the normal force, independent of the position of external force and also independent of shear force. Similarly, the output voltage of strain gages 5, 6, 7, and 8 is proportional to the shear force only.

As shown previously in the block diagram of the force sensor in Fig. 3.2, an RC filter was introduced followed by the operational amplifier. This filter with a 150 Ω resistor and a 1 μF capacitor was used to suppress the noise of frequencies higher than 1 kHz. After the signal passed through the filter, the noise level in terms of the read-out count in A/D board was about ±2.5 count for both normal and shear forces, which was about ±4 mN after calibration.

The calibration constants were obtained by the following calibration steps. As shown in Fig. 3.14, three different angles were applied. In the first procedure, the indentor was reversed facing up and different weights were put upon it. This was to measure the calibration constant in the normal direction. The results showed that putting the weights in different places of the indentor did not influence the read-out values too much. In the

second procedure, force sensor was rotated by 90° and the weight was put right behind the indentor. This step measured the constant in shear direction. To detect if the normal and shear effects were coupled or not, we used a 45° angle and hung the weights on it. In principle, if these two effects are isolated, the force component in shear direction will not influence the read-out value of the normal direction, and vise versa. In fact, it was found out that the coupling effect was very small and it could be ignored without losing the accuracy in our resolution range.

Another important aspect of using the force sensor was to make sure that one stayed within the safety range. The safety range was limited by the range of output voltage, which in our case was ± 10V, and also by the yielding strength of the cantilever beam, which was made of aluminum. The yielding strength of aluminum is about 276 Mpa, and with some calculations it was found that the maximum tolerable normal force was 3 N, and 2 N for shear force, with safety factor of 2. The limit of the force constrained by the output voltage was higher than all these.

3.1.5 A/D Board

The A/D board used in this setup was a National Instruments AT-MIO-16X board. This board is a 16-bit device which combines compounds for analog to digital, digital to analog, and timers on it. This board is provided with a set of built-in C library functions, through which the board can be configured and programmed to work in customized conditions. The 16-bit specification represents that the input and output signals have 65536 counts. For example, in our setting for both force and position, the bipolar voltage ranging from -10V to +10V matched to the digital counts from -32767 to +32768. That is,

if the noise was only in the Least Significant Bit, the resolution was 10/32768V. The timers of this board can be set to sample at a rate of up to 100 kHz.

Two digital to analog (D/A) channels were used in this experiment to send out signals to the two motors. The computer program calculated the desired output torques using the control strategy difference equations, and then sent out the voltages to these motors. Two analog to digital (A/D) channels were utilized to convert the read-in voltages from two potentiometers to digital signals for recording or further processing, and two other A/D channels were used to convert the read-in voltages from force sensors to digital signals for recording. All the D/A and A/D channels were configured to the differential mode. The differential mode has the advantage for setting the isolated reference signal so that the output is not influenced by the shifting of the ground level. Also the differential mode can help with reducing the pick-up noise and increase common-mode noise rejection.

The built-in timer could be programmed to sample different frequencies. In our experiment, the control rate was set to be 2 kHz. This control rate was selected by two criteria. The first was that higher frequency made the system more stable. Because the motors of this setup were servomotors, the torque sent to the motor was to change the positions of the motors as well as the linkage mechanism. If the time period between two control signals was too long, the motor would move too far and might cause the system to be unstable. Thus, high frequency control loop was desired to maintain the stability of the system. During our trial runs, the mechanism became observably unstable when the frequency was below 1 kHz. However, the other criterion was that the frequency could not be set too high because of the limit of the computation time of each running loop. In our case, the work between two control signals included the calculation of the next

desired position and velocity, read-in of the previous position and force data, send-out of the new position signal. These steps involved I/O processing and some elaborate computations. From our trial runs, it was found that 2 kHz was the frequency that was always able to complete all the steps between two control signals and high enough to keep the stability. Therefore, the control frequency was set as 2 kHz through the timer setting in the A/D board. That is, each count of the timer was 1/2000 second.

The force and position data sampling rates could also be set to 2 kHz. However, we were not interested in such a high frequency where most signals were from the surrounding noise. Also, since we did not want to cause overflow of the memory of the computer system, 500 Hz sampling rate was selected. It could cover the useful frequency domain up to 250 Hz Nyquist frequency, where no aliasing occurred. The sampling rate was set through programming such that for every four control loops one datum was sampled.

3.1.6 Position Control

In fact, the fundamental issue of position control was to reach the desired trajectory with the smallest error while at the same time preserving the stability of the system. In this case, the position control of the system utilized the proportional-integral-differential (PID) control strategy. The proportional term was to use the high gain to get a smaller error; the integral term was to accumulate the error as the feedback reference and eliminate error one order higher than the proportional control; and the differential term was to introduce the damping as well as stability. The application of these terms was achieved by programming with difference equations. To determine the parameters of

these terms, we used the Ziegler-Nichols PID tuning (Franklin, *et al.,* 1990) to reach this goal.

The Ziegler-Nichols PID tuning method is also called the stability-limit method. The steps of this method are as follows:

1. Use proportional control only
2. Increase gain K slowly till continuous oscillations occur
3. Record control gain Ku, and oscillation period Pu
4. Use the PID control combined with the following forms:

$$P: u(k) = K_p e(k)$$

$$I: u(k) = u(k-1) + K_p \frac{T}{T_i} e(k)$$

$$D: u(k) = K_p T_d (V_d(k) - V_c(k))$$

where e(k) is the difference between the desired and feedback positions,

T is the reciprocal of control frequency, that is 1/2000 sec in our case,

$K_d = 0.6K_u$,

$T_i = P_u/2$,

$T_d = P_u/8$,

V_d is the desired velocity, V_c is the current velocity.

In our case, V_c was computed by measurements taken at two positions that were ten control samplings apart, that is, (u(k)-u(k-10))/10T. This was done so that sudden noise was averaged (reduced) and this ensured a more stable control.

After getting the Ziegler-Nichols parameters, the difference equations were formed and then implemented in the program to see the performance. The performance was

acceptable except that the parameters needed to be adjusted a little to get the best result, that is, the smallest error with the most stability.

3.2 Videomicroscopy System

The videomicroscopy system in our experiment was used to capture the image sequences of the fingerpad in real time when the fingerpad was stroked by transparent plates. The captured image sequences were then saved for further analysis. Fig. 3.15 shows the schematic plot of this system. This system was first built up by Chen (1996).

The system was composed of a fiber optic illumination source, a zoom lens, a gray scale CCD camera, a video monitor, and a frame grabber hosted by a 80486 PC. The light source was Fostec 8375 DC regulated source, which had low voltage ripple. A Fostec 8130 DDL quartz halogen lamp was installed as the light source. This DDL lamp had uniform light output. A Fostec 8920 fiber backlight was then connected to the lamp. This whole setup constituted the illumination part. In order to get the images of the fingerpad,

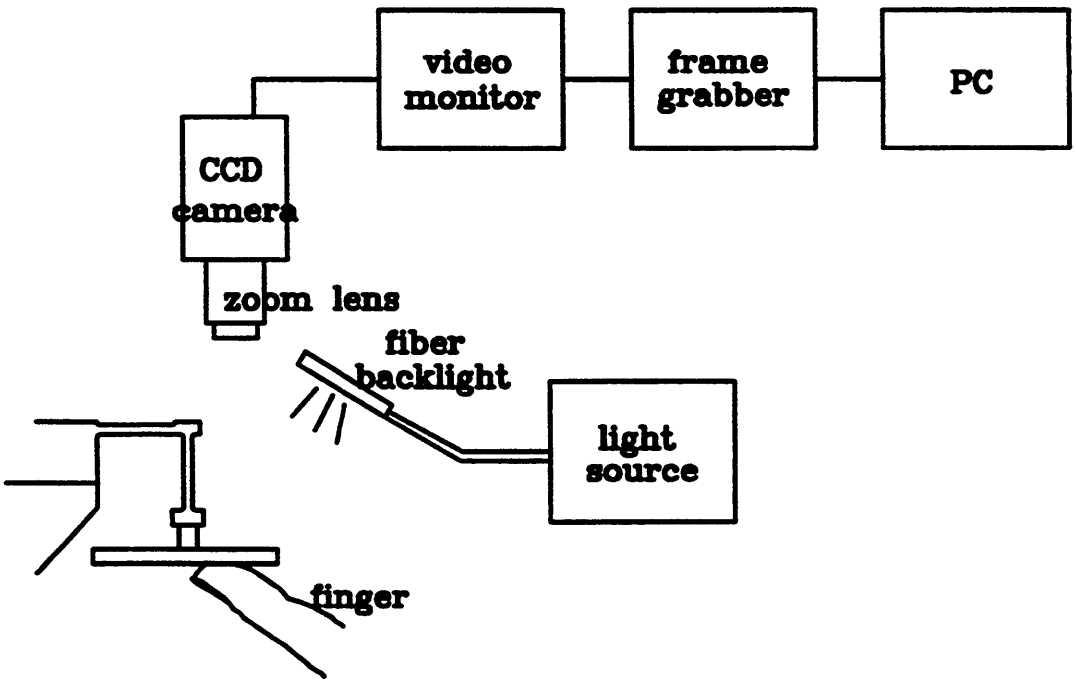

Figure 3. 15 The schematic plot of the videomicroscopy system.

the light and the indentor needed to be adjusted to a suitable angle so that the contact region was illuminated and most of the light was reflected into the high resolution Hitachi KP-M1U CCD camera. The Unitron 1:6.5 zoom lens in front of the CCD camera was utilized to change the magnifications of the images, and also the distance between the lens and the indentor could be adjusted to focus on the images. The image signals were sent to a Hitachi video monitor, through which we could observe the motion of the fingerpad and finger ridges in real time. The signals were then digitized by the BitFlow VESA local-bus VideoRaptor frame grabber and saved in the 80486 computer.

The image of each frame was a 8-bit gray scale 640x480 image, so it took 307.2 Kbytes for each frame. Considering the limit of the I/O and CPU speed of the system, the timer inside the frame grabber was set to 1 kHz and at every sampling 640x10 pixels were captured. That is, it took 48 ms to finish a complete frame capturing. We added up 2 extra void samplings to make the sampling rate 50 ms per frame. Thus, 20 frames could be captured in 1 second. Due to the limit of computer memory, which was 32 Mbytes, the maximum the system could capture was 90 frames per trial, so we could at most capture 4.5 seconds continuously. The time needed to finish one trial depended on the stroke length as well as the stroke velocity, which will be discussed in the next chapter.

3.3 Synchronization of Systems

From previous two sections, it is clear that one computer system took care of the position control as well as the position and the force data recordings, while another computer system captured image sequences. The requirement for using two different computers was because both tasks needed large amounts of operations in the central processing units (CPU) as well as memories of the computers. In order to use two

computers in each of the experiment trials, synchronization was necessary for matching the force data, position data and images. This is very important to properly interpret the behavior of force data at a certain time point with the corresponding image in the exact same time.

The synchronization of these two systems was developed by Chen (1996). The major electronic components in the synchronization circuit were the 8253 programmable interval timer and the 8255 programmable peripheral interface. Both computers had the same synchronization circuit in it. The 8253 programmable interval timer had three independent 16-bit counters which could be programmable to a desired sampling rate. The timer in each computer had the same sampling rate to achieve the synchronization. The 8255 programmable peripheral interface worked as the I/O interface between two computers. In this application, the interfaces in both computers were set to mode 0, the basic I/O mode. There were 3 ports in each 8255 chips, as A, B and C in Fig. 3.16, and each port contained 8 bit. In our configuration, the port A worked to send out data, the port B worked to receive data, and the port C worked as the handshaking element, which

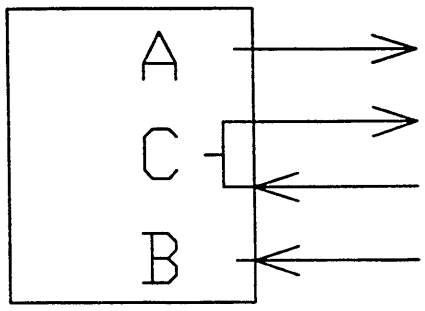

Figure 3. 16 The configuration of the 8255 programmable peripheral interface.

means it took care of the communication between two computers. The upper 4 bit of port C was set to be output and the lower 4 bit was set to be input.

The conceptual plot of the work of 8255 interfaces in both computers is shown in Fig. 3.17. In our setting, the computer for the videomicroscopy system worked as the master and the computer for the stimulator worked as the slave. That is, communication could be in both directions, but data could only be sent from master to slave. A sequence of work for sending data is as follows. Before there were data in the port A buffer of the master, both the master and the slave set the value of communication port C to 0. When the data appeared in port A buffer of master, which marks as 1 in the sequence plot, the output of port C changed the value to 1, as step 2 in the plot. This output port in master was connected to the input of port C in slave, and the value changed coincidentally. At the moment when input of port C in slave changed the value from 0 to 1, the port B in slave

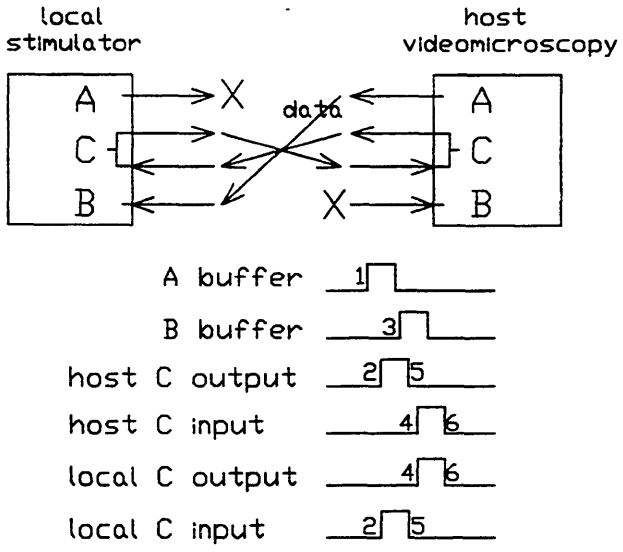

Figure 3. 17 The connection between two I/O in both computers and the order of a data sending process.

opened and received the data from master. As the port B in slave got the data in step 3, the output of port C in slave sent the confirmation back to master in step 4 and then both master and slave turned the value in port C back to 0 in steps 5 and 6 for another data transportation. In our case, the data could be the starting flag or stopping flag of experiment, or even the trial names and numbers.

Up to this point, we have described how the stimulator and how the videomicroscopy system were set up, and the synchronization was accomplished. That is, most of the hardware as well as software needed for the experiment have been described. The next step would be to use these tools in the design of the experimental procedure and to run the experiment, which will be introduced in the next chapter.

Chapter 4

Experimental Procedure

4.1 Experimental Protocol

The experimental protocol is shown schematically in Fig. 4.1. Before the experiment, each subject was asked to wash his or her hands for about 2 minutes with clean water only, to minimize the effects of contaminants on the skin. The subject then sat comfortably in a chair and placed the index finger of the right hand upon the inclined finger support, as shown in Fig. 4.2. The finger was fastened by Velcro and the fingernail was glued to the support with the fingerpad facing upwards so that the indentor could indent and stroke the fingerpad. Prior to each trial, the indentor surface was wiped first with an alcohol pad and then with a dry wiping tissue, followed by a 1 minute wait before starting the trial to ensure dry conditions. This process was repeated for each stroke to keep the indentor surface in the same state of cleanliness and dryness.

Before running the stimulator, there were a few minor steps for good performance of results and good machine maintenance. First, the Ethernet cable was unplugged from the computer and the network was unloaded. The network was a serious noise source and this noise level could have corrupted the data. Prior to turning on the power of linear amplifiers, the experiment was run once with power off so that the residual torques inside

motors could be removed and set to 0. When turning on the power for the amplifiers, the linkage mechanism was held carefully to avoid sudden movement due to residual torques.

The fingerpad had to be preconditioned before the experiment, because the internal tissues tended to shift significantly in the first few trials (Fung, 1993). In our experiment, the fingerpad was indented and stroked with the same stimuli for 8 times, which was found to be the maximum number of trials needed to achieve stable data in all the subjects.

After the preliminary steps mentioned above, the fingerpad was subjected to indentation and stroking by the test surfaces, as shown in Fig. 4.3. First, the indentor was

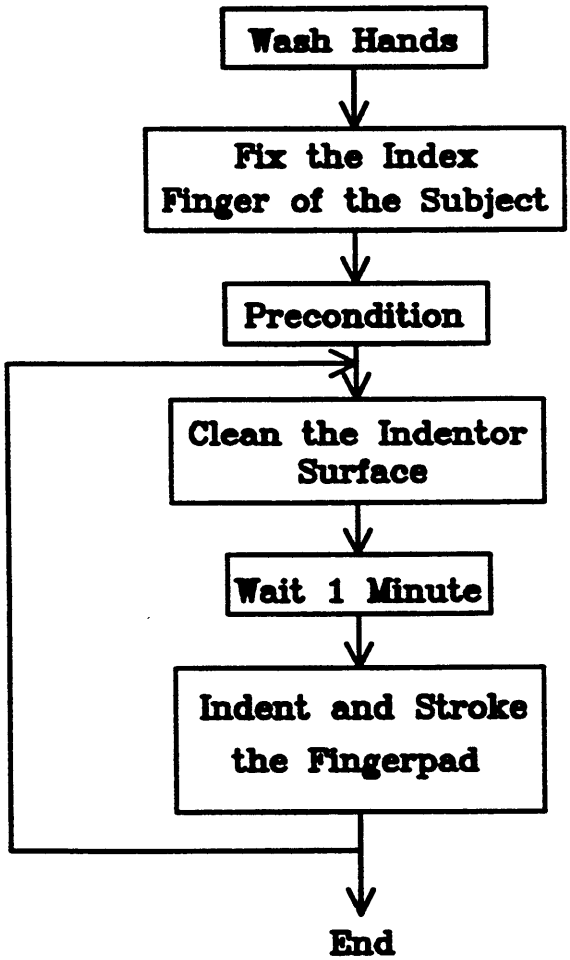

Figure 4. 1 The experimental protocol.

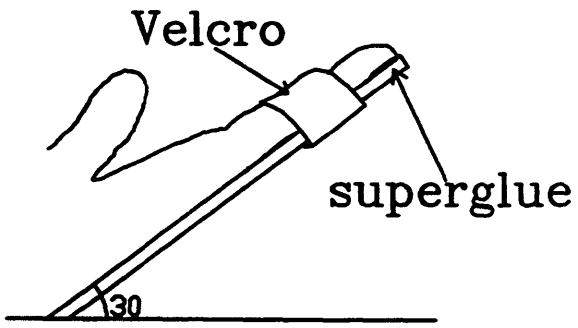

Figure 4. 2 Fixing the finger by superglue and Velcro.

controlled to barely contact the fingerpad. The "bare contact" could be detected mainly by the image when only a small contact spot was seen, and was also felt by the subject. At this time, a very low value of normal force was registered and then the indentor indented the fingerpad vertically down at a certain velocity to a specific indentation depth. The indentor was then held at that depth for 5 seconds, which allowed the normal force to reach a steady state (Gulati and Srinivasan, 1995, 1997). The indentor then stroked the fingerpad horizontally at a certain stroke velocity over a stroke distance. The stroke directions could be from distal to proximal, or from proximal to distal. During stroking, position and force data were recorded synchronously for further analysis. When stroking

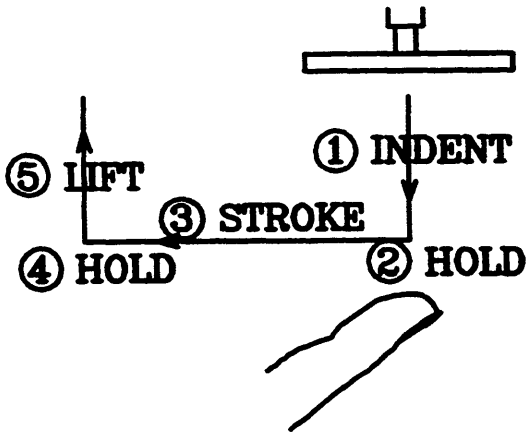

Figure 4. 3 The processes of indentation and stroking.

was completed, the indentor was lifted off the fingerpad and moved back to the original position. The indentor surface was then cleaned again and the next trial began.

In the experiment, there were several stimuli and different parameters that could be changed. As described above, the indentation depth, the indentation velocity, the stroke distance, the stroke velocity, and the stroke direction could all be varied. Because of the time limit for the project, only some combinations of these stimuli could be done and they were selected based on results from preliminary experiments. The indentation depth, which influences the contact force and the stretching of the fingerpad under stroking, was regarded as one of the important factors and selected as a variable. The indentation velocity, with which the indentor moved vertically down, was, however, only crucial for transient response during the first few seconds after indenting (Gulati and Srinivasan, 1995, 1997), but did not affect stroking after a 5 second hold. Therefore a constant velocity 4 mm/s was selected as the indentation velocity for all trials. The stroke distance was the length for the forces to achieve steady state. Once the steady state was reached, no significant change in the forces occurred. From the images, we found 10 mm was enough for the force values of all subjects to reach the steady states in most of the trials, so it was chosen and was not treated as a variable. The stroke velocity and the stroke direction were found to be related to the shear force induced by stroking, so both were treated as variables in our experiment. The indentation depth, stroke velocity, and stroke direction were the three experimental parameters studied and will be discussed in the next section.

4.2 Experimental Stimuli

As discussed above, there are three parameters in our experimental stimuli, the indentation depth, stroke direction, and stroke velocity. In each of the experimental trials, only one parameter was changed and other two were fixed, so that the influence of that parameter could be investigated.

The indentation depths in the experiment ranged form 0.75 mm to 2.25 mm, with a 0.25 mm increment. That is, 7 different indentation depths were applied. The smaller depths are associated with the general deformation of the fingerpad when we explore the surfaces of objects. The larger depths are associated with the deformation of the fingerpad during typical manipulation tasks. The fingerpad can have even larger deformation in terms of depth when exerting higher force on objects, but this could not be investigated with our setup due to the limitations of the force sensors.

Two stroke directions were investigated in the experiment, as shown in Fig. 4.4. One is from distal to proximal, named the forward direction as in the plot, and the other one is from proximal to distal, named the backward direction. The forward direction moves the

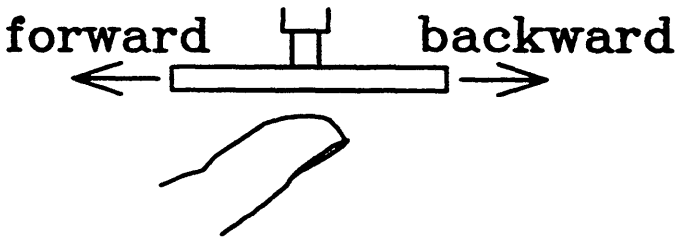

Figure 4. 4 Two stroke directions of the experiment.

finger tissue away from the fingernail, so that the tissue right in front of the fingernail becomes thinner. The backward direction does the opposite: the indentor strokes the finger tissue toward the fingernail and more tissue accumulates in front of the fingernail. This difference should make the results deviate for two directions.

Four stroke velocities were applied in the experiment, 2, 4, 8, and 16 mm/s. These velocities covered roughly the range of speeds with which people explore objects using fingerpads. The logarithmically increasing velocities covered a wide range of velocities with only 4 different values.

The list of all the stimuli used is shown in Table 4.1.

Indentation Depth (mm)	0.75, 1.00, 1.25, 1.50, 1.75, 2.00, 2.25
Stroke Direction	forward, backward
Stroke Velocity (mm/s)	2, 4, 8, 16
Indentor	glass, polycarbonate, acrylic
Subject	cw, fs, ws, ck, yc

Table 4. 1 The experimental stimuli and the experimental parameters.

4.3 Trajectory

Once the lengths and velocities for both indentation and stroking were selected, the trajectory of one complete trial could be defined. We already introduced the tools such as inverse kinematics and position control strategy. Now these tools will be combined to follow a desired trajectory.

The trajectory could be separated to two parts. The first part was to move the indentor to the starting position where the indentor barely touched the fingerpad. In this part of motion the indentor could be moved in any trajectory provided no obstacle was in the path of the trajectory and the system was stable. The second part was to control the

indentor to indent and stroke the fingerpad with prescribed positions and velocities, that is, the experimental trajectory.

To move the indentor to the starting position, we used the easiest way for the trajectory, that is, we moved only one motor at each sub-trajectory. In Fig. 4.5, two major links were shown to understand the motion of the links step by step. Before an experimental trial started, these two links were at rest as shown in the first panel. Then, the upper link moved up with a certain angle, while the other link was at rest, which means no power was added to the motor for the lower link. The next step was to keep the upper link at the same angle, and move the lower link forward to the desired position. The last step was to keep the lower link at its angle and move the upper link down to the bare contact position. If the indentor did not touch the fingerpad yet, fine adjustment could be done on-line, so that the desired starting position was reached.

During each of the motor angular motion, cubic spline was used to fit the path of each sub-trajectory. For example, to move the upper link upward to some angular position in a certain time, the cubic spline equation for this link was as follows:

$$\phi(t) = a_3 t^3 + a_2 t^2 + a_1 t + a_0$$

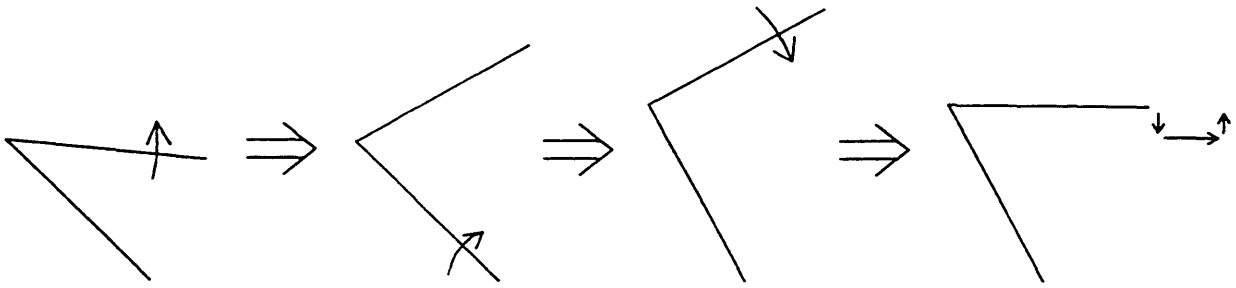

Figure 4. 5 The motion of the linkage for achieving the "bare contact" position.

where t was time, and ϕ was the angular position of the upper link. The coefficients a3, a2, a1, a0 were evaluated by the conditions at the beginning and the ending of this path, with the velocities both set to 0. That is, $\phi(0) = \phi_0, \dot{\phi}(0) = 0, \phi(t_1) = \phi_1, \dot{\phi}(t_1) = 0$, where ϕ_0 was the starting angular position, ϕ_1 was the desired ending angular position of this sub-trajectory, and t_1 was the prescribed time for reaching ϕ_1. In our experiment, we set t_1 for each step as 2 seconds. That is, it took 6 seconds to reach the bare touch position. In the above conditions, both starting and ending velocities being set to 0 was to make the trajectory of the continuous three steps even smoother.

The second part was to move the indentor to indent, hold, and stroke the fingerpad, with prescribed positions and velocities. Let us replot this part of the trajectory in Fig. 4.6. In each straight line path, regardless of whether it is vertical or horizontal, the velocity should be from 0, the stage of hold, to a constant velocity, the indentation velocity or the stroke velocity, to another 0 velocity, another stage of hold. Therefore, it consisted of acceleration and deceleration portions. A schematic velocity curve is shown in Fig. 4.7. In each straight line sub-trajectory, for example, the indentation path in Fig. 4.6, 5% of the total time to complete this path was set as constant acceleration, and also

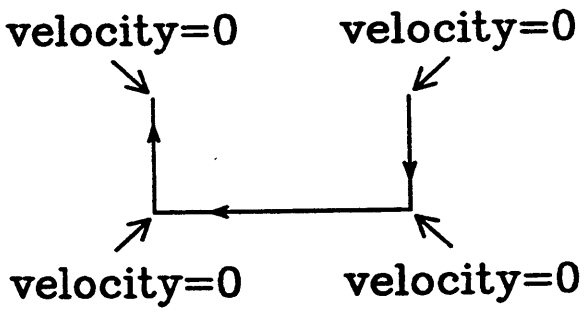

Figure 4. 6 The velocity characteristics of the experimental trajectory.

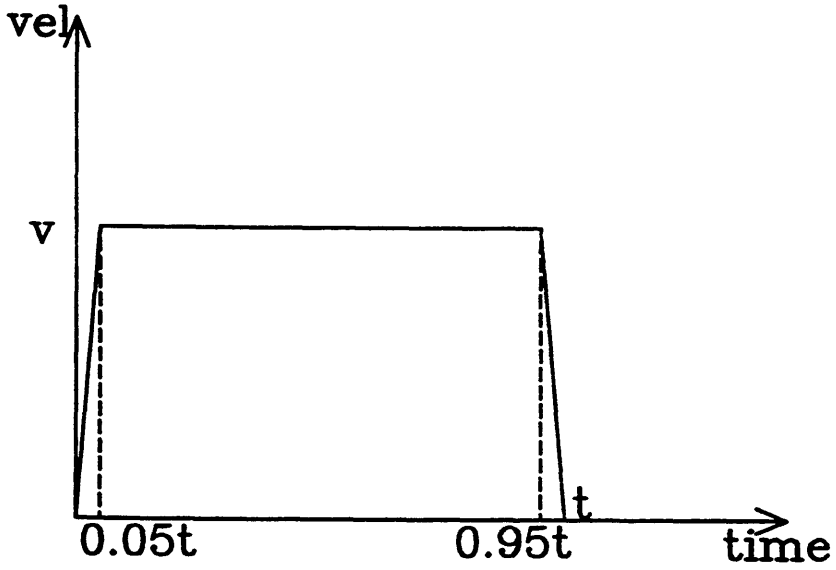

Figure 4. 7 The idealized velocity profile for each straight line trajectory.

the last 5% time was set as constant deceleration. Therefore, only during the middle 90% time the indentor had a constant desired velocity. This was good compared with not prescribing the 5% time for acceleration and deceleration in that without 5% acceleration, the system would try to reach the desired velocity in much shorter time, and it produced the system overshoots and the system oscillated even longer than 5% of the total time. With the prescribed velocity curve, the desired moving length, i.e., the indentation depth or the stroke distance, was equal to the area under the curve in Fig. 4.7. Thus, the desired positions and velocities through the whole trajectory could be calculated.

4.4 Indentors

There were three kinds of materials used as the flat plate indentors in our experiment: glass, polycarbonate, and acrylic. These three materials were selected because they are transparent, which was needed for image capturing. It may be asked if these three kinds of indentors, which look so similar, could represent the frictional behavior of human

fingerpads in contact with huge amounts of different kinds of materials in the world. Though it is almost certain that the three materials did not span the range of frictional behaviors, it will be shown that two distinct frictional phenomena appeared with these three materials. That is, the materials we used did show the radically different frictional properties, so further research may be directed towards finding a classification of the frictional behavior of human fingerpads in contact with different kinds of materials.

The glass plate indentor was that used for VWR micro-slides. The material was soda-lime glass and processed by Fourcault sheet glass procedure. The polycarbonate plate was GE Lexan sheet. The acrylic plate was Atohass Plexiglas MC sheet. One important comparison between these three indentors was the roughness of them. A Dektec profilometer was utilized to get the surface micro-profile and typical results are shown in Fig. 4.8. The peak-to-valley values of the glass, polycarbonate, and acrylic were about 700 A, 1300 A, 1100 A, respectively. These values will be relevant to the discussion of results (Chapter 6).

4.5 Subjects

There were five subjects in this experiment, 3 males and 2 females, all of whom were MIT students. The selection of subjects was based on the availability. The limited number of subjects was because of the time limit of the experiment. In the experiment, it might have been possible to find people in light or heavy industrial work jobs or older ages. However, because of the limited number of subjects in the experiment, it was considered to be better from the statistical point of view to have all five subjects with little variation in professions and ages, so the data could at least be representative of university students.

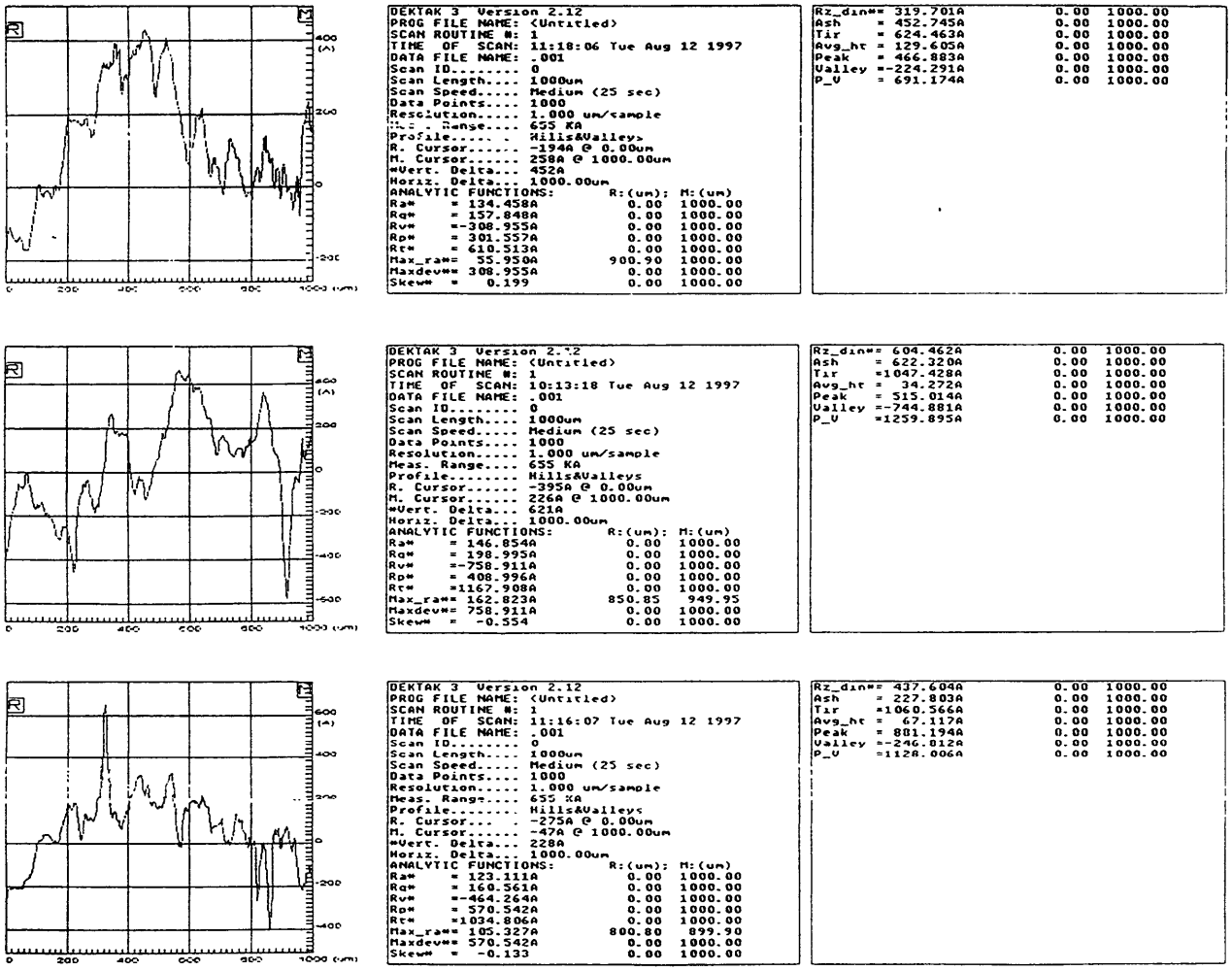

Figure 4. 8 The surface roughness of the three different indentors, tested by the profilometer.

The five subjects had the gender and the age shown in Table 4.2. We set five subjects from number 1 to 5, and will use these numbers in the later discussion. The ages were in a small range, from 24 to 27 years old. All five subjects used the right hand as the dominant hand. We used the right hands of all the subjects in the experiment.

subject	number	gender	age
cw	1	M	27
fs	2	F	25
ws	3	F	24
ck	4	M	26
yc	5	M	26

Table 4.2 The data of all five experimental subjects.

4.6 Image Capture

For capturing the images, two computers for the stimulator and the videomicroscopy system were synchronized, as described in the previous chapter. The videomicroscopy system first turned on the mode of showing the live video, which means the on-line image could be observed from the computer. With the help of the live video, we could adjust the light, the magnification, as well as the focus. Then by pressing a key in the computer of the videomicroscopy system, a START command was sent to the computer of the stimulator. The experimental trajectory of the stimulator was, as stated previously, composed of three main stages: indentation, holding steady for 5 seconds, and stroking. In our setting, when the holding reached 4.5 seconds, the stimulator received the START command and moved continuously with prescribed path. This means we captured the image sequence 0.5 second before the process of stroke started. This 0.5 second helped to observe if there was any change developed during the static holding. Then, the

videomicroscopy system continued capturing images through the stroking process, till the maximum frames were reached. The maximum frames the system could capture were 90 frames, but for safe use of memory, only 80 frames were captured for each trial. After all 80 frames were captured, the image data were saved and the memory was released for the next trial. This system then sent a START command again and wait for the stimulator system to receive it. The loop worked repeatedly until a key was hit or the maximum trial number was reached.

There were fewer stimuli for the experiment with image capture, due to the time limit of the experiment. We had one magnification, which allowed us to observe the whole contact area of the fingerpad during stroking. When a small portion of the fingerpad contact region was interesting, the zoom-in tool in MATLAB was applied. Two kinds of indentors were used: the glass plate and the polycarbonate plate. The indentation depth was 1.5 mm for all trials, and the stroke velocities were 2 and 4 mm/s. Due to the limitation of the maximum frame number, 90, in each trial and the frames captured per second, 20, the stroke velocity influenced whether we could observe the whole 10 mm stroke distance or not. In the case of 4 mm/s, about 2.5 seconds were spent in the stroking process, which means that at most 50 frames were enough for obtaining the full image sequence. While in the case of 2 mm/s, the frame number was doubled to become 100 and the system was unable to capture all of them in one trial. To overcome this problem, the images were captured twice, once for the first half and once for the second half in two separate trials.

The calibration of the videomicroscopy system consisted of two stages. The first stage was to compute how many pixels did the image shift in two contiguous frames, and the

second stage was to relate the pixel numbers to the real length. In this experiment, only the first stage was done. For achieving this calibration, a small point was drawn in the surface of the indentor. As the indentor moved during the stroking process, the point moved at the same velocity as the indentor, so from the images the velocity of the indentor in terms of pixels could be obtained. This stage of calibration was helpful for the analysis of the relative motion of the fingerpad and the indentor, which will be described later.

4.7 Image Processing

The images of the fingerpad captured during the stroke process were utilized to understand the subtle changes in the contact area and to detect the static or kinetic friction states more carefully. In order to provide qualitative visualization as well as to conduct quantitative analysis of these images, image enhancement techniques were applied. The techniques used in this research were mostly based on the image processing work by Chen (1996), but some of them were improved and newly developed with the help of the MATLAB image toolbox. The image processing techniques used in this research were simple thresholding, morphological processing, scan-line processing, and image shifting.

The images in our experiment were all gray scales with values from 0 (lowest intensity) to 256 (highest intensity). The contact region between the fingerpad and indentor had lower image intensity and the non-contact region had higher image intensity. The simple thresholding selected a gray scale value as the threshold. Scanning through all the pixels of an image frame, if the gray scale value of a pixel was higher than the threshold value, then set it to 256, while if it was lower than the threshold value, set it to 0. Therefore, the image became a binary image.

Furthermore, this binary image could be processed with erosion, one of the basic techniques in morphological processing (Gonzalez and Woods, 1992). The erosion was achieved by logical operators such as AND or OR on neighboring pixels. In our images, the contact region between the fingerpad and the indentor had 0 intensity after simple thresholding. To apply the erosion to this kind of images, a 3x3 mask scanned through the images. If a pixel and its eight neighboring pixels were all 0 intensity, then the gray value of this pixel kept 0. Otherwise, the pixel gray value changed to 256, the same as the non-contact region. Through this process, the boundaries of the image were eroded. Subtracting the original image by this eroded image, we got the outline of the contact region. This was very useful in detecting the distance moved by the indentor frame by frame.

A faster way to measure the motion between different frames was scan-line processing. Selecting a row of the image matrix and then plotting it with respect to pixel number, we could get the gray scale distribution across that scan line. The difference between frames then was identified by the subtraction of two frames.

In our experiment, because the fingerpad was stretched and deformed by the indentor, the finger tissue in the contact portion might be shifted a certain distance. To detect the shifting amount of the images, a processing tool called image shifting was used. In MATLAB, the shifting of image was applied by just moving the column of the image matrix, and then the shifted image was obtained. Using the image shifting combined with the morphological processing or the scan-line processing, two or even more images could be combined in the same frame and the comparison among them became easier.

Chapter 5

Results

5.1 Glass Surface

5.1.1 Indentation Depth

The experimental data for the glass plate recorded during the 10 mm horizontal stroke distance is shown for various indentation depths in Fig. 5.1. This experiment was conducted in the forward direction (distal to proximal), with a stroke velocity of 4 mm/s and on the fingerpad of subject 2. Data for other subjects are presented in Appendix. The seven curves in each panel represent the seven different indentation depths from 0.75 to 2.25 mm at 0.25 mm increments. Panel A shows the nearly constant indentation depths through the whole stroke, demonstrating good control at high positional resolution. Panel B shows the corresponding normal forces. The initial values of the normal forces at 0 mm stroke distance represent the steady state values of the forces after transient response of the fingerpad to indentation have died down. These normal forces remained approximately constant for small indentation depths, but ramped up during the stroke to steady state values for large indentation depths. The steady states at each of the higher depths were reached after a maximum of 6 or 7 mm of stroke distance. Through the whole 10 mm stroke, the higher the indentation depth, the higher was the corresponding normal force.

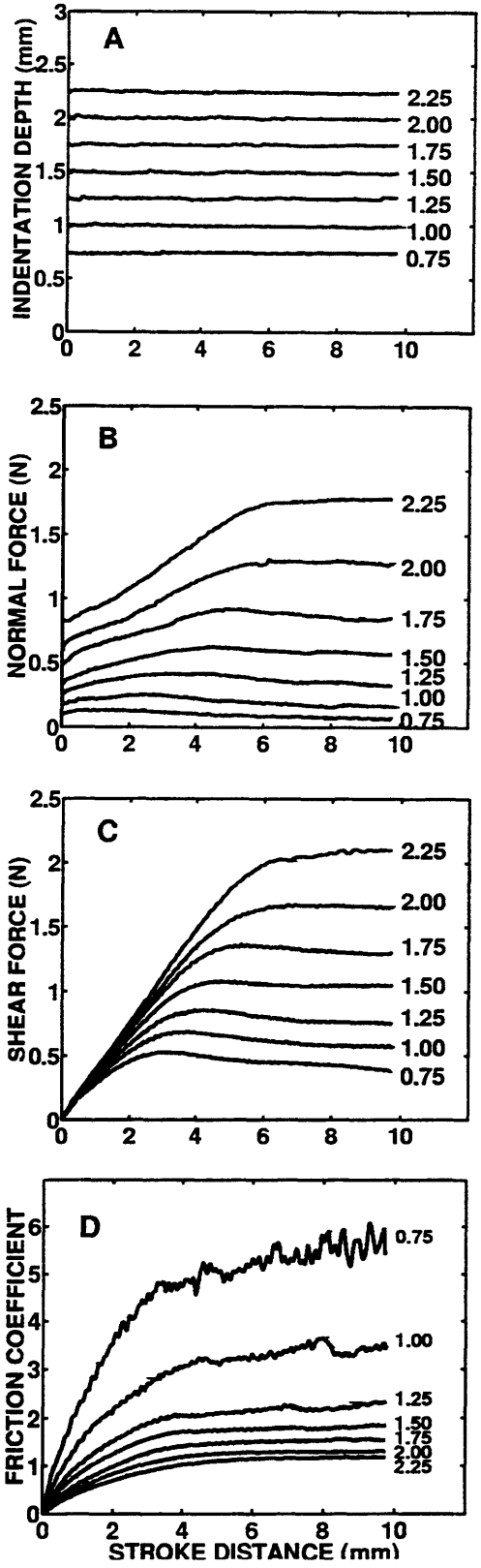

Figure 5. 1 The indentation depths, the normal forces, the shear forces, and the friction coefficients for different indentation depths on the fingerpad of subject 2, with 4 mm/s stroke velocity and forward direction.

Panel C shows the shear forces, where the traces grew from 0 to a steady state value, with higher slopes and higher steady state values for higher depths of indentation. In each trace, in the beginning there is a region where the fingerpad skin moved with the plate without relative motion. This portion represents the shear force - displacement relationship of the fingerpad, and the corresponding slope is a measure of the shear stiffness of the fingerpad. After a skin stretch up to certain distance, slip, or relative motion between the glass and skin surfaces began to occur. The shear force continued to increase and a steady state was achieved at about the same location where the normal force also reached its steady value. In a later section, the transition from no slip to slip will be shown by analyzing the corresponding image sequences.

The ratio of shear and normal forces demonstrates a different behavior than that of either the normal or the shear force. By definition, this ratio is the friction coefficient, a measure of the difficulty of moving one object relative to the other. Panel D of Fig. 5.1 shows that for each depth of indentation, the friction coefficient increased in a nonlinear fashion and reached an approximately steady value. As the indentation depth increased, however, the friction coefficient decreased. In the traces shown, for smaller indentation depths, the noise seems larger because its value in the shear force signal was amplified when divided by small values of normal forces.

The left panel of Fig. 5.2 shows an inverse relationship between the friction coefficients and the indentation depths for all five subjects. The friction coefficients in this plot are the mean values during the last 1 mm of stroke distance. The data for each of the five subjects show a common trend, but are distinctly different. This difference is

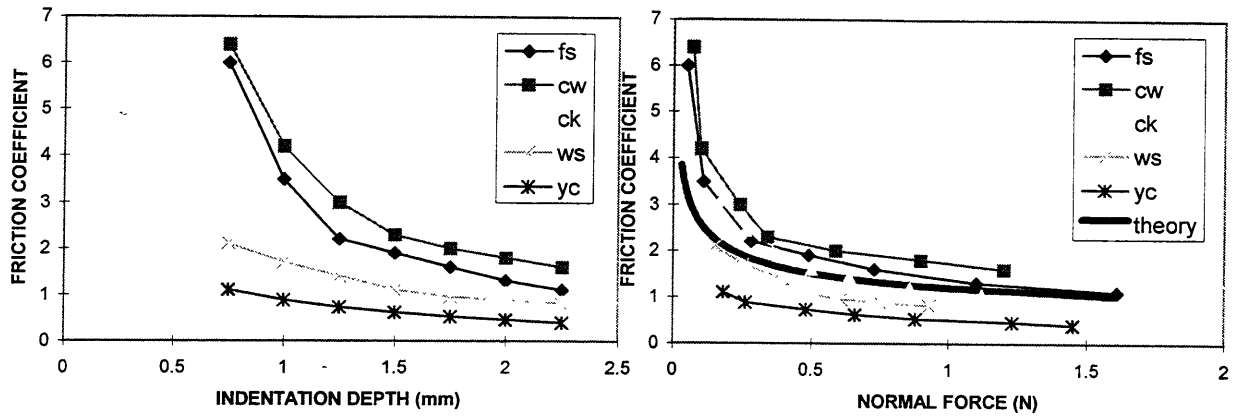

Figure 5. 2 The inverse relationships between the indentation depth and the friction coefficient, as well as the normal force and the friction coefficient, for all five subjects.

possibly due to the variability among the fingerpads of subjects, such as in the size of fingerpad, the type of finger ridges, and the amount of sweating.

The right panel of Fig. 5.2 shows the inverse relationship between the friction coefficients and the normal forces (the mean values over the last 1 mm of stroke distance). The traces for the subjects are more overlapping than in the left panel. The figure also shows that the inverse relationship can be predicted to a first order of approximation from Hertz's solution for the mechanics of contact between a rigid flat plate and an elastic sphere. In this case, the Hertz's formula for small deformation is (Johnson, 1985):

$$a = 2\left(\frac{F_n R}{2E}\right)^{1/3}$$

where F_n is the normal force, R is the radius of the elastic sphere, E is the Young's modulus of the sphere, and a is the radius of the nominal contact area between the rigid flat plate and the sphere. Because the fingerpad is a soft material similar to rubber, it can

be assumed that the shear force is proportional to the nominal contact area (Schallamach, 1952), i.e., $F_s \propto A$. Also, the nominal contact area A is proportional to the radius square, a^2. Thus,

$$F_s \propto F_n^{2/3}$$
$$\frac{F_s}{F_n} \propto F_n^{-1/3}$$

whose trace is shown in Fig. 5.2 as a bold line with the proportionality constant chosen such that the line fits the mean of the traces for all the subjects. It is seen that this proportionality of the friction coefficient to $F_n^{-1/3}$ exhibits the same inverse trend as the experimental data.

5.1.2 Stroke Velocity

The experimental record for various stroke velocities is shown in Fig. 5.3. The normal forces, shear forces, and friction coefficients are plotted with respect to stroke distance in three panels for subject 1. The indentation depth was 2 mm for all four velocities of 2, 4, 8, and 16 mm/s. Panel A shows that the normal forces for all four stroke velocities are almost totally overlapping. The recorded normal force was the response force due to the compression of the finger tissue in the normal direction. When the stroke velocity changed while the indentation depth was kept constant, the elastic response in the normal direction was almost the same, and therefore the normal forces were the same regardless of the change of stroke velocity. In panel B, it can be seen that when the stroke velocity was higher, the shear force as well as the friction coefficient became larger. This can be explained by considering the fingerpad as a viscoelastic material (Gulati and Srinivasan, 1995). When the fingerpad is loaded by shear force, as the stroke velocity increases, the

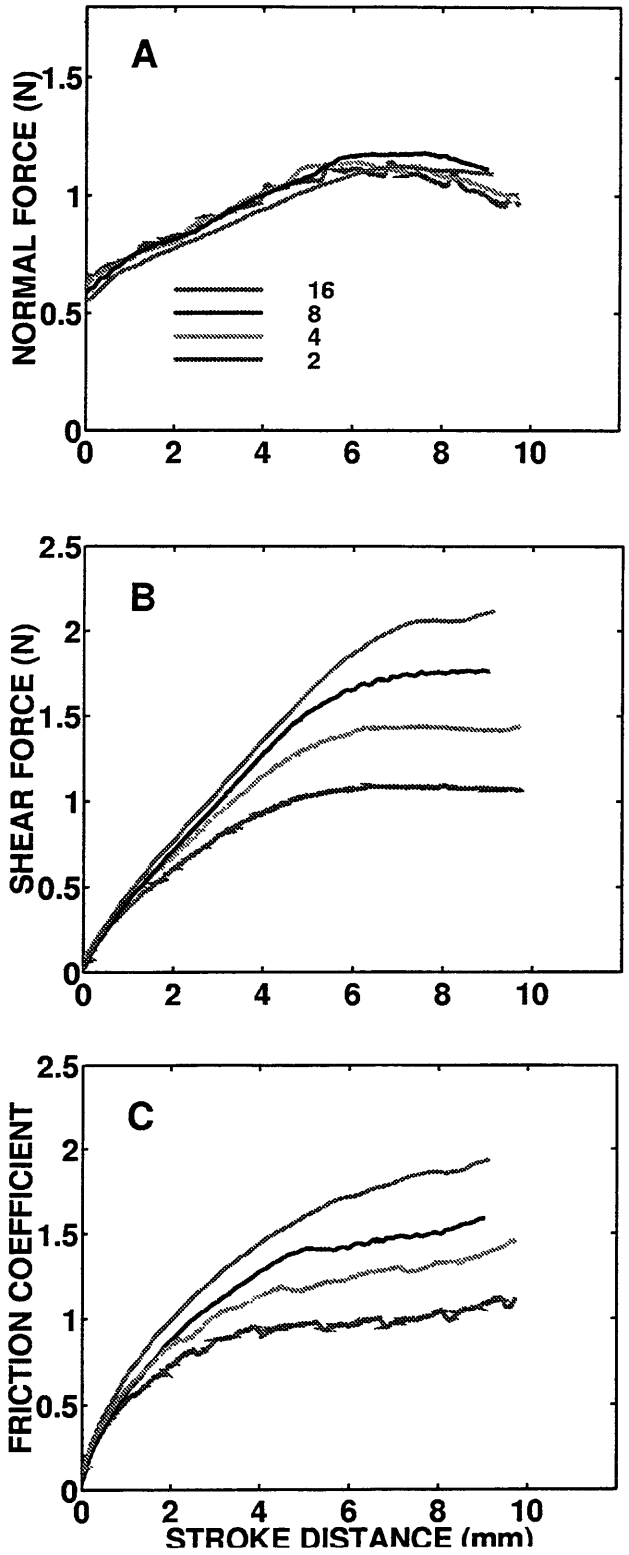

Figure 5. 3 The normal forces, the shear forces, and the friction coefficients for different stroke velocities on the fingerpad of subject 1, with 2 mm indentation depth and forward stroke direction.

contribution of the viscous property of the fingerpad to the resistive force grows, and a higher shear force is necessary to balance the increase of the viscous force so that computer-controlled constant velocity of motion can be maintained. Thus for larger stroke velocities, the shear force is larger, and consequently the friction coefficient is also larger, as shown in panel C.

A minor observation from Fig. 5.3 is that the normal force and friction coefficient with smallest stroke velocity indicate periodic value changes. This was due to the heart beat of the subject. For these curves, the stroke velocity was 2 mm/s, so it took about 5 seconds for the 10 mm stroke. It can be seen that about 7 pulses occurred in this period of time, so the frequency was around 1.4 Hz, which was 84 pulses/min, close to the average human pulse rate.

5.1.3 Stroke Direction

Fig. 5.4 shows the normal forces, shear forces, and friction coefficients for both the forward direction in the left panels and the backward direction in the right panels. The data shown for various indentation depths are for a constant stroke velocity of 4 mm/s captured from the trials on the fingerpad of subject 5. It can be seen that the trends in the data for normal forces were different for the two directions while the trends for both shear forces and the friction coefficients were mostly the same.

In the forward direction, the normal forces grew up to a certain value that depended on the indentation depths and then dropped gradually from a stroke distance of 4 mm to 10 mm. In the backward direction, the normal forces decreased from the beginning of the stroke and continued to decay with larger decreasing slopes than in the forward direction.

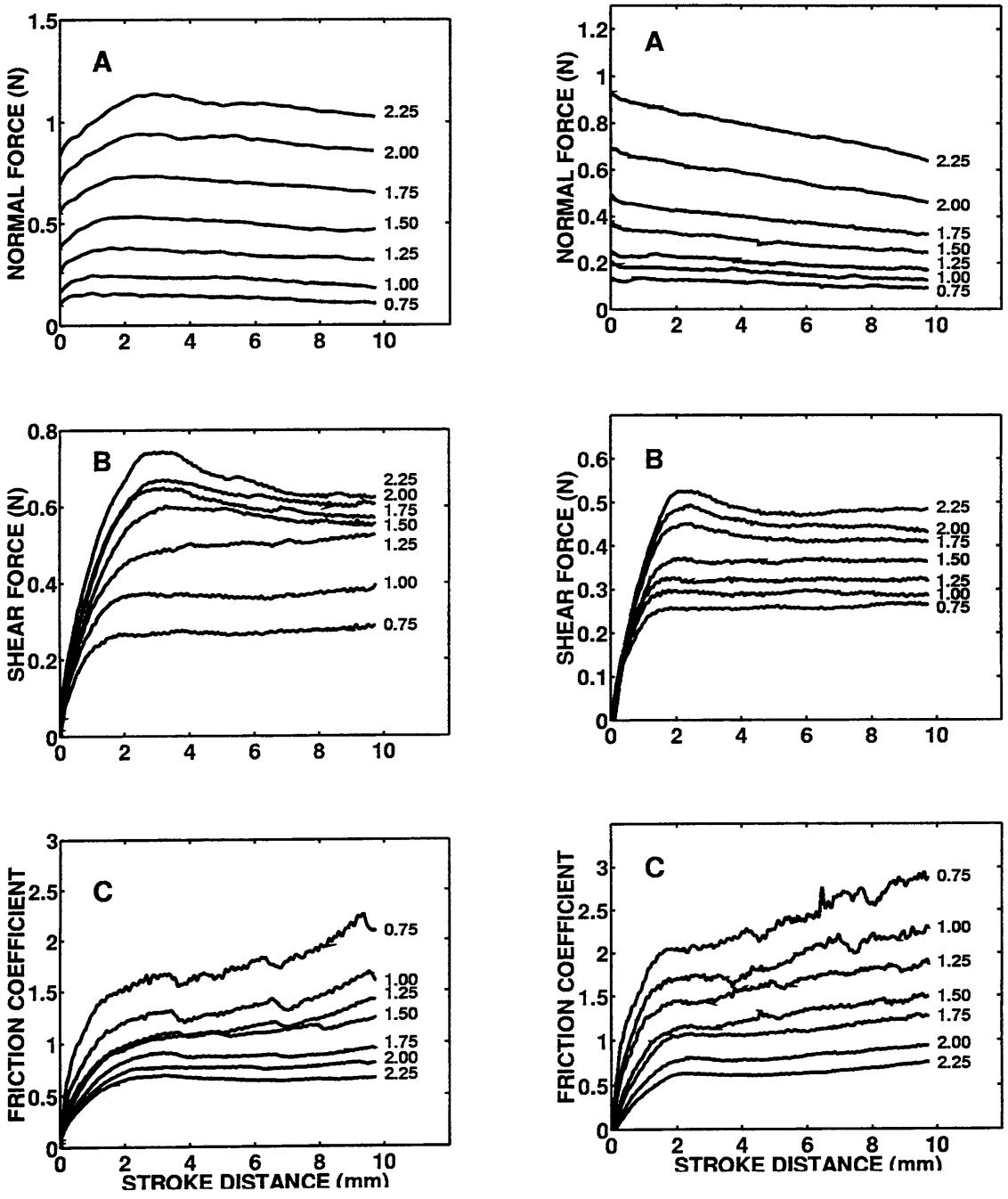

Figure 5. 4 The comparison of data of different indentation depths in forward direction, the left side panels, and in the backward direction, the right side panels. Data were obtained from subject 5 with 4 mm/s stroke velocity.

The difference of normal forces between the forward and backward directions could be due to the different boundary conditions in the two cases. As stated before, when stroking in the forward direction, which means the indentor moved from the distal side to the proximal side, the finger tissue was squeezed to the proximal side, where the available space ahead of the contact region is larger than in the distal side. Thus, in the case of forward direction, the finger tissue could be moved to the proximal side gradually, while for the case of backward direction, the distal side has the finger nail right close to the contact portion of the fingerpad, and the tissue accumulated very fast to a saturated state. Though the difference between the two directions was understood, the increasing and decreasing trend of the curves need further analysis with the help of specific finger tissue models.

In the panels B and C in both sides of Fig. 5.4, the basic trend was similar. For small indentation depths, the shear forces grew during the first few seconds of stroking, and reached steady states toward the end. For larger indentation depths, the shear forces grew to higher values and then dropped down to steady states. This was slightly different from the case we observed previously from the data of subject 2, and it in fact depends on the different fingerpad structures of different subjects. However, it can be seen from the data in the Appendix that the curves for the same subject always have a similar pattern.

Most of the data for two different stroke directions were recorded in different days and different sittings. The force data from different days varied from each other, though the basic trends , the shape of curves, of the same stimuli were the same. For the trials of two stroke directions as in Fig. 5.4, the force data during indentation and 5 second hold right before stroking, the portion where the stroke direction has not been an effective influence,

should be the same. Therefore, if the material properties of the fingerpad did not change, at least the starting value (the value for 0 stroke distance) of the normal forces for both cases should be the same in Fig. 5.4. However, the shifting of initial force values could be observed, and in some data from other subjects (see Appendix), the shifting was even larger. This could be explained that the moisture, the body health condition, or the external loading history, such as typing on the keyboard, could all influence the properties of the tissue day by day, so the data in different sittings may always change. Also in two different sittings, the finger of the subject could not be fixed in the exactly same angle, so the contact portion was not exactly the same. Though the data were shifting, which implies the quantitative comparison between the data of different sittings was not so meaningful, fortunately the basic trend was similar for the same subject, and the data from one sitting could give us reasonable information through careful analysis.

Fig. 5.5 shows the comparison between the data for forward and backward directions for different stroke velocities. The indentation depth was 2 mm and data were obtained from subject 4. As previously observed in Fig. 5.3, the normal forces were almost the same regardless of the change of stroke velocity. For the shear forces and the friction coefficients, the higher the stroke velocity, the larger the values for stroke distances greater than about 2 mm. Thus, for the backward direction, the previous explanation for the frictional behavior can be applied.

5.1.4 Images: Observation of Skin Stretch and Slip

A captured frame of image is shown in panel A of Fig. 5.6. This was from the frame number 1 of an image sequence in a typical stroke. In all the experimental trials, a stroke contained 80 frames. The frames recorded at the exact moment when the stroking began

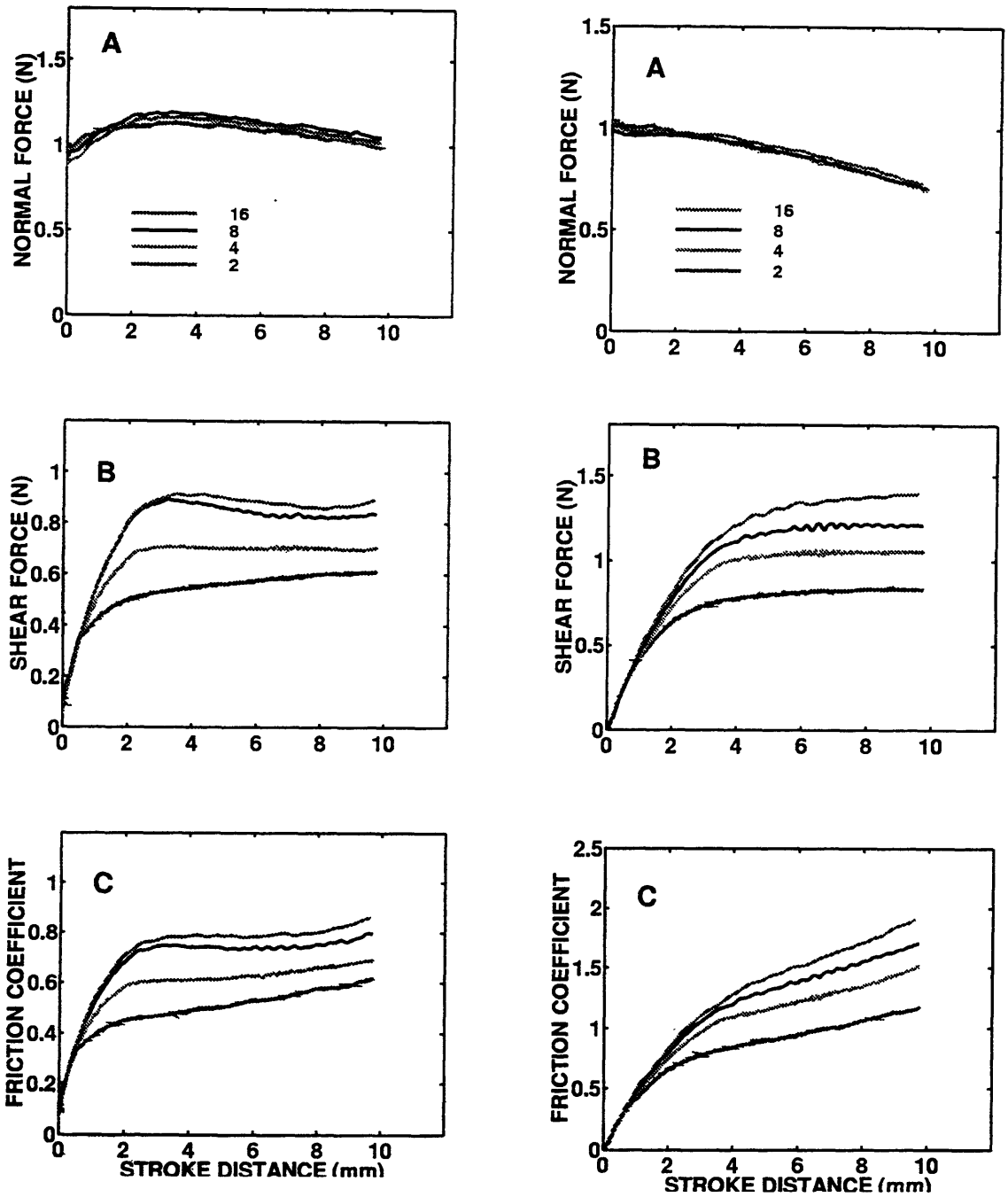

Figure 5. 5 The comparisons of data of different stroke velocities in the forward directions (left panels) and backward directions (right panels). Data were obtained from subject 4 with 2 mm indentation depth.

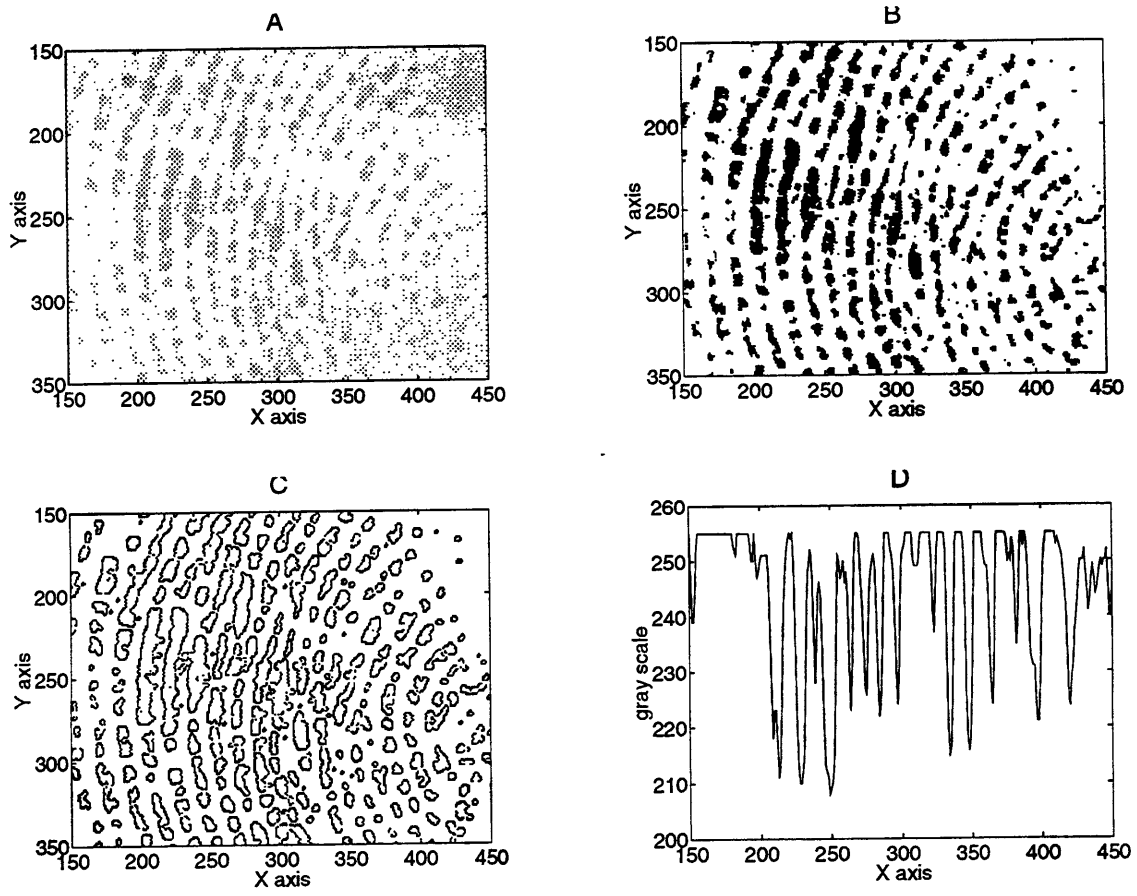

Figure 5. 6 A typical fingerpad image captured by the videomicroscopy system. Panel A shows the raw image; panel B shows the processed binary image; panel C shows the outline image; panel D shows the scanline image. The numbers on the both axes in panels A, B, and C as well as on the horizontal axis of panel D indicate pixel counts.

was numbered as 1, and the following frames were numbered consecutively. In panel A of Fig. 5.6, the dark pixels of the image represent the contact region with the fingerpad. Three kinds of image processing tools have been used to enhance the images, so that the motion of the finger ridges during stroking could be further analyzed. Panel B of Fig. 5.6 shows the binary image, which was obtained through simple thresholding. Panel C demonstrates the outline of the contact finger ridges. This was done through the

morphological erosion process. Panel D shows the scanline in one selected pixel line, which in this figure corresponds to pixel no. 240 on the y-axis in the other three panels. Using all these image processing tools, the global as well as local motions of the finger tissue were analyzed.

For all the image data shown later, the indentation depth was 1.5 mm, the stroke velocity was 4 mm/s, and the subject was number 2. The time interval between two successive image frames was 50 ms. Fig. 5.7 displays the motions of finger ridges. The upper two panels are from frame 15, and the lower two panels are from frame 20. Selected top left regions of the left panels are shown magnified in the right panels. From

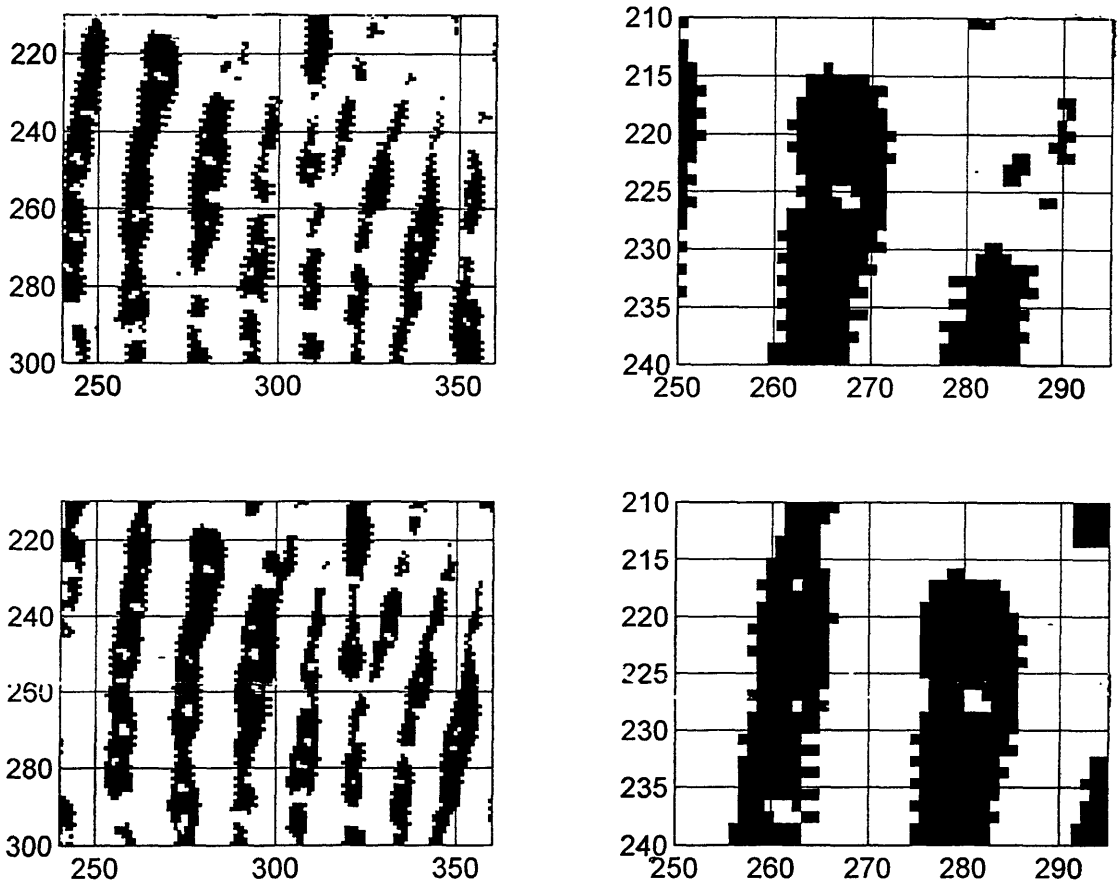

Figure 5. 7 The motion of the finger ridges. The upper panels belonged to frame 15 of a image sequence, and lower panels belonged to frame 20 of the same image sequence.

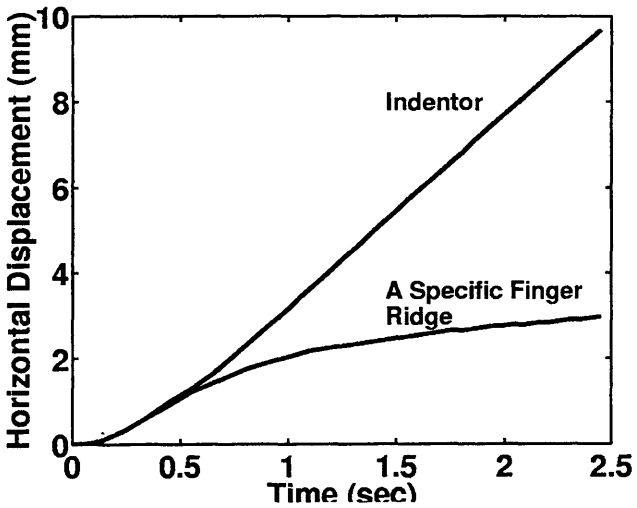

Figure 5. 8 The horizontal displacement of the indentor and of one selected finger ridge, observed from an image sequence.

the comparison of the upper and lower right panels, we found that the original finger ridge between horizontal pixels 260 to 270 (the finger ridge with a sweat hole in the center) moved to the place around pixel 280 with almost no change in shape. Thus, we could keep tracing the positions of finger ridges and obtain the displacement profile of finger ridges. Also, we marked a point on the glass plate indentor, so that we were able to also trace the displacement of the indentor frame by frame.

Figure 5.8 shows both the horizontal displacement of indentor and the horizontal displacement of one specific finger ridge in a sequence of images. The specific finger ridge was selected randomly from the center portion of the contact area. From this figure, we found that at the beginning of these two curves the displacements were the same, which implies no relative motion between that specific finger ridge and the indentor. After a distance of about 1.5 mm, they started to separate. The indentor kept moving with a constant velocity, while the finger ridge moved with a continuously decreasing velocity.

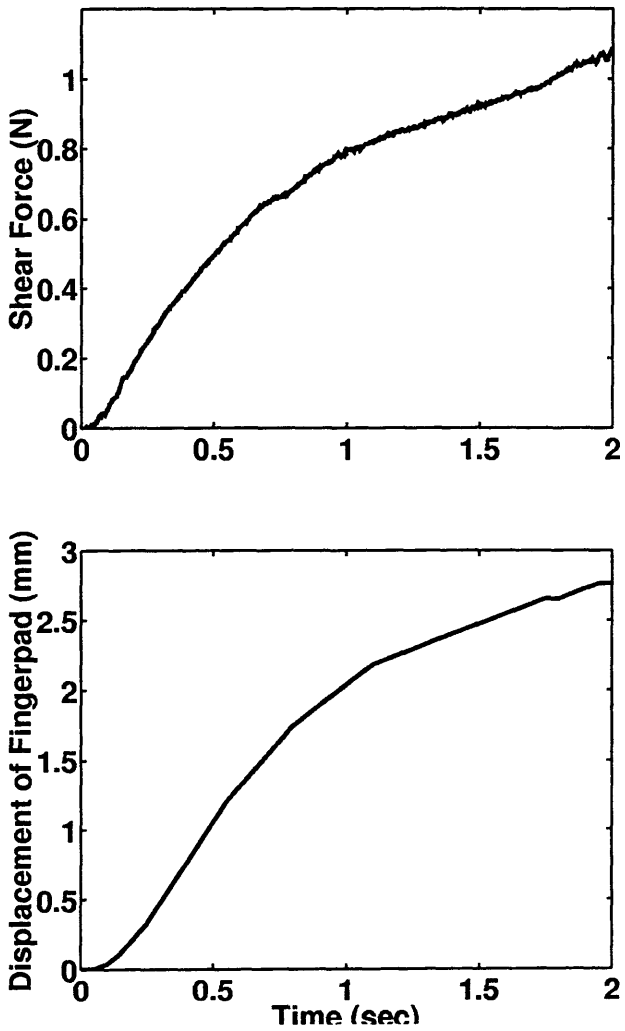

Figure 5. 9 The comparison of the shear force and the displacement of a selected finger ridge.

In our previously shown force data, the shear force had reached the steady state after stroking some distance, while in the case here, the stroke length might not have been long enough so that at the end the steady state still had not been reached. However, the finger ridge velocity did continue to reduce, and had the tendency to go to 0 velocity, the steady

state. Fig. 5.9 demonstrated the matched shear force data and the displacement of that finger ridge, both from the same experimental trial. It is clear that the trend of two curves are almost the same. Thus we can conclude that the magnitude of the shear force should be approximately proportional to the deformation of the fingerpad.

The previous figure of the displacements of the indentor and of the finger ridge demonstrates that there was a portion where no relative motion occurred between the indentor and the finger ridge. We are interested in when the slip started and whether the slip occurred faster in some parts of the contact area and slower in other parts. Fig. 5.10 shows the utilization of the morphological processing to compare two images and to detect the relative motion. Because the videomicroscopy system was stationary while the indentor was moving during the experiment, if there was no relative motion between the indentor and the fingerpad, which means both had the same velocity in the motion direction, we should see that the finger ridges moved the same amount of pixels as the indentor. Thus, using the recorded displacement of the indentor frame by frame, we could shift back the amount of pixels which the indentor moved between two frames, and superimpose the two images to see if relative motion occurred or not. In Fig. 5.10, the upper panels show frame 7 (the darker lines) superimposed over frame 6 (the lighter lines) without shifting. The right panels are only the zoomed-in versions of the left panels. From these upper panels it can be seen that the finger ridges moved by some pixels. The lower panels shows the shifting back of frame 7 by 3 pixels, the same amount by which the marked point in the glass plate moved between these two image frames. The two images mostly overlap to each other, so it is concluded that almost no relative motion

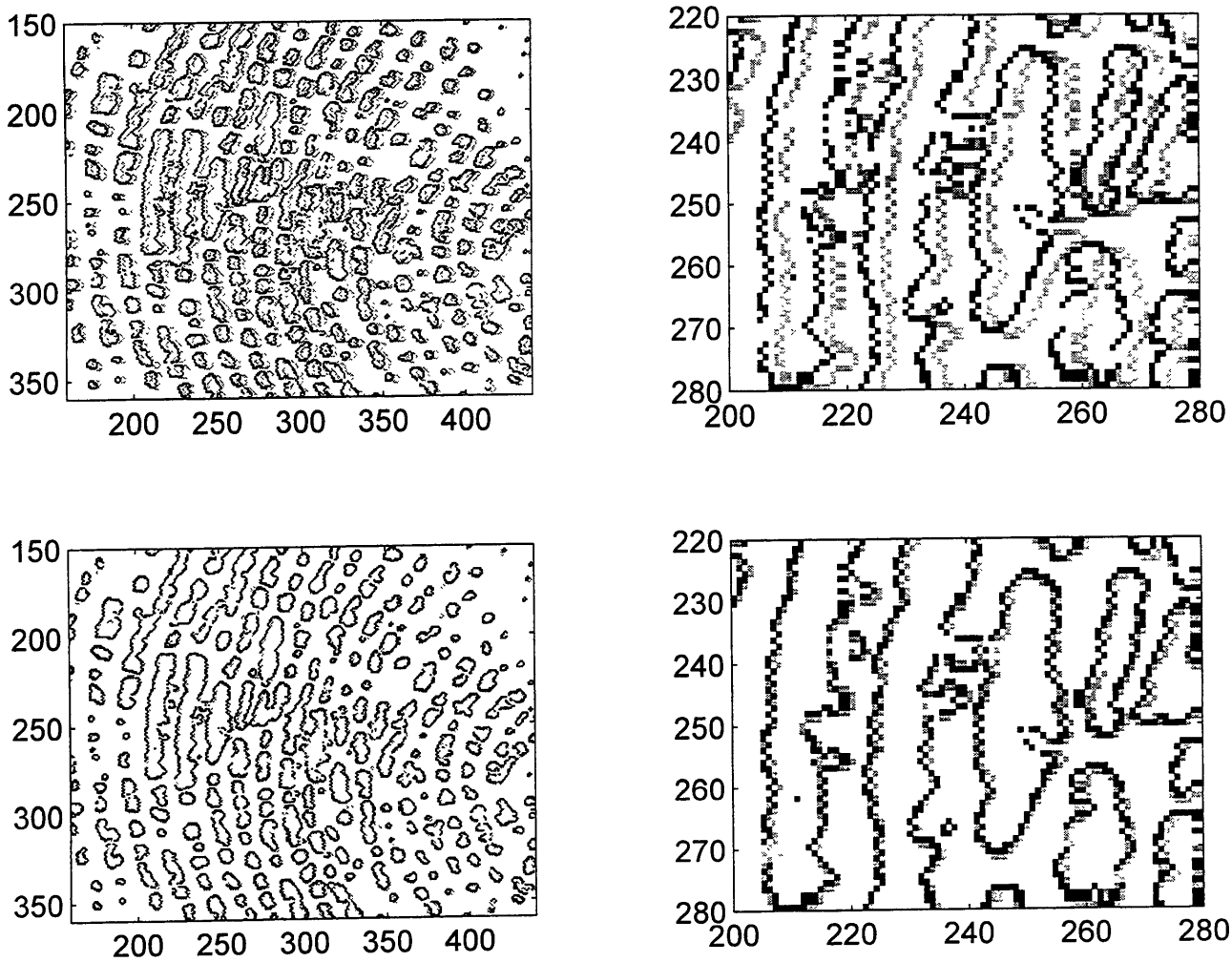

Figure 5. 10 The shifting back process of two successive images.

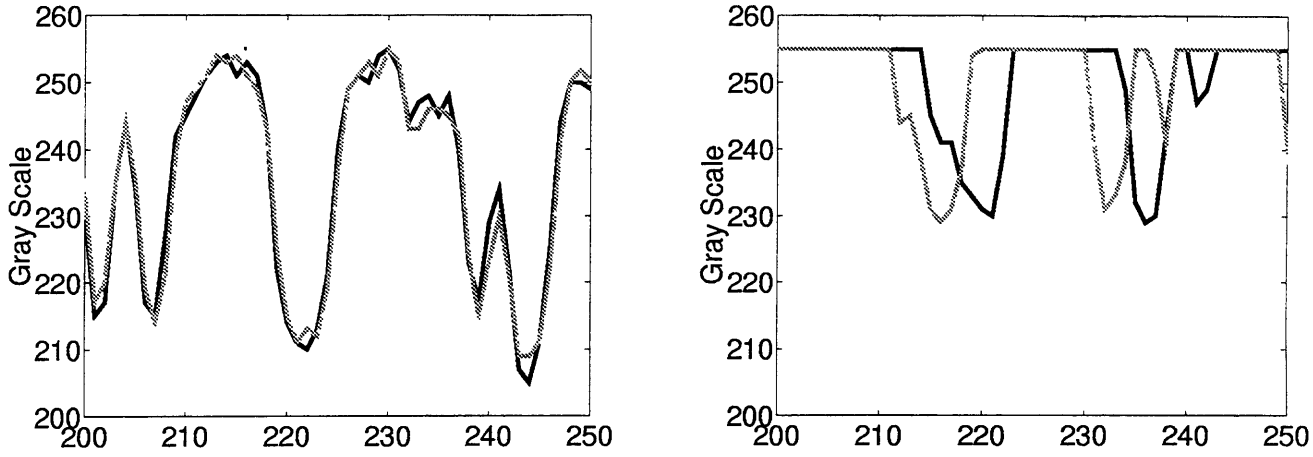

Figure 5. 11 The comparison of images by scanline process.

occurred between these two frames. It should be noticed that some parts of the figure do have one pixel difference between two images. However, because the indentor motion might be with a non-integer distance, say 3.368 pixels, while the image could only be shifted back an integer number of pixels, the outline may not overlap exactly even when no relative motion occurred.

The relative motion could also be inferred by using the scanline processing. Fig. 5.11 shows a small portion of scanlines. The left panel has two scanlines which belonged to frames 3 and 4, with shifting back of the scanline of frame 4; the right panel has two scanlines of frames 20 and 21, with shifting back of the scanline of frame 21. It shows that the scanlines of frames 3 and 4 almost overlap each other, while the scanlines of frames 20 and 21 have ridges with some pixels apart, even though we already shifted the amount of pixels by which the indentor moved. This implies that relative motion, or slip, occurred between the plate and the fingerpad. Although scanline processing is good for

detecting relative motion, we used the morphological processing to realize the behavior for the whole contact area because it used the full 2-dimensional data from the images.

Fig. 5.12 shows a series of images for perceiving the motion of the finger ridges. The first panel contains frame 1 only; the second panel contains frame 1 and frame 2 shifted by the amount of pixels the indentor moved between frames 1 and 2; the third panel contains frame 1, shifted frame 2, and frame 3 shifted by the amount of pixels the indentor moved between frames 1 and 3; and so forth for all the following panels. From the series of images, we observe that the peripheral portion of the image moved first (starting from frame H), and then the moving portion propagated from the peripheral portion toward the center portion, and finally the last panel containing images from frame 1 to frame 14, demonstrates slip over the entire contact area of the fingerpad. If we zoom in to a small portion around a peripheral region, as shown in Fig. 5.13, we can find that superimposing shifted images from frames 1 to 6 show no significant relative motion, while adding images from frame 1 to 7 indicate at least two pixels difference in the superimposed finger ridge images. Thus, we can infer that the slip in the peripheral region started at the frame 7. To figure out when the slip occurred totally through the whole contact area, we zoom in to the central region where the slip occurred last and plot in Fig. 5.14. The left panel shows the adding images from frame 1 to 10, where the center finger ridge (around pixel (200,230)) was likely stationary. The right panel shows the adding images from frame 1 to 11, and the center portion is more blurred and it implies all the finger ridges in this region moved some pixels, and therefore we can conclude that over the whole contact region slip occurred around frame 11.

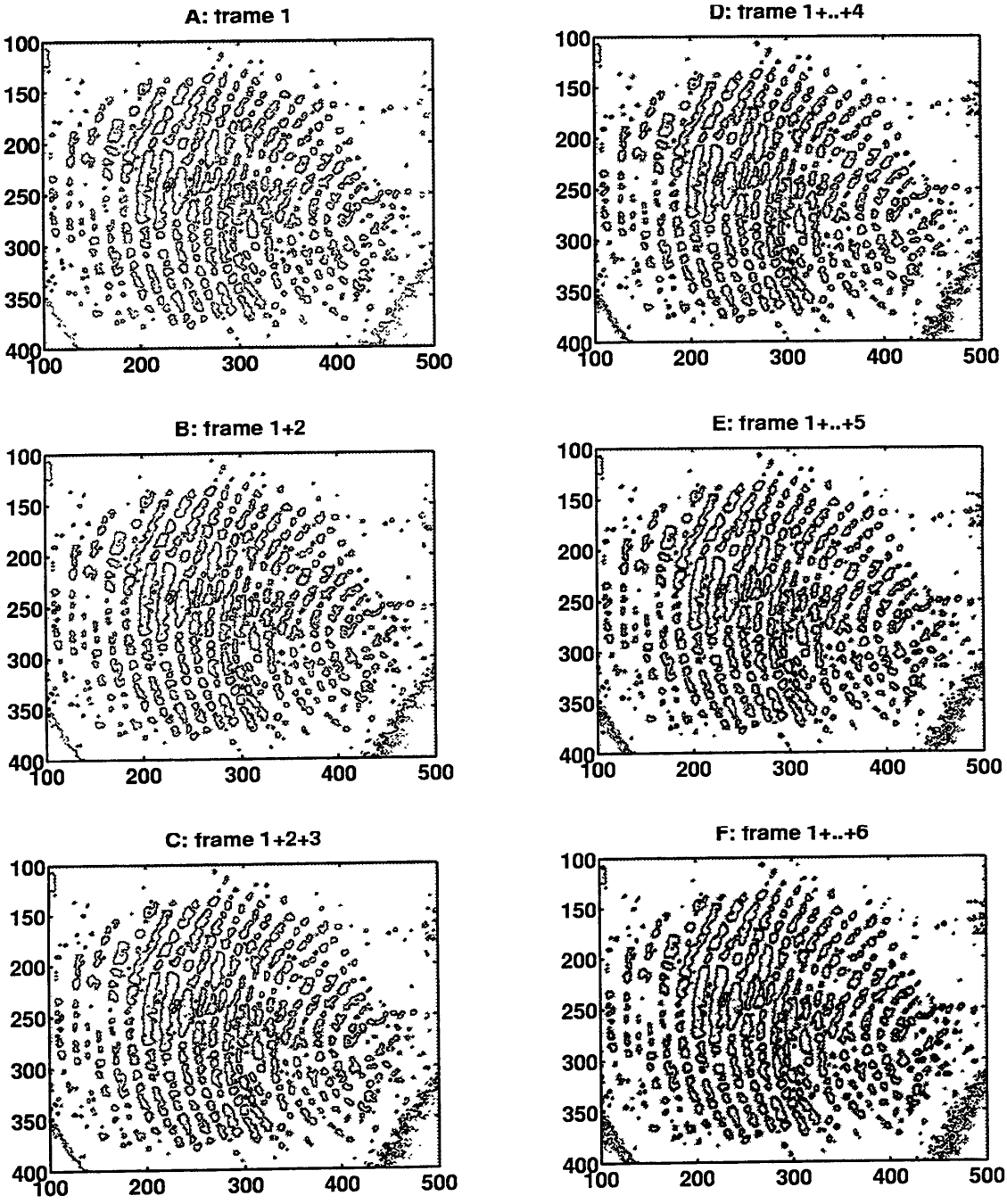

Figure 5. 12 A series of images to demonstrate the relative motion between the fingerpad and the indentor, from peripheral parts to center parts.

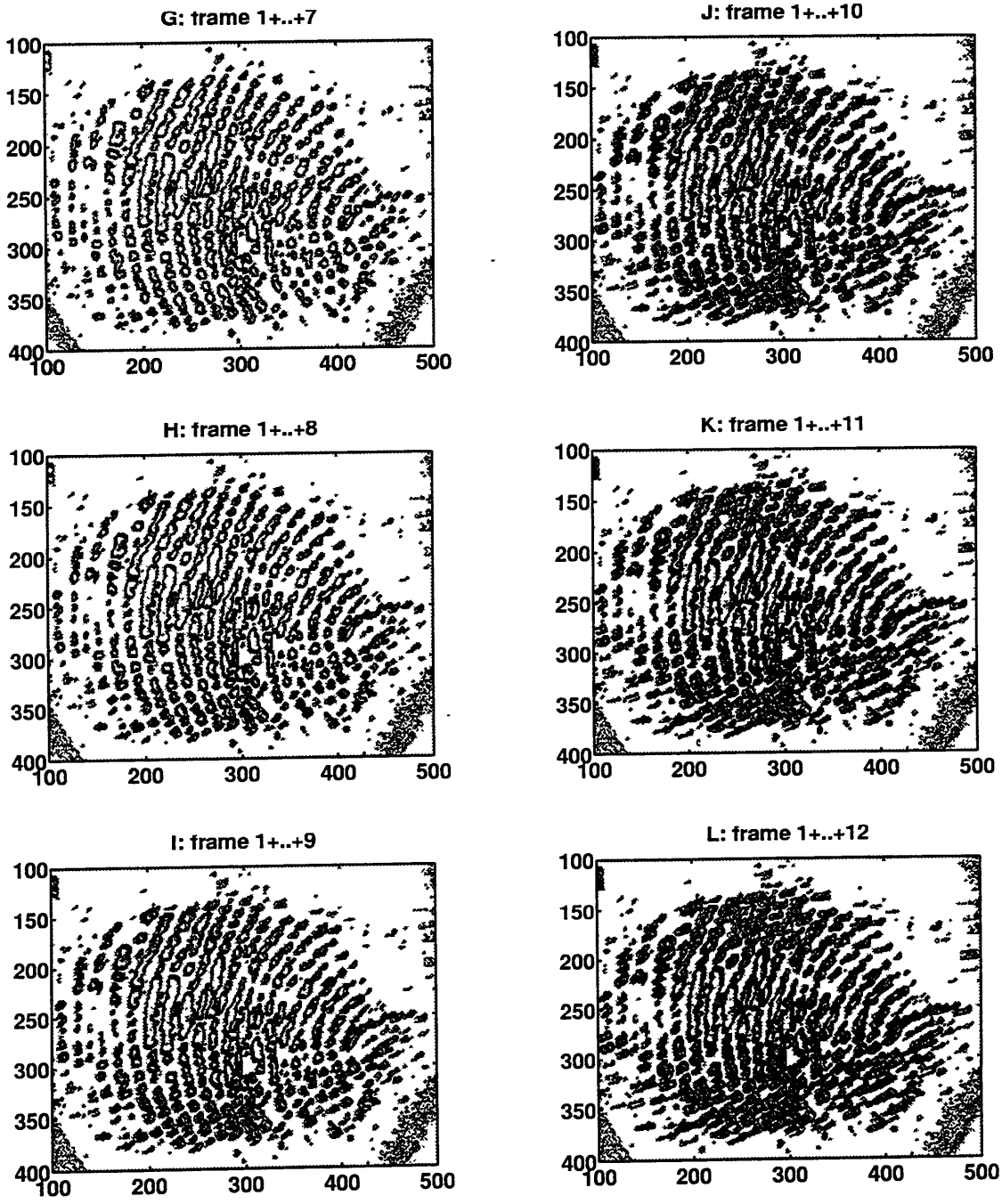

Figure 5. 12 (cont.)

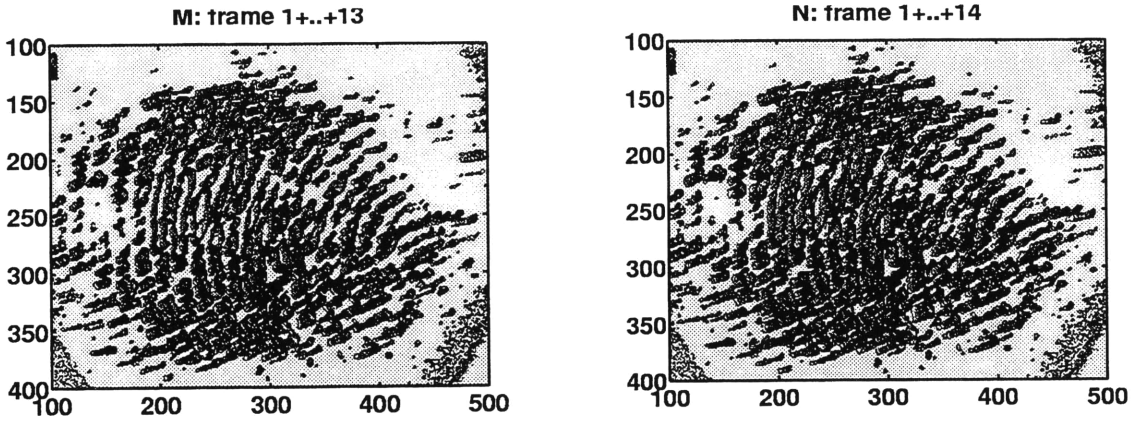

Figure 5. 12 (cont.)

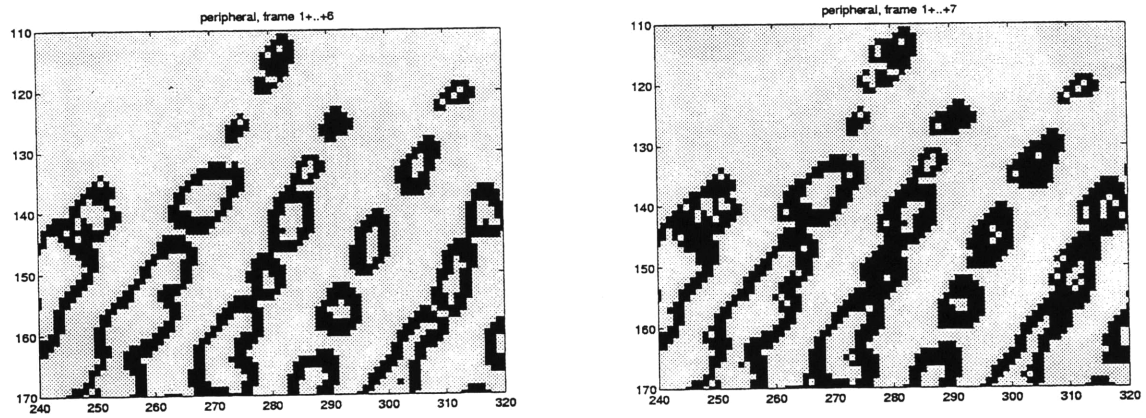

Figure 5. 13 The relative motion in one peripheral part.

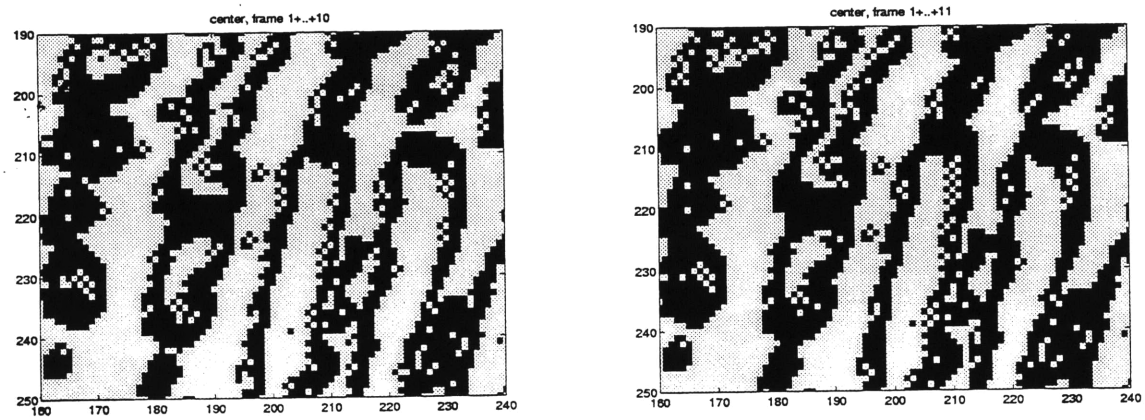

Figure 5. 14 The center part where the relative motion occurred latest.

Because the motion of each part of the fingerpad was not the same, we would like to understand the distribution of the displacement field in the contact area. To reach this goal, frame 1 and frame 49 were compared, as shown in Fig. 5.15. These two frames were 48 frames apart with 2.4 seconds time difference and about 9.6 mm of indentor movement. Clearly all the finger ridges moved to the right, and the region bounded by points marked A-I in the upper panel moved to the corresponding region in the lower panel. 25 points in this region were selected and as in Fig. 5.16 the displacements of all these points with respect to the original pixel coordinates of the points are plotted. This is a 3-D plot, the X,Y axes correspond to the axes in Fig. 5.15, and the Z axis represents the amount in pixel numbers the selected points moved. It is seen that the center of the Y axis has the highest value across this axis, which means the portion in the center of Y axis moved further than the two sides, i.e., the indentor stretched the fingerpad more in the center of Y axis. Also, we can find that as the X coordinate becomes smaller, the displacements of the points are larger. That is, the portion with smaller X coordinate was stretched more than the portion with larger X coordinate. This can be seen in Fig. 5.15 that the A-I enclosed region was squeezed to a thinner band, and thus finger ridges on the left moved more than ones on the right.

5.2 Polycarbonate Surface

5.2.1 Indentation Depth

Typical experimental force data (obtained from subject 2) for the polycarbonate plate is shown in Fig. 5.17. Panel A shows the approximate constancy of the indentation depth over a stroke distance of 10 mm. Panel B displays the normal force record at several indentation depths during stroking. Because of the complexity of these traces, compared

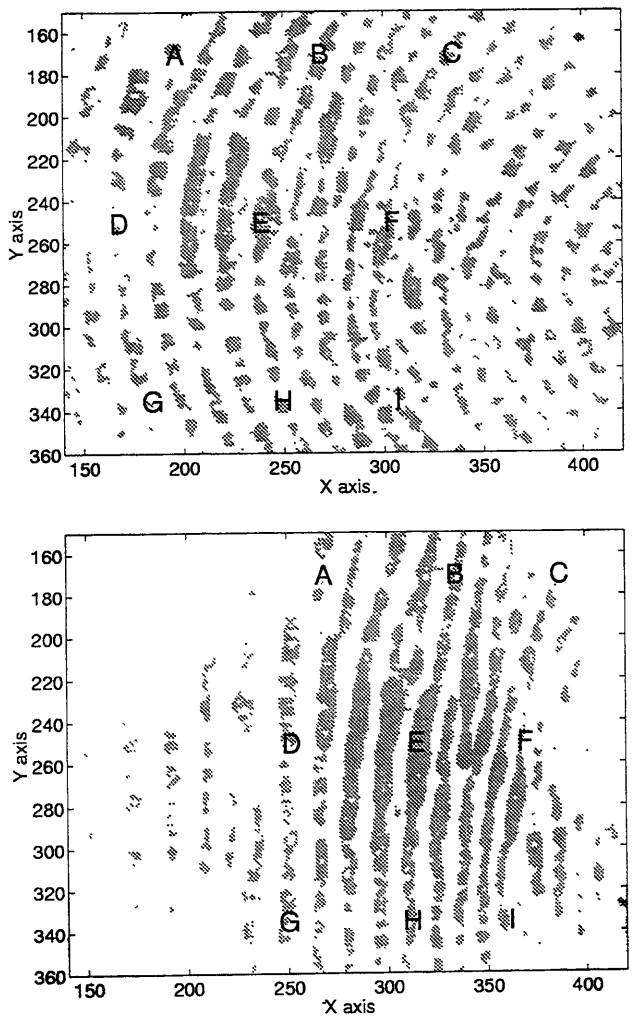

Figure 5. 15 The comparison of the images of frame 1 and frame 49.

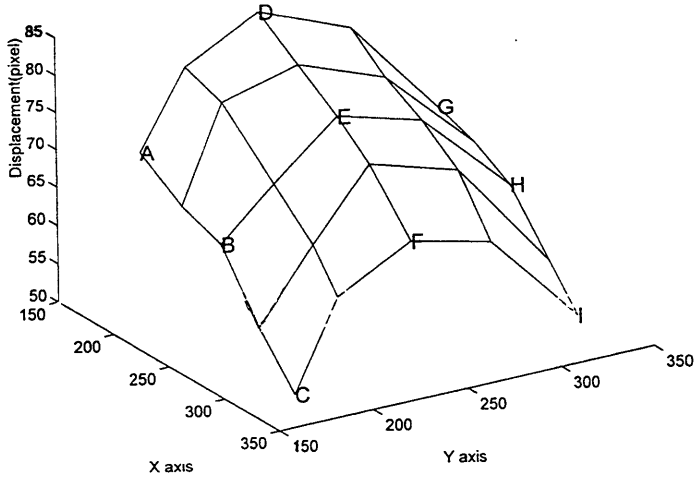

Figure 5. 16 The displacement field, from frame 1 to frame 49, of different points on the fingerpad.

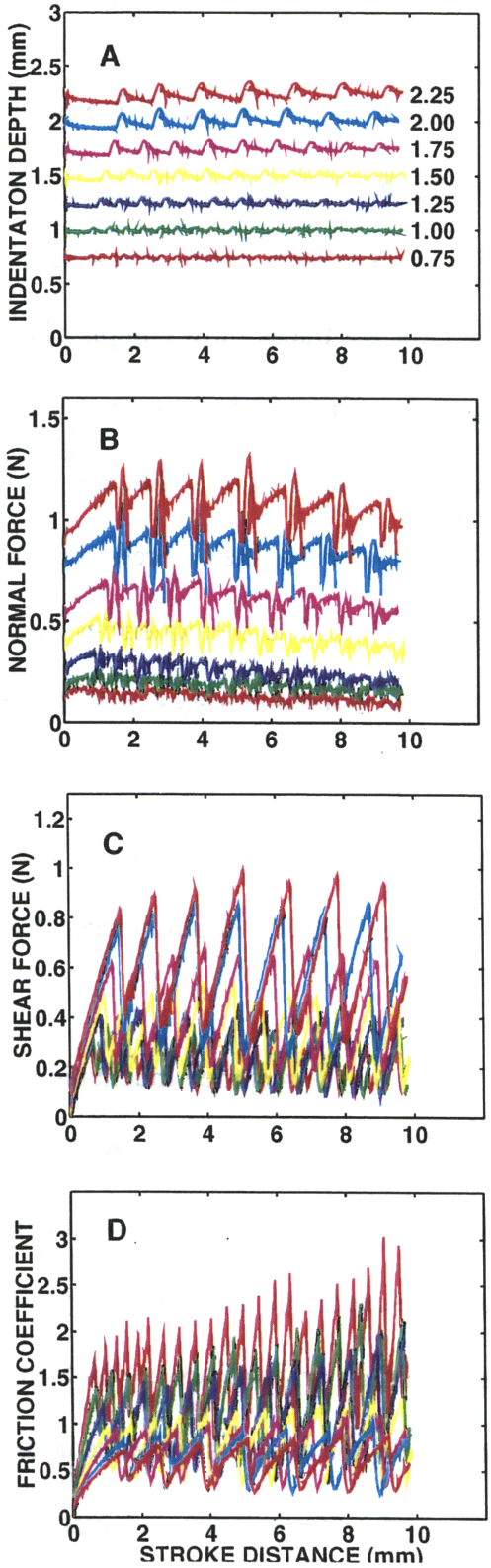

Figure 5. 17 The indentation depths, the normal forces, the shear forces, and the friction coefficients for different indentation depths on the fingerpad of subject 2, with 4 mm/s stroke velocity and forward stroke direction.

to those in Fig. 5.1, color figures are used here; for all the other data in the Appendix, only three different indentation depths are shown in the interest of clarity. As in Fig. 5.1 for glass, the stroke velocity for all these three depths was 4 mm/s. In contrast to the data obtained from the glass surface case, the traces show complex but periodic oscillations in both normal and shear force records, arising from the occurrence of stick-slip all through the stroke. Comparison of panels B and C shows that the normal forces had smaller amplitudes of oscillations than those for the shear forces, but the frequencies were the same for a given depth of indentation. These frequencies decreased as the depth of indentation increased. Panel D shows that the presence of stick-slip caused oscillations of the same frequency in the friction coefficient as that of the normal and shear forces, with the shape of the waves being triangular, similar to that of the shear force. The mean friction coefficient decreased as the indentation depth increased, just as in the case of the glass surface.

Fig. 5.18 captures a small portion of the recorded indentation depth, normal force, and shear force from Fig. 5.17, but is plotted with respect to time. The desired indentation depth here was 1.5 mm. In this figure, a few repeated cycles of stick-slip behavior can be easily seen in all three panels. The recorded indentation depth ranged from about 1.47 mm to 1.55 mm, implying a maximum error of about 4% from the desired value. The controlled value of the indentation depth was not as good as in the case of glass plate, but was still within a reasonable range of $\pm$ 50 μm in this indentation depth.

Let us trace through the curves starting from the point where the shear force (in the third panel) reached the maximum right before time at 8.1 sec. At this time point, relative

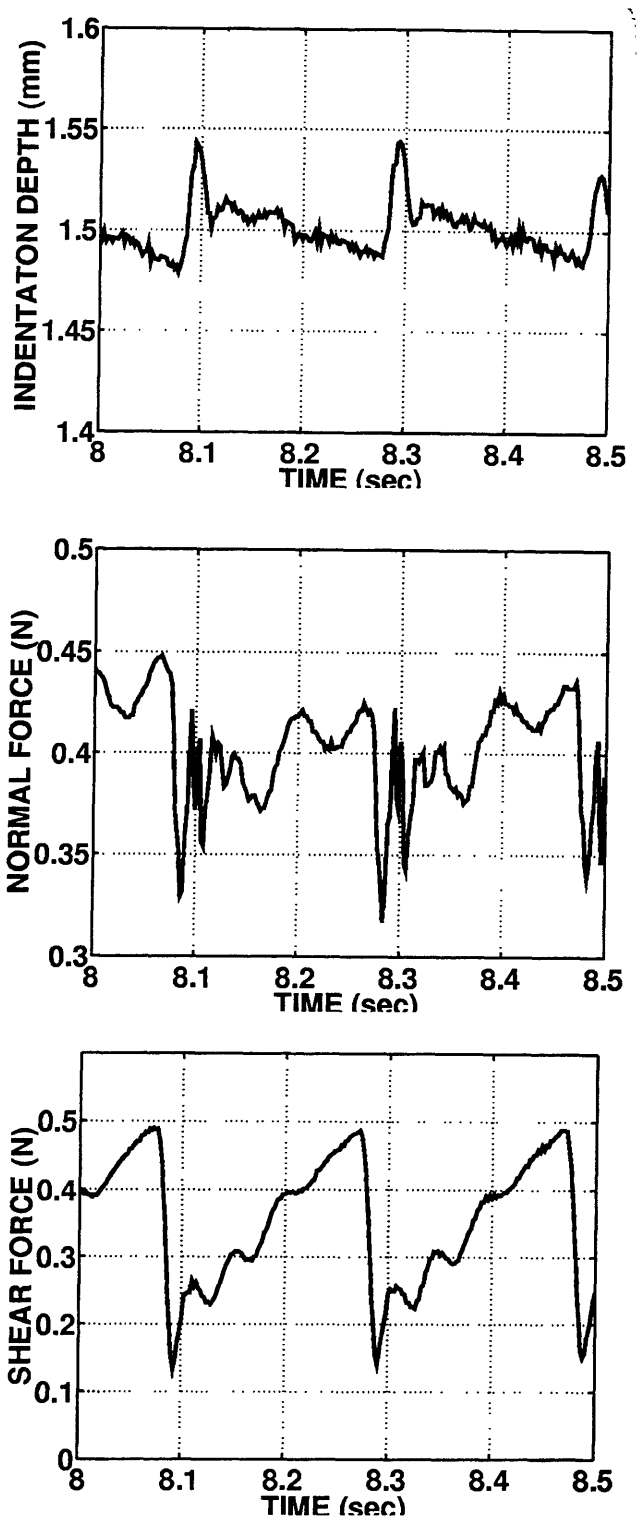

Figure 5. 18 The stick-slip behavior in a few cycles.

motion occurred between the polycarbonate indentor and the fingerpad. This maximum shear force was because the contact surfaces could not sustain any higher shear force and the two surfaces separated. The first panel shows that this time point corresponds to the minimum value of indentation depth. The normal force was not at its maximum value exactly at that time, but was relatively high and it can be observed that there was a slope change at that point. After this point, the normal force as well as shear force dropped down to the minimum in a very short period of time, smaller than 0.02 second, and the indentation depth grew to a maximum. The increase of the indentation depth was because before the slip occurred, the sticking behavior between the indentor and the fingerpad resisted the indentor from reaching the exact 1.5 mm depth for a period of time. Due to the integral control strategy, the previous error accumulated and once the slip occurred, where the resistant effect was not so strong, the indentation depth grew to an even higher value than the desired one. At this moment when relative motion occurred, the indentor kept moving forward while the finger tissue bounced back due to the stored elastic energy inside it. The sudden release of the system also caused the cantilever beams of the force sensor in both normal and shear directions to oscillate at their own natural frequency. Thus, the normal force vibrated with a higher frequency (compared to the stick-slip frequency) while the damping effect of the finger tissue in the normal direction also contributed to the change of the magnitude and the frequency of oscillation. The shear force oscillated with its natural frequency corresponding to its own of the cantilever sensor, while the value still increased gradually due to increase in friction. At the portion where the normal force increased again around 8.25 seconds (from about 8.23 to 8.27 seconds), the sticking behavior resumed and the shear force increased with a slightly

different slope. The indentation depth around here was close to 1.5 mm, implying better control than in other portions. There was a small drop in normal force (around 8.23 seconds) before the slip behavior repeated. This is still not clearly understood and it should be investigated in the future. After the shear force went up to the maximum again, the stick-slip cycle repeated itself again and again through the whole stroke length.

Two important parts of the stick-slip data are the stick-slip frequency and the stick-slip force magnitude. In this experiment, because the force data were periodic, the relationship between the indentation depth and the frequency, as well as the relationship between the stroke velocity and the frequency, were investigated. The first panel of Fig. 5.19 shows the peak values of shear forces for all five subjects at different indentation depths. The stroke velocity for the data in this plot was 4 mm/s. The peak values, as shown before, were maximum forces the contact surfaces could sustain without separation. This panel shows that as the indentation depths increased, the peak values of shear forces increased in an approximately linear behavior. The second panel of Fig. 5.19 shows a certain inverse power function relationship between stick-slip frequency and indentation depth. Another view point for this data is from that of the wave length. The stick-slip wave length, which is defined as the ratio of the stroke velocity to the stick-slip frequency, was the distance between two peak values of shear forces, or it could be regarded as the distance between two successive sticking locations on the polycarbonate plate. An approximately linear relationship between the indentation depth and the stick-slip wave length is shown in the third panel of Fig. 5.19.

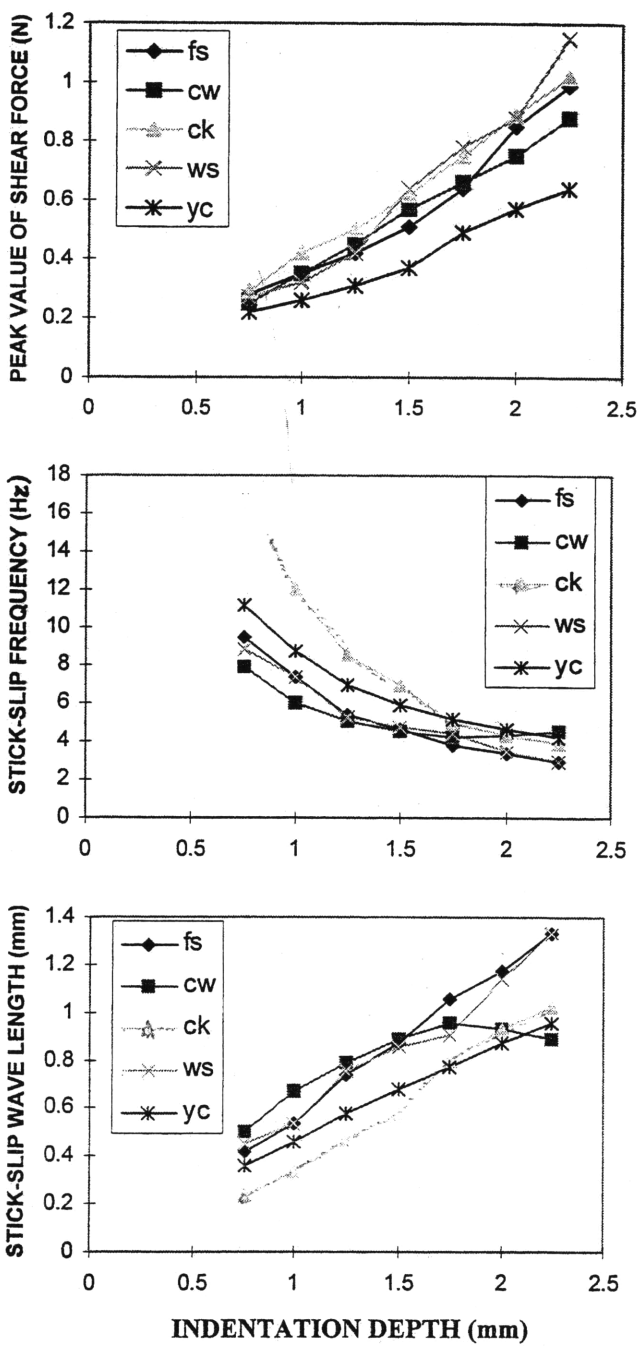

Figure 5. 19 The relationships between the indentation depths, and peak values of shear forces, the stick-slip frequencies, the stick-slip wave lengths, respectively, for the data from all 5 subjects.

The consistent relationship between the peak shear force and the indentation depth can be explained in terms of the deformation of the fingerpad. When the normal loading is larger, which means the indentation depth is larger, the contact region is bigger, and therefore larger shear force is needed to cause the separation between the fingerpad and the polycarbonate plate. Thus the higher indentation depths cause the corresponding peak values of shear forces to be higher. It has been shown earlier in the case of the glass plate that the shear modulus like properties of the fingerpad remained almost the same for different depths of finger tissues. In addition, panel C in Fig. 5.17 shows that the increasing slopes of all shear force curves were almost the same. Therefore, if the shear force grew to a higher value, it should take a longer time to reach that value. That is most likely to be the reason why the larger indentation depths resulted in larger wave lengths.

5.2.2 Stroke Velocity

The force records for various stroke velocities of the polycarbonate plate are shown in Fig. 5.20. The indentation depth in this case was 2 mm and the data were obtained from subject 1. Basically, it is not easy to distinguish the four curves in all three panels, which means that the values of four curves have almost the same magnitude. To better observe the data, in Fig. 5.21 we replot the normal and shear forces shifted in the y axis, but keep the scale of all the curves the same as in Fig. 5.20. It can be seen that both normal and shear forces behaved very similar to the data shown in the case of various indentation depths (Fig. 5.17), and the corresponding normal and shear forces with the same stroke velocity had exactly the same stick-slip frequency.

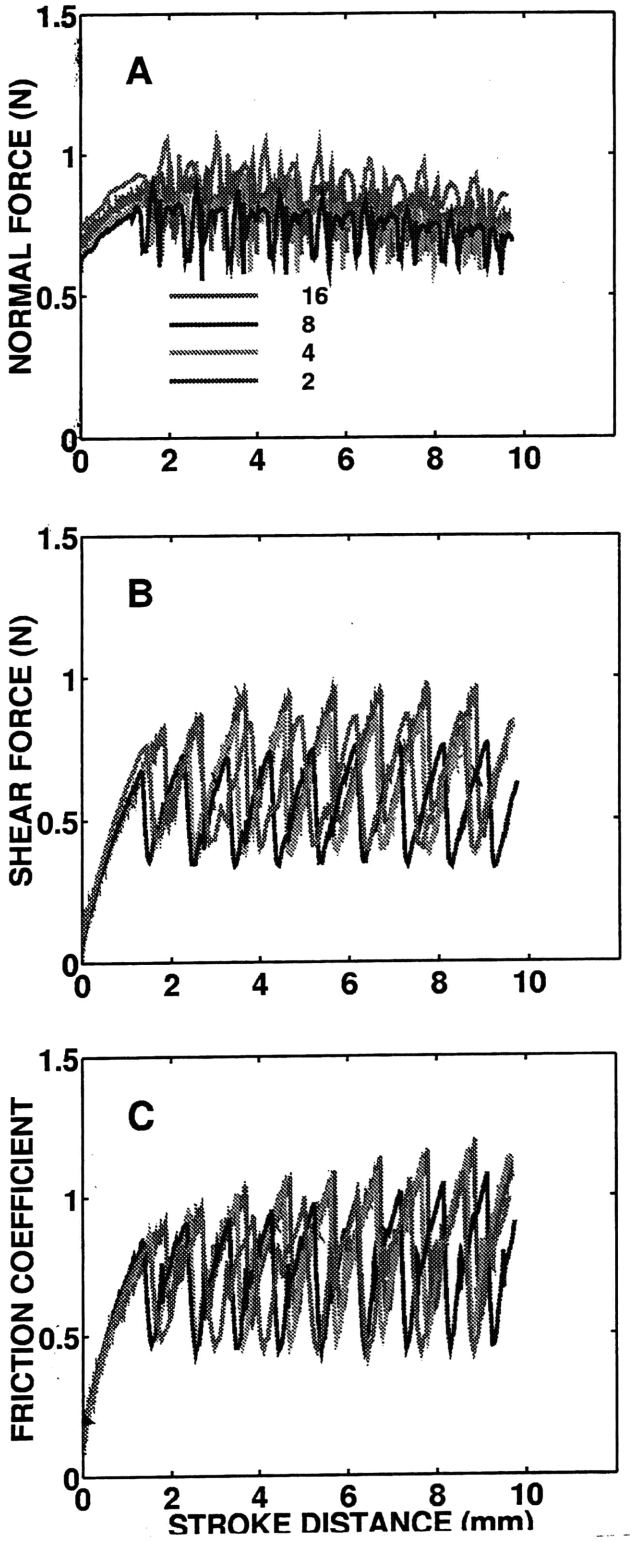

Figure 5. 20 The normal forces, the shear forces, and the friction coefficients for different stroke velocities on the fingerpad of subject 1, with 2 mm indentation depth and forward stroke direction.

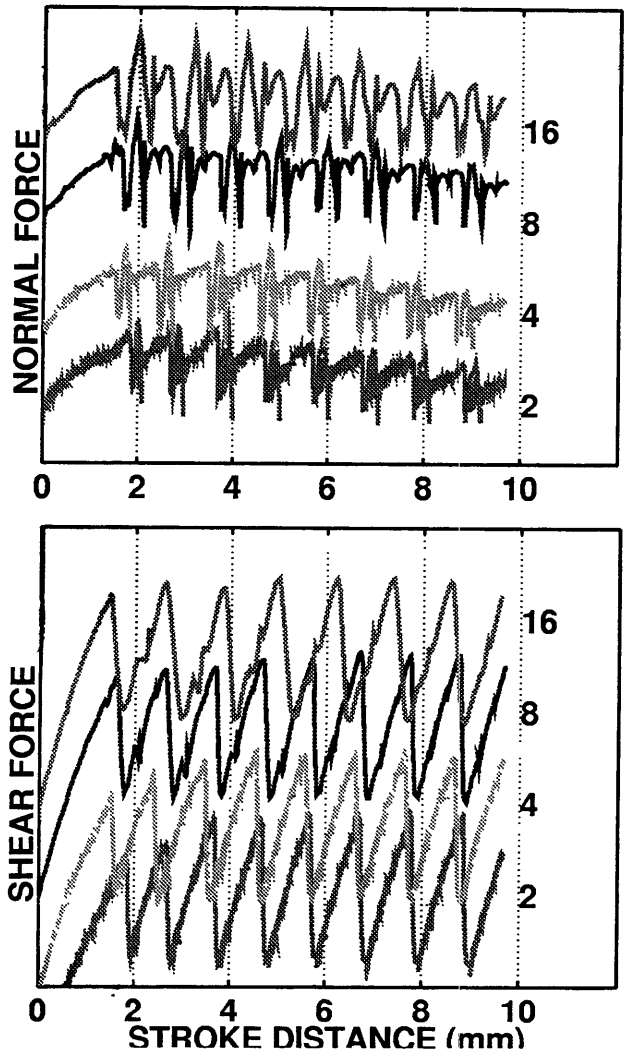

Figure 5. 21 The shifting data of Fig. 5.20.

For the comparison of the data for various stroke velocities, we should look at the details in Fig. 5.21. In the panel for the normal force, the basic trend for all four velocities was the same, but the data of higher stroke velocities had more jagged shapes and the larger oscillating amplitudes. This was because in the case of higher stroke velocities the

stimulator introduced more kinetic energy into the system, and the stick-slip induced natural frequency oscillations would have larger amplitude and the curve looks more jagged. In the panel for the shear force, the oscillating magnitudes of all four curves are quite close to each other, but if observed carefully it can be seen that the data for smaller stroke velocities had slightly larger magnitudes. Also, another obvious observation is that the distances between two shear force peak values, which has been defined previously as the wave length, were almost the same for all four velocities.

Fig. 5.22 shows the relationships between stroke velocity and peak values of shear forces, stick-slip frequencies, stick-slip wave length, respectively, for all five subjects. In the first panel, it is shown that the peak values of shear forces decayed a little for higher stroke velocities. This amount of decay was small compared to the average of peak values of shear forces for different stroke velocities. In the second panel, as the stroke velocities increased, stick-slip frequencies grew linearly. The proportional relationship between frequency and stroke velocity implies that the wave length, the ratio between stroke velocity and frequency, was invariant regardless of the change of stroke velocity. As shown in the third panel, the wave length was almost constant for different stroke velocities. The invariance of the wave length means that the distances between two sticking locations on the polycarbonate plate were always the same regardless of the change of the stroke velocities. This might imply that stick-slip behavior was a spatial phenomenon, but not a temporal phenomenon. The reasons for both slight decaying of peak value of shear force with increasing stroke velocity and the invariant stick-slip wave length still need to be investigated in the future.

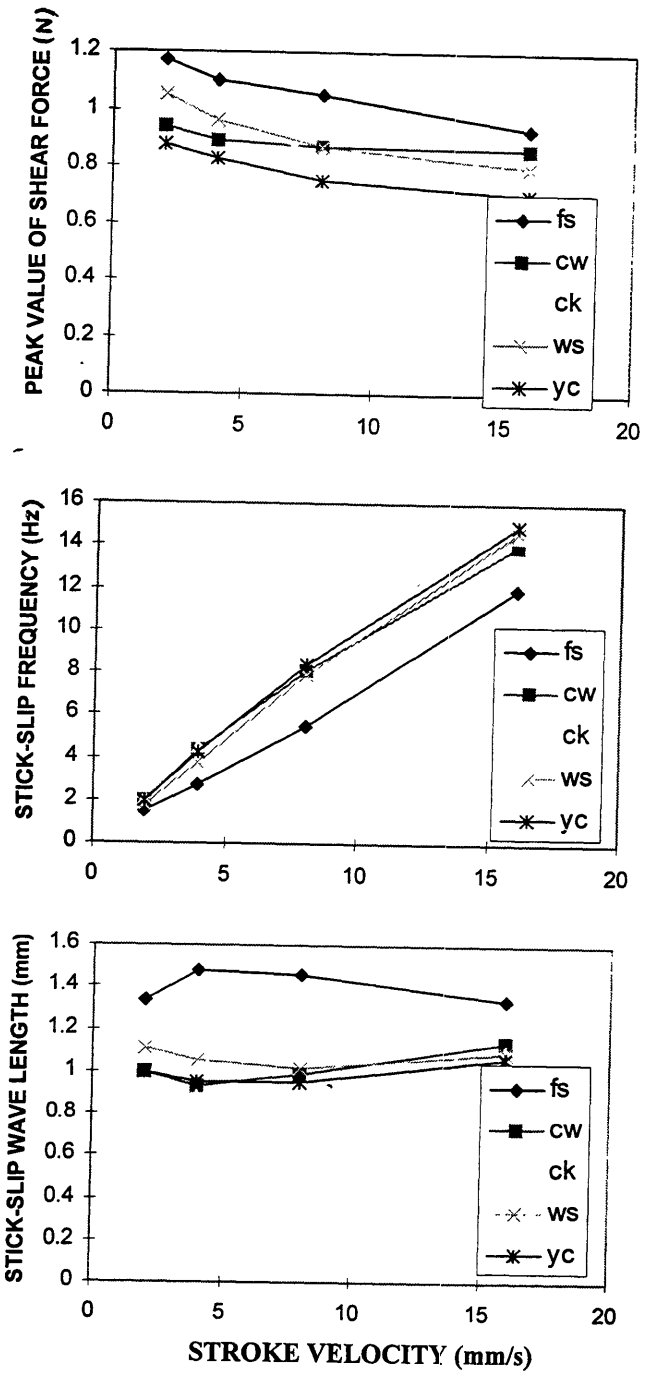

Figure 5. 22 The relationships between stroke velocity, and peak values of shear forces, the stick-slip frequencies, and the stick-slip wave lengths, respectively, for the data from all 5 subjects.

5.2.3 Images: Observation of Stick-Slip

Using the same image processing tools described before, we can also trace the motions of the polycarbonate indentor and the finger ridges frame by frame. Fig. 5.23 shows the displacement of the indentor and the displacement of one selected finger ridge in the center region. From this figure, we observe that at the beginning of the stroke, for about the first 0.5 second, the indentor and the finger ridge moved together at the same velocity. The same velocity means no relative motion occurred between two surfaces, just as in the case of the glass plate (Fig. 5.8). After a skin-stretching displacement of about 1 mm, the slip started to occur and both curves show the subsequent stick-slip occurrences. Looking carefully at the middle portions of both curves, we find that there were mainly two

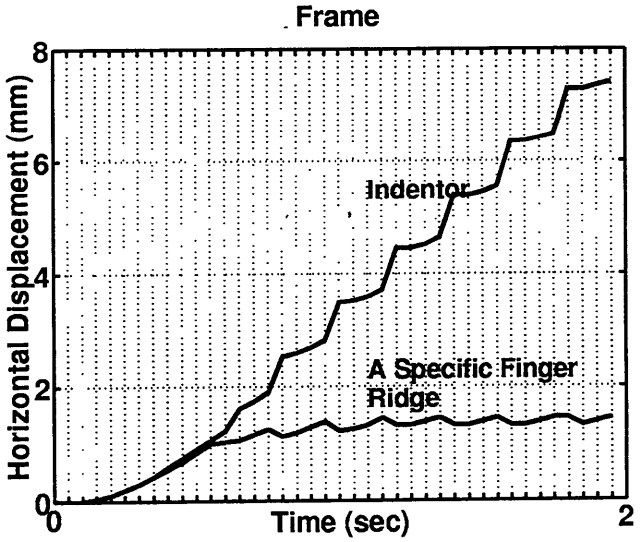

Figure 5. 23 The horizontal displacements of the indentor and of one selected finger ridge, observed from an image sequence.

different slopes for the displacement of the indentor, and also two different slopes for the displacement of the finger ridge. The slopes of these curves represent the moving velocities of the indentor and the finger ridge. Tracing through the curve for the displacement of the finger ridge, we find that the finger ridge moved forward in a period of time, and then moved backward by about the same distance in a shorter period of time. The slope of the moving forward part is almost the same as the slope in the curve of the displacement of the indentor during that period of time. The same slope means both contact objects had the same velocity, i.e., no relative motion. This period of time is the so-called stick portion of a stick-slip phenomenon. After this portion, the indentor moved forward with a lower velocity, while the finger ridge bounced back due to the stored elastic energy inside the fingerpad. This period of time is relatively short and is the slip portion of the stick-slip phenomenon.

A sequence of images for the stick-slip behavior is shown in Fig. 5.24. The four panels are from frames 23, 24, 25, 26, corresponding to the times 1.1, 1.15, 1.2, 1.25 seconds, of the experimental trial of Fig. 5.23. The black spot in the upper left side of the first panel was the marker on the polycarbonate indentor. All the other black spots are the contact finger ridges. From frame 23 to frame 24, the marker moved to the right, and the finger ridge in the lower part also moved to the right. From frame 24 to frame 25, the indentor moved several pixels to the right side, while the finger ridge bounced back a few pixels. From frame 25 to frame 26, the indentor moved forward again and so did the finger ridge. Thus one cycle of the stick-slip phenomenon was completed and another cycle followed immediately.

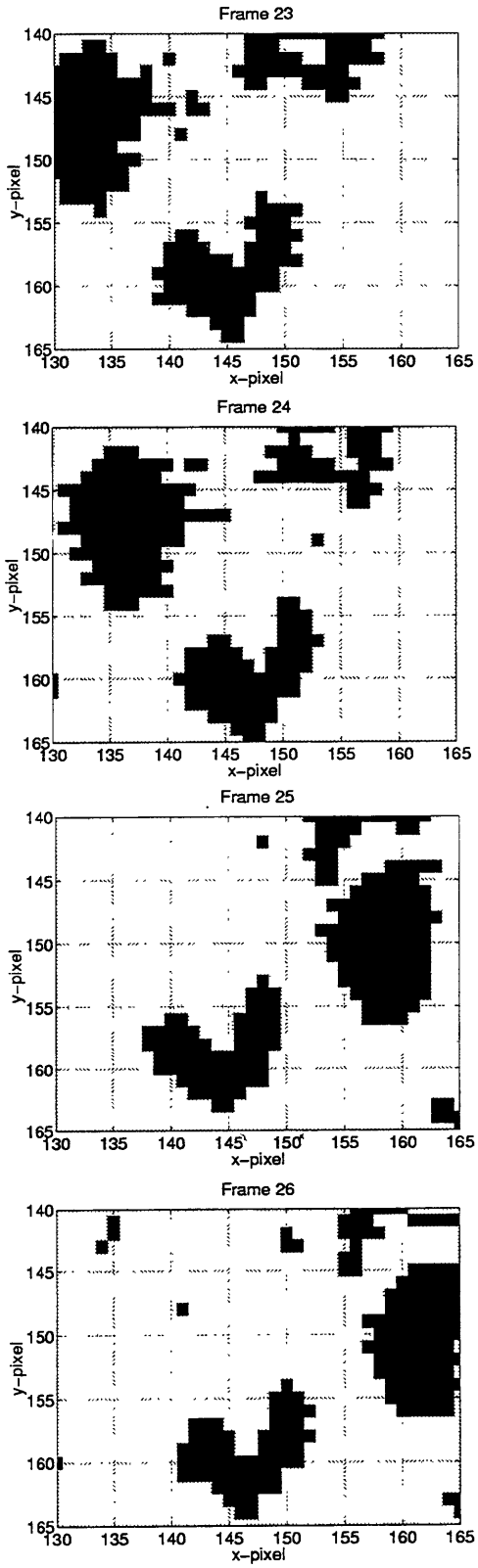

Figure 5. 24 Demonstration of stick-slip-stick from the observation of the motion of the indentor and a finger ridge.

Fig. 5.25 shows the corresponding shear force and the displacement of a finger ridge. From this figure, we find that the frequency for the shear force periodic oscillation was the same the frequency of the stick-slip displacement. The magnitude, however, was not exactly proportional between these two quantities. Especially for the first peak of the shear force, no correlated peak is found in the displacement of the finger ridge. One important comment about the image data is about the very short time for the drop of shear force when slip occurred. According to previous description, the time scale from a local

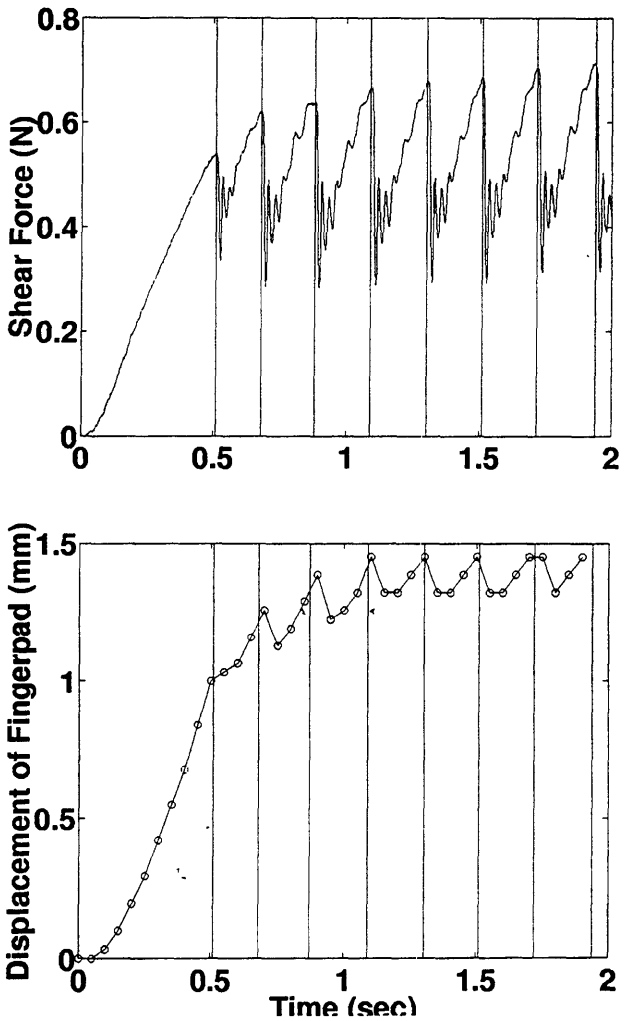

Figure 5. 25 The comparison of the shear force and the displacement of a selected finger ridge.

maximum shear force to a local minimum shear force was about 0.02 second, or 20 ms. However, the sampling rate of images was 50 ms, which was too large to capture the detailed phenomenon of the slip. The lighter lines in Fig. 5.26 show our speculation about the actual displacement of a finger ridge relative to the data obtained from videomicroscopy, shown as a darker line. This kind of uncertainty was due to the limitations of the videomicroscopy system.

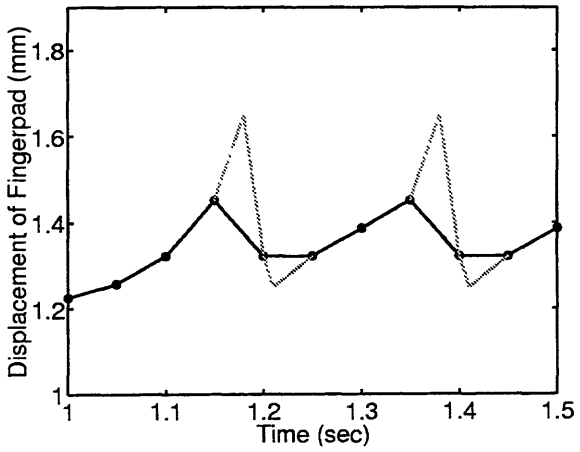

Figure 5. 26 A possibility of the displacement of the fingerpad.

5.3 Acrylic Surface

The data for the acrylic indentor with three different indentation depths are shown in Fig. 5.27. The stroke velocity of this experiment was 4 mm/s and the subject was no. 3. Compared to the data shown for the polycarbonate indentor (Fig. 5.17), the patterns for all four panels were all about the same. The data for all the other subjects shown in Appendix also ascertained this similarity. Therefore, the discussion in the next chapter will only focus on the data from the polycarbonate plate for stick-slip behavior.

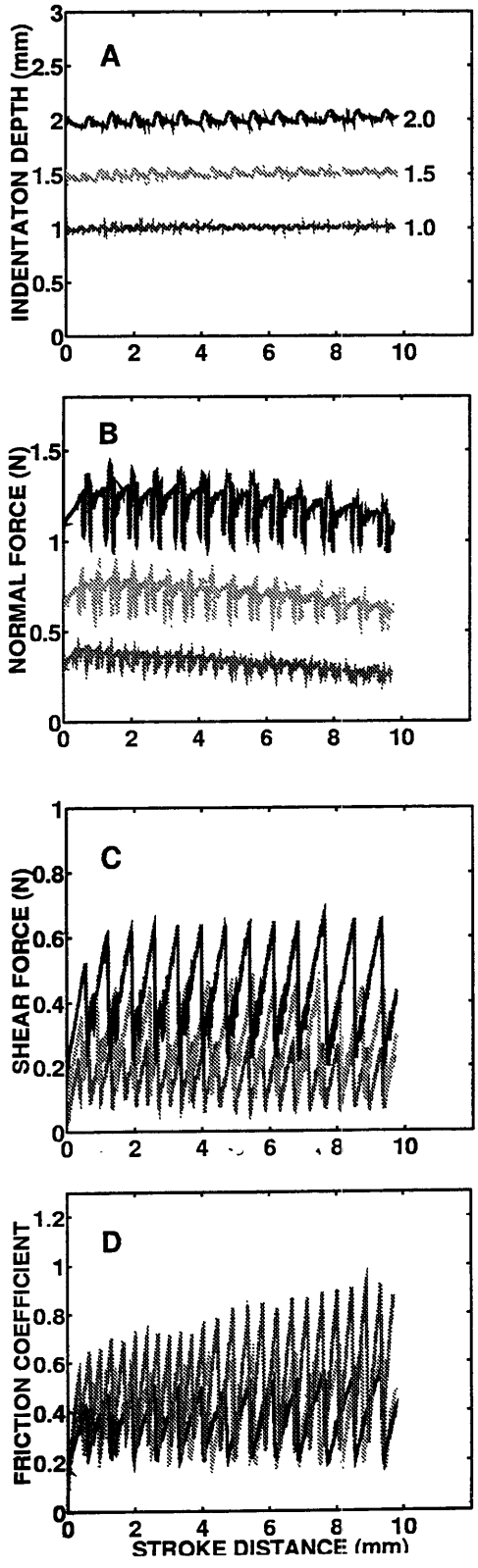

Figure 5. 27 The indentation depths, the normal forces, the shear forces, and the friction coefficients for different indentation depths on the fingerpad of subject 3, with 4 mm/s stroke velocity and forward stroke direction.

Chapter 6

Discussion

6.1 Three Frictional Factors in the Human Fingerpad

The theory of friction can be used to interpret the results in more detail both for the cases of the glass plate and the polycarbonate plate. As described in the introduction, there are three major components that contribute to the frictional behavior: asperity deformation, adhesion, and plowing. In our experiment, because the stimulus surface is smooth and the stroke velocity is small compared to the typical velocity that occurs in situations such as abrasion in grinding machines, plowing effect is not apparent. Therefore, the influence of plowing is neglected and only deformation as well as adhesion effects are considered. Asperity deformation depends mainly on the mechanical properties of contacting materials -- the surface properties of both materials such as roughness, and the bulk properties such as moduli. As shown before (Fig. 4.8), the peak-to-valley heights, one of the roughness indicators, for glass and polycarbonate plates were about 70 nm and 130 nm, respectively. Since these heights are about 1/1000 in scale compared to the approximate height of human finger ridges, which is in the range of around 100 microns, the roughness difference between glass and polycarbonate was quite small. Therefore, we expect that roughness of the indentor surface did not have a strong influence on the frictional behavior of the human fingerpad. It is also obvious that the

bulk modulus of the human fingerpad is much smaller than that of the glass plate and the polycarbonate plate, that is, the fingerpad is considerably more deformable. For the effect of the asperity deformation to be significant, the fingerpad should dominate the data from both in the glass and the polycarbonate cases. Then, when the fingerpad in both cases was of the same subject, it should have the same effect in the results for the two cases. Therefore, the radically different behaviors observed were perhaps not because of the effect of the mechanical properties, but due to distinctly different properties in adhesion.

6.2 Adhesion -- Junction Forming and Junction Breaking

Adhesion is the effect of junctions between two surfaces while in contact. This effect can be separated into two parts: junction forming and junction breaking. When two surfaces contact each other, the normal force is equal to the contact force between them. As the normal force is larger, the true contact area between surfaces is larger. Junction forming then occurred in the contact region and contribute to adhesion between the two surfaces. The adhesion phenomenon between the fingerpad and the indentors can be easily identified by pulling the finger apart from the indentors, and adhesion force is felt by the fingerpad. The junctions between two surfaces can sustain the force in the shear direction and junction shear strength is influenced by the surface characteristics in term of physical and chemical properties of both materials. The normal force acting on the surfaces affects the number of junctions formed. Junction breaking has a different mechanism from junction forming. It is basically a cutting or tearing process to destroy junctions. When the local shear stress is larger than the junction shear strength, the junction breaks. From a global view, if relative motion occurs between two surfaces, it implies that the junctions cannot sustain the applied force anymore, and they have to

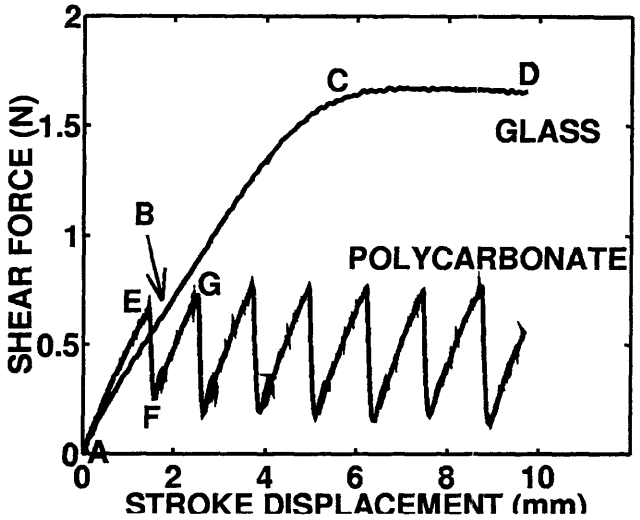

Figure 6. 1 The comparison of the shear forces in the case of the glass surface and in the case of the polycarbonate surface.

break apart. This statement also infers that the more the junctions are, the larger the shear force can be sustained. That is, the number of junctions decide the largest shear force which can be transmitted from one surface to the other.

One of the data comparisons between the shear forces in the case of the polycarbonate plate and that of the glass plate is shown in Fig. 6.1. The two curves of this plot had the same indentation depth, stroke velocity, and subject, but only the indentors were different. It can be seen that although the glass plate had a smoother curve, it had a higher shear force at the end of the stroke. The question here is: why is it that the shear force in the case of the glass plate could increase to a quite high value very smoothly without any drops, while in the case of the polycarbonate plate even at a relatively low value of shear force, the periodic stick-slip behavior is encountered. This is intuitively not obvious, because when we stroke surfaces in our daily life, the smooth feeling may indicate low friction, while if sometimes the stick-slip phenomenon happens, the surface should be very 'sticky' so that we cannot smoothly stroke across the surface. To resolve this

question, we propose the adhesion effect as the main reason for the difference between the results in the cases of the glass plate and the polycarbonate plate. Therefore, some predictions about junction forming rate, junction breaking rate, and number of junctions, are proposed in order to get reasonable explanations of the data.

6.2.1 Glass Surface

We can divide the data from a single stroke between the glass surface and the fingerpad, shown as the smooth curve in Fig. 6.1, into three stages: no relative motion (region A-B in Fig. 6.1), relative motion with continuously growing shear force (region B-C), and relative motion in the steady state (region C-D). Proposed junction forming rate and junction breaking rate curves with respect to the shear force are plotted in Fig. 6.2. The junction forming rate is influenced by the surface characteristics and the normal force, so it is supposed to be independent of the shear force, as the constant dashed curve shown in Fig. 6.2. The junction breaking rate, the solid curve in Fig. 6.2, however, is related to the shear force. A threshold shear force value is proposed for an abrupt change

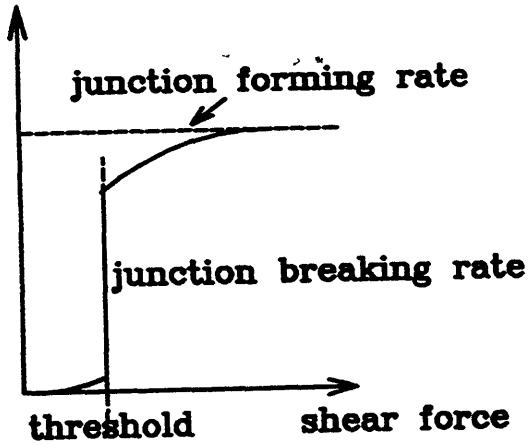

Figure 6. 2 The proposed curves for the junction forming rate and the junction breaking rate with respect to shear force in the case of the glass plate.

breaking rate. Below this threshold, the breaking rate is relatively small, while across this threshold value of shear force, the breaking rate increases suddenly. Above this threshold, the breaking rate increases gradually with the increase of shear force, and saturates at a value equal to the value of junction forming rate. This threshold shear force value is a function of the junction strength and the number of junctions. That is, when the shear force is high enough to overcome the resistance of the junction strength over all junctions, the possibility of junction breaking rapidly becomes higher. When the shear force is even larger, this possibility grows gradually with increasing shear force. Another hypothesis we propose for the glass case is that the junction forming rate is mostly larger than the junction breaking rate, and that these two rates are equal for a high enough shear force.

As mentioned before, these junctions transmit the shear force between two surfaces. In an experimental trial, some junctions had already formed during indentation and hold, right before the process of stroking. When the controlled indentor started to move, these junctions were still strong enough to prevent from breaking, that is, the junction strength was enough to resist the external shear force acting on these junctions. The external shear force on the junctions was the transmitting force between the fingerpad and the indentor, which was equal to the elastic force inside the fingerpad when this fingerpad was pulled to one side. Because the junctions were mostly not broken, these two surfaces moved in the same velocity without relative motion. This was the first stage of a stroke (A-B in Fig. 6.1). As long as no relative motion occurred between two surfaces, the fingerpad was stretched by the same distance as the movement of the indentor, and therefore the elastic force in the fingerpad grew accordingly. When this elastic force, which was the same as the shear force transmitted by junctions, grew to the shear force threshold value, the

junction breaking rate increased suddenly. Because the forming rate was still larger than the breaking rate, the total number of junctions still increased. However, the net increasing rate of junctions, the forming rate minus the breaking rate, was smaller than before. During this time, the indentor was still controlled to move in a constant velocity. If the fingerpad skin in contact with the plate were to move at this same velocity, i.e., no relative motion, then the increasing rate of the elastic force inside the fingerpad should be the same as before. However, those junctions could not support this increased elastic force, so the fingerpad could not be stretched at the same velocity as the indentor. Therefore relative motion occurred at this moment (at B in Fig. 6.1). Because the net number of junctions still increased, the shear force which could be transmitted through junctions still increased, and the fingerpad was continuously stretched with slower velocity (as Fig. 5.8). This was the second stage of this stroking process (B-C in Fig. 6.1), and junction forming and breaking of this stage are shown schematically in Fig. 6.3. Finally, at point C in Fig. 6.1, the junction forming rate was equal to the junction breaking rate, so that the number of junctions remained almost a constant. Thus at this third stage (C-D in Fig. 6.1), the steady state in shear force was reached.

6.2.2 Polycarbonate Surface

For the case of the polycarbonate plate, the proposed curves for the junction forming rate and the junction breaking rate with respect to the shear force are shown in Fig. 6.4. The only difference with respect to the curves for the case of the glass plate is that the junction forming rate is lower, so that above the threshold shear force value, the breaking rate jumps up over the forming rate, and thus the net number of junctions decreases.

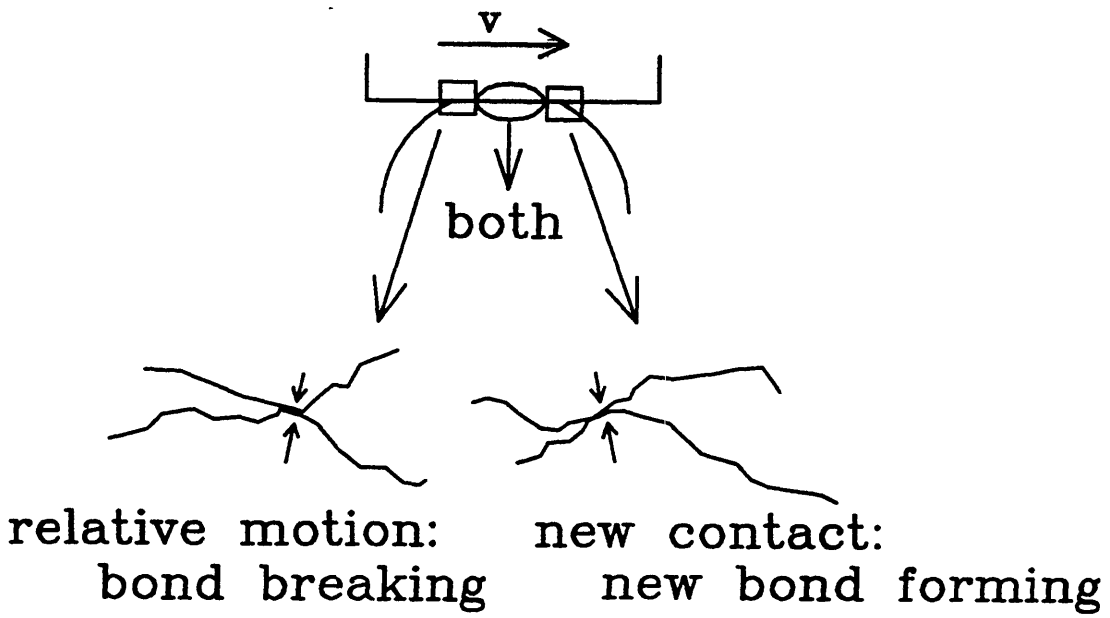

Figure 6. 3 The conceptual plot of the junction forming and the junction breaking.

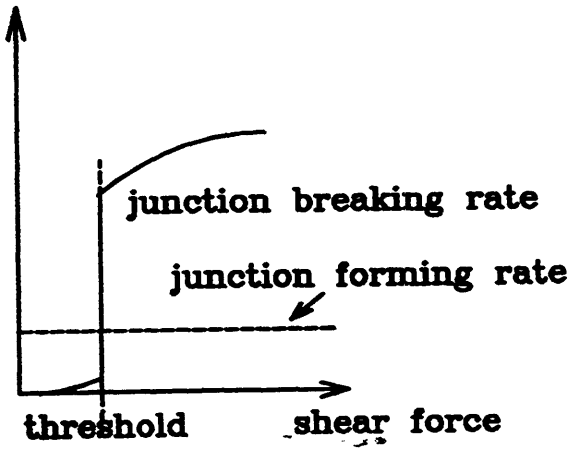

Figure 6. 4 The proposed curves for the junction forming rate and the junction breaking rate with respect to shear force in the case of the polycarbonate plate.

Let us trace through a stick-slip curve as in Fig. 6.1. At the beginning of stroking (region A-E), as in the case of the glass plate, no relative motion occurred between the polycarbonate surface and the fingerpad. The junctions were strong enough to overcome the gradually increasing shear force. When the shear force hit the threshold value

(corresponding to E in Fig.6.1), the net number of junctions decreased, and thus the shear force which could be transmitted through these junctions also decreased. From the point view of the fingerpad, two forces acting on it were the internal elastic force and the external shear (friction) force transmitted from junctions. At this point E, the shear force decreased suddenly, so the two forces could not balance and the unbalanced force accelerated the fingerpad skin in the backward direction (region E-F in Fig. 6.1), which is the slip portion of a stick-slip behavior. This can also be regarded as the release of the stored elastic energy inside the fingerpad. As the shear force between two surfaces dropped to point F in Fig. 6.1, the situation went back to the part below the threshold of Fig. 6.4, and the number of junctions started increasing again in region F-G of Fig. 6.1. During the first part of this period F-G, the external shear force on the fingerpad increased due to the increasing number of junctions, while the elastic force still continuously decreased due to the viscoelastic behavior of the fingerpad, which caused the slower release motion (ref. to Fig. 5.25) compared to the suddenly drop of the shear force. Later, the shear force from junctions was able to balance the elastic force as well as to change the velocity of the fingerpad, the fingerpad started to decelerate in the backward direction, stop, and accelerate in the forward direction. As the fingerpad reached the velocity of the indentor again, no relative motion happened between two surfaces and they stuck together again. At this moment no force was needed to accelerate the fingerpad, so the shear force from junctions was again equal to the elastic force from the fingerpad. This is the stick portion of a stick-slip behavior. The fingerpad moved with the indentor velocity until the shear force threshold value occurred again, and the stick-slip cycle then followed continuously.

6.3 Visualization

The image data on the movement of the fingerpad contact region supports the description above. Fig. 6.5 shows the displacements of the indentor and the fingerpad for both the cases of the glass plate and the polycarbonate plate. From this figure, we can see that the average stroke velocity of both plates was the same. The displacement of the fingerpad in the case of the glass plate continuously increased, with decreasing velocity. This behavior has been described and explained by the junction forming and breaking effects. In contrast, the displacement of the fingerpad in the case of the polycarbonate plate oscillated, which means the fingerpad was stretched forward and then bounced back repeatedly. The portion of stretching forward generally moved the same number of pixels as the movement of the polycarbonate indentor, which was the stick portion without relative motion. The portion of bouncing back was the release of the elastic energy stored in the fingerpad. From comparison between the case of the glass plate and the case of the

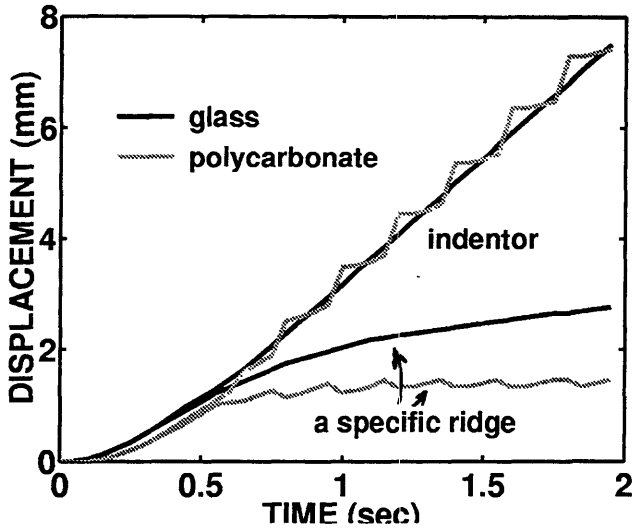

Figure 6. 5 The comparison of the displacements of the indentors and of a specific finger ridge for both the cases of glass and polycarbonate plates.

polycarbonate plate, we find that the displacement of the fingerpad in the case of the glass indentor grew to higher values than in the case of the polycarbonate indentor. This is the same as the comparison of the shear force, as shown previously in Fig. 6.1. The proposed junction characteristics for both cases explain this difference. Because in the stick-slip case the shear force dropped suddenly when slip occurred, it was never possible to stretch the fingerpad above a certain distance. In the smooth friction case, because the adhesion effect was always active, the number of junctions could continuously increase, and the fingerpad could be stretched until the junction breaking rate and forming rate were equivalent. Thus both the shear force and the displacement of the fingerpad in the case of the glass indentor had higher final values.

Another observation described previously is that in the case of the glass plate, the relative motion started from the peripheral parts of the contact area. Let us focus now on the pressure distribution in the contact area. Because the indentor was a flat plate and the fingerpad surface was initially curved, the indentation caused more tissue to be compressed in the center. Therefore, the center had higher pressure than the peripheral portion. If the local pressure is higher, there should be more asperities in contact between two surfaces, and the number of junctions should be larger. Furtherfore, according to the proposed curve for junction breaking rate, the shear force threshold to cause the start of relative motion also depends on the number of junctions. Thus, for the center portion of the fingerpad in contact, because the pressure was higher than the peripheral portion, the number of junctions per unit area was larger, and the shear force threshold per unit area was higher. Consequently, it was more difficult to have relative motion in the center portion than in the peripheral portion. This explanation is also valid for the case of

different indentation depths. The relative motion should occur earlier in the smaller indentation depth than in the larger one.

One more important inference from the image data is the 3-D representation of the displacement field of different finger ridges, as previously shown in Fig. 5.16. We recall from Fig. 5.15 that the displacement in the side A-D-G moved faster than in the side C-F-I, and the middle part D-E-F moved faster than in the upper side A-B-C and the lower side G-H-I. The comparison of displacements of the middle part and the upper, lower parts can be again explained by the pressure distribution. The pressure of the middle part D-E-F was higher, so it contained more junctions and had the ability to transmit larger shear force to stretch the fingerpad. The difference of the displacements in the side A-D-G and in front side C-F-I can be explained by the accumulation of the finger tissue. When the fingerpad was stretched toward the side C-F-I, more and more tissue was accumulated in that side, which formed a strong resistive force. The indentor continued to move the contact part of the fingerpad to the side C-F-I, so the finger ridges were squeezed to a thin band. Thus the finger ridge in the side C-F-I moved slower than the finger tissue in the side A-D-G, as shown in that 3-D plot.

6.4 Comparison with Rubber-Like Materials

Rubber-like materials basically have similar frictional behaviors as the human fingerpad. Roth *et al.* (1942) showed that for rubber-like materials as the stroke velocity increased, the friction coefficient increased, and the curves are plotted in Fig. 6.6. Though these curves are not the same as what were obtained in our experiment with the glass plate (Fig. 5.1 and 5.3), the basic behavior, gradually growing and then reaching the steady states, is

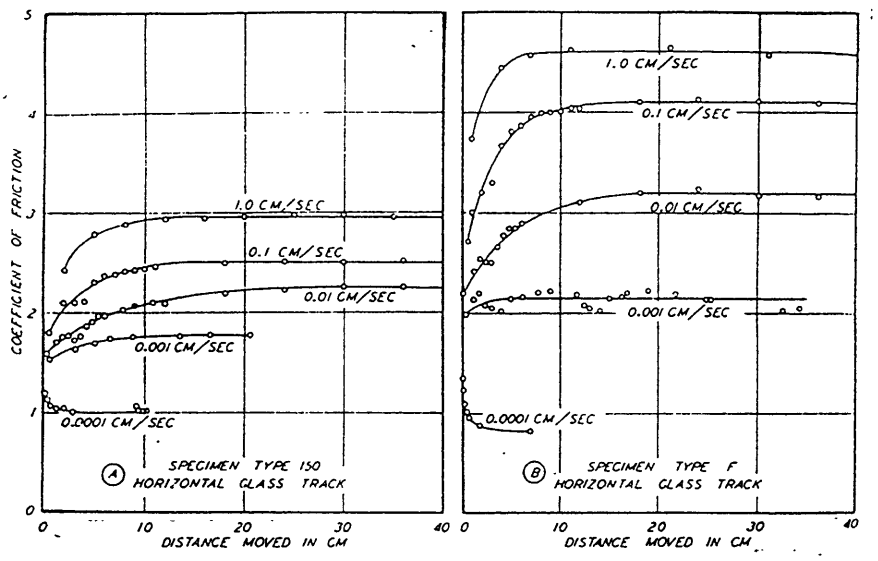

Figure 6. 6 The record of friction coefficients with different stroke velocities in two types of rubber (Roth, et al., 1942).

the same. The cause for the velocity dependent behavior of rubber is the hysteresis and viscoelastic properties (Grosch, 1963), which can also be the explanation of the velocity dependent behavior of the human fingerpad. The influence of normal force on rubber friction coefficient has been investigated by Schallamach (1952) and is shown in Fig. 6.7. It is obvious that the curves have almost the same behavior as in the fingerpad/glass plate case, as shown in the right panel of Fig. 5.2. Therefore, the possibility of using rubber-like materials to simulate the behavior of fingerpad may be considered. However, there is one unusual phenomenon in rubber called Schallamach wave propagation (Schallamach, 1971). When the sliding speed between rubber and a solid surface falls into a specific regime, detachment waves could be observed in the contact area. These detachment waves propagated through the contact region, from the leading side to the trailing side, with the propagation velocity was larger than the sliding velocity. This phenomenon has not yet been observed in our fingerpad experiment. Furthermore, although stick-slip behavior did occur between rubber and some kind of materials - chromium oxide and

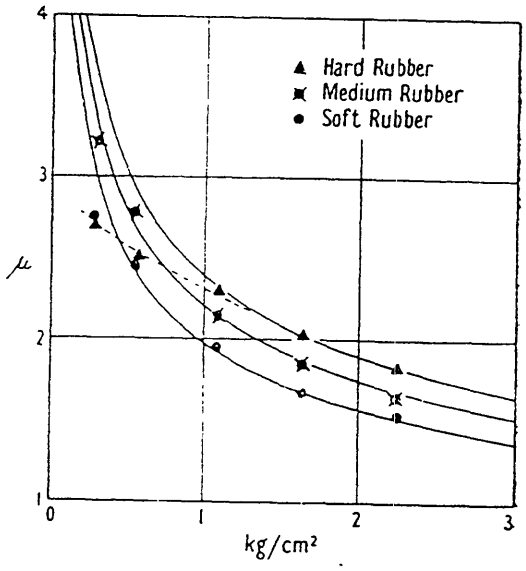

Figure 6. 7 The relationship between the friction coefficient and the normal apparent pressures for three different kinds of rubber (Schallamach, 1952).

glass (Rorrer, *et al.,* 1992), the resulting data were not similar to the data we observed in the fingerpad/polycarbonate plate case. Therefore, while the overall behavior of rubber-like materials is similar to that of the human fingerpad, the difference in the micro-scale between the fingerpad and rubber, such as surface texture and surface characteristics, may cause several differences as well.

Appendix Data of All Five Subjects

The following plots show the data from the experiments with different indentors, subjects, and stimuli. It contains:

1. Indentor = glass
    a. Stroke velocity = 4 mm/s, stroke direction = forward, and 7 different indentation depths = 0.75 to 2.25 mm.

    b. Stroke velocity = 16 mm/s, stroke direction = forward, and 7 different indentation depths = 0.75 to 2.25 mm.

    c. Indentation depth = 2 mm, stroke direction = forward, and 4 stroke velocities = 2, 4, 8, and 16 mm/s.

    d. Stroke velocity = 4 mm/s, stroke direction = backward, and 7 different indentation depths = 0.75 to 2.25 mm.

    e. Indentation depth = 2 mm, stroke direction = backward, and 4 different stroke velocities = 2, 4, 8, and 16 mm/s.

2. Indentor = polycarbonate
    a. Stroke velocity = 4 mm/s, stroke direction = forward, and 3 different indentation depths = 1, 1.5 and 2 mm.

    b. Indentation depth = 2 mm, stroke direction = forward, and 4 different stroke velocities = 2, 4, 8, and 16 mm/s.

3. Indentor = acrylic
    a. Stroke velocity = 4 mm/s, stroke direction = forward, and 3 different indentation depths = 1, 1.5, and 2 mm.

All Depths
Velocity: 4 mm/s
Direction: Forward
Indentor: Glass
Subject: 1

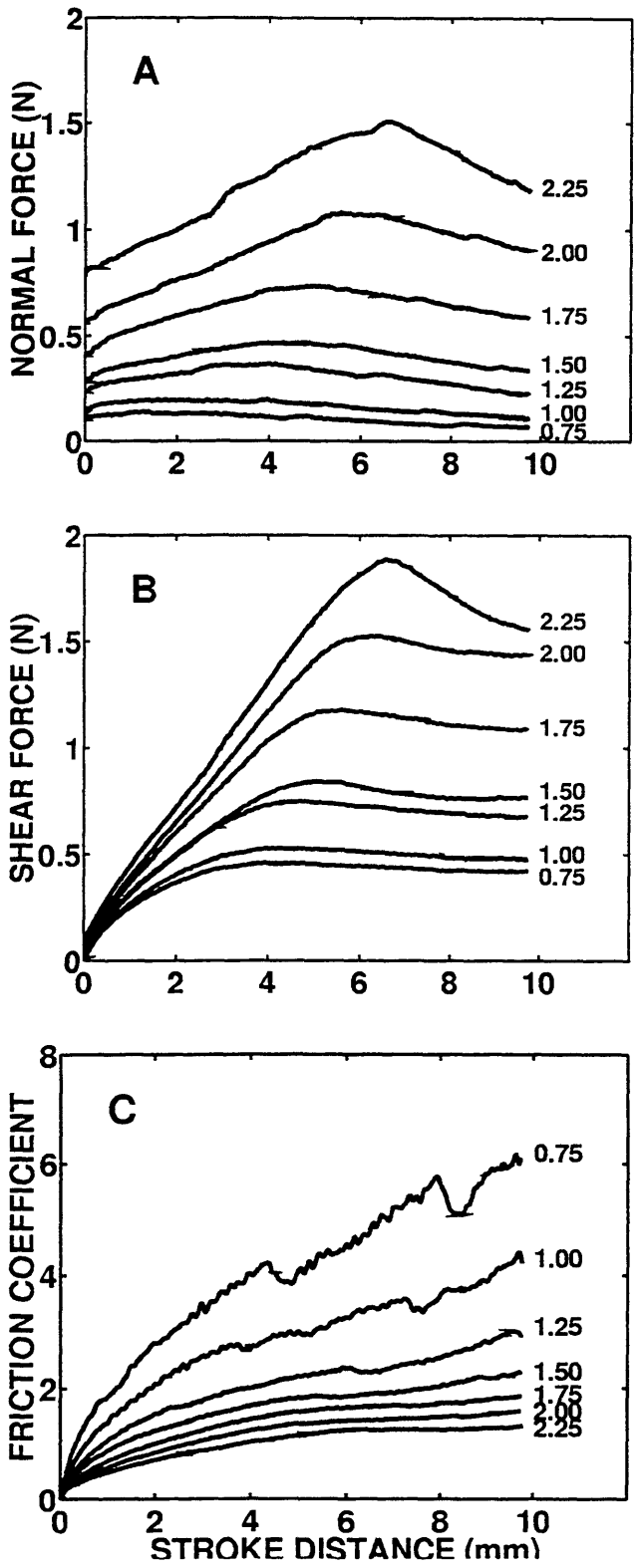

All Depths
Velocity: 4 mm/s
Direction: Forward
Indentor: Glass
Subject: 3

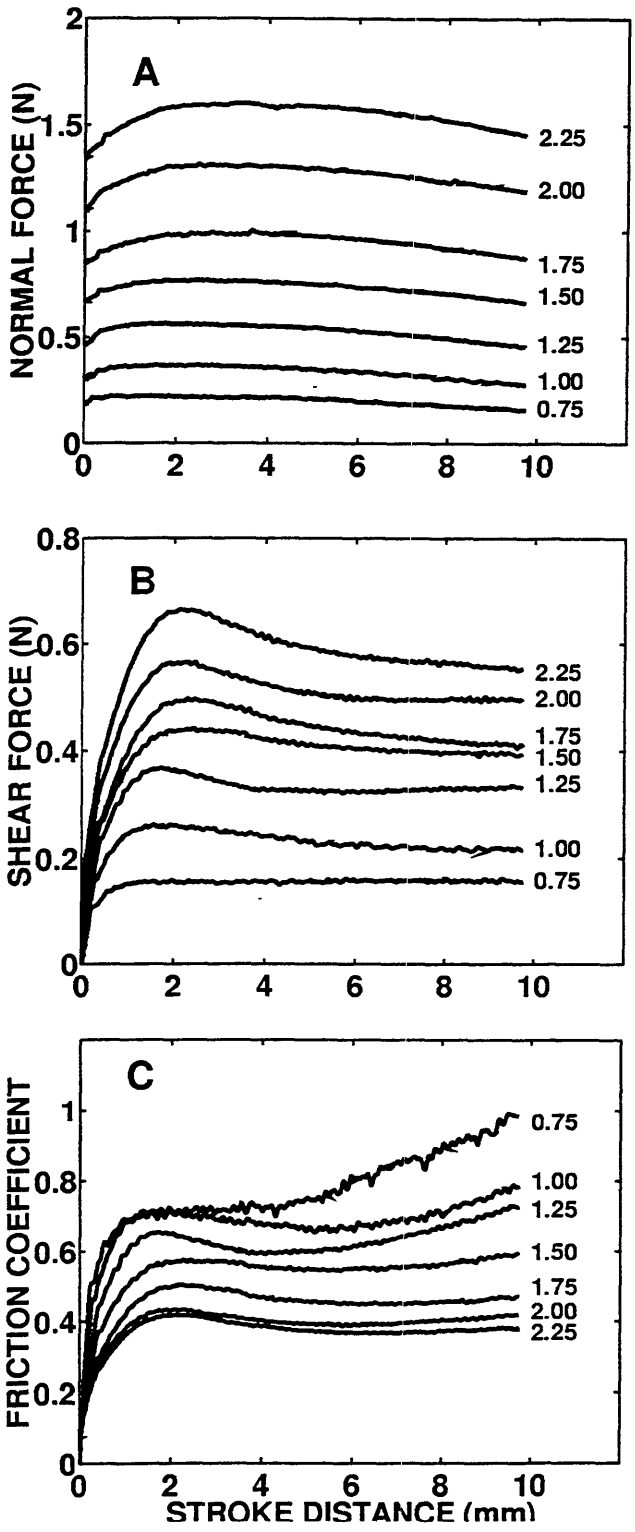

All Depths
Velocity: 4 mm/s
Direction: Forward
Indentor: Glass
Subject: 4

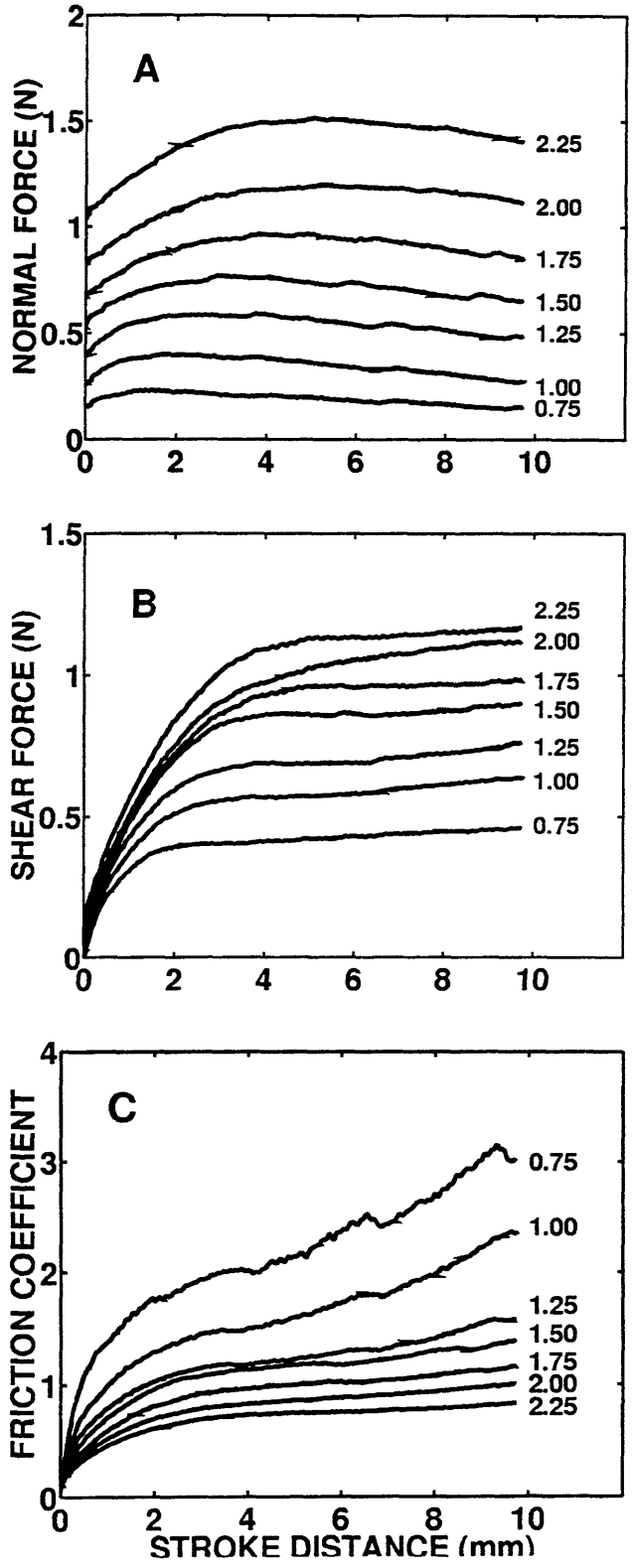

All Depths
Velocity: 16 mm/s
Direction: Forward
Indentor: Glass
Subject: 1

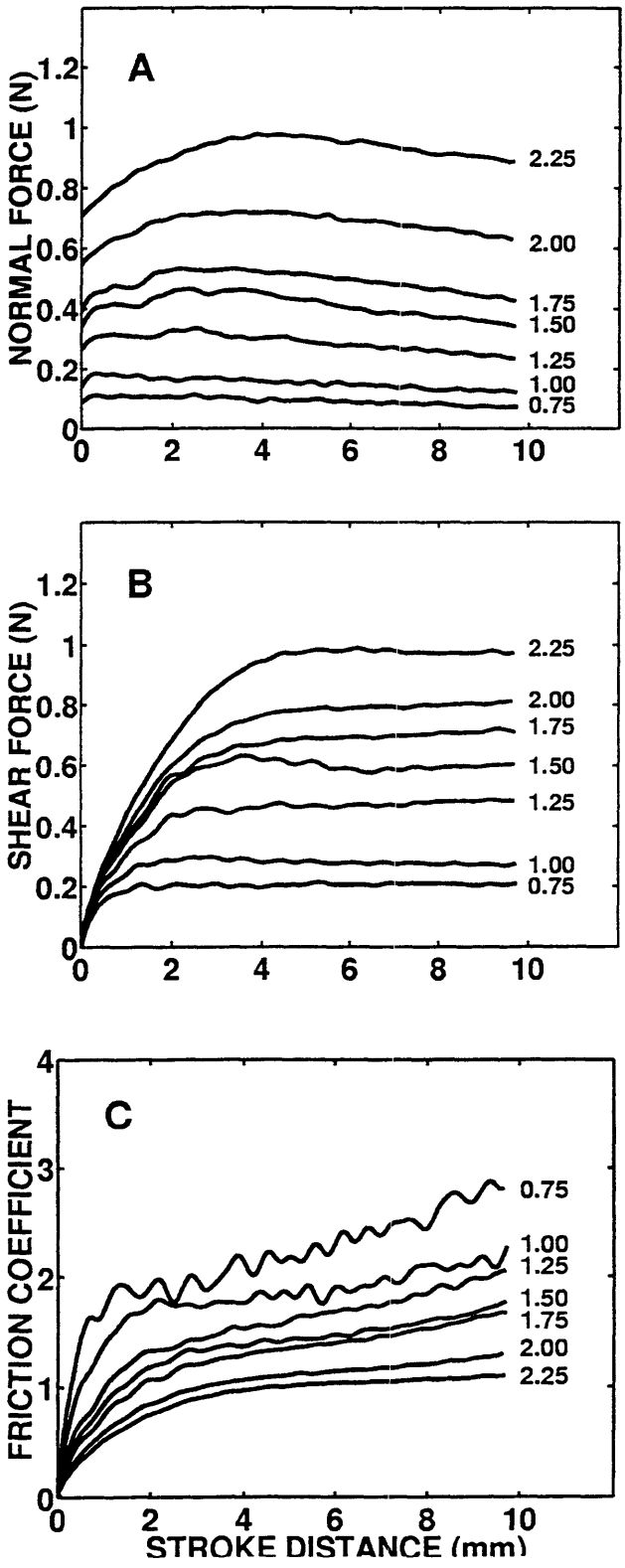

All Depths
Velocity: 16 mm/s
Direction: Forward
Indentor: Glass
Subject: 2

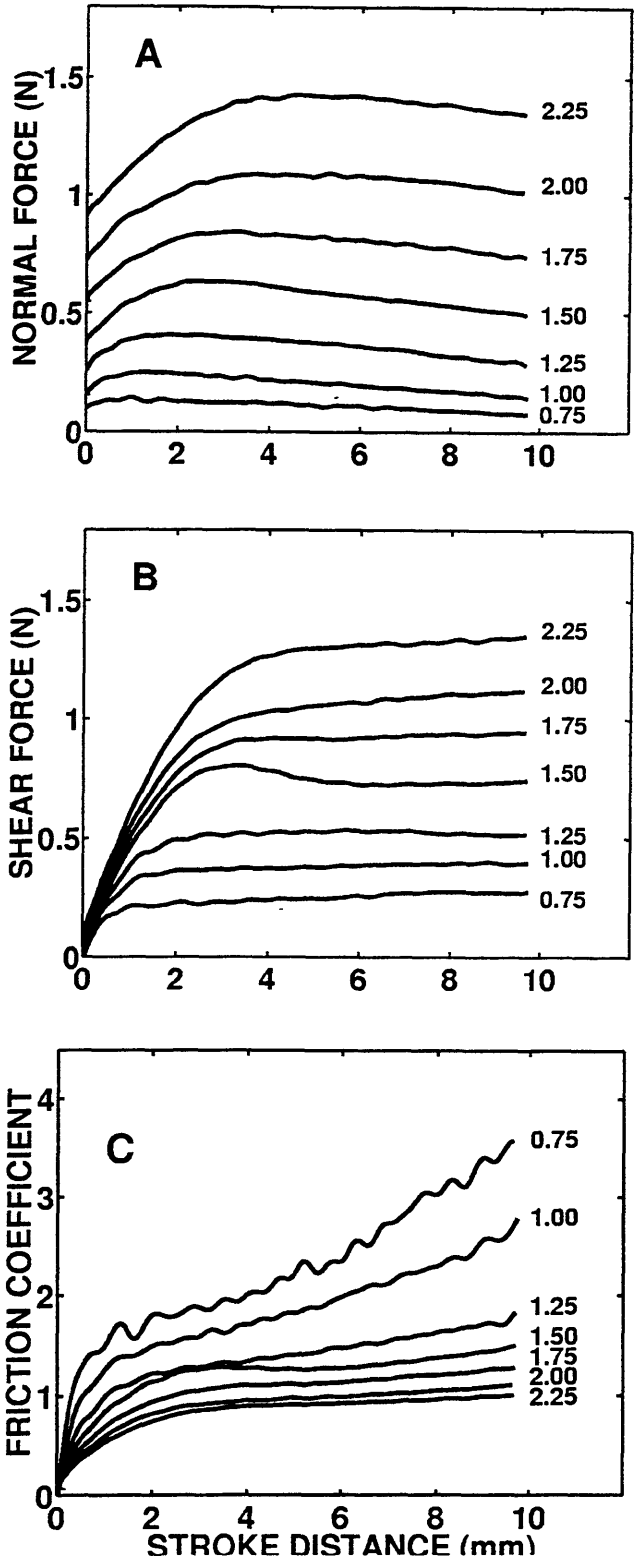

All Depths
Velocity: 16 mm/s
Direction: Forward
Indentor: Glass
Subject: 3

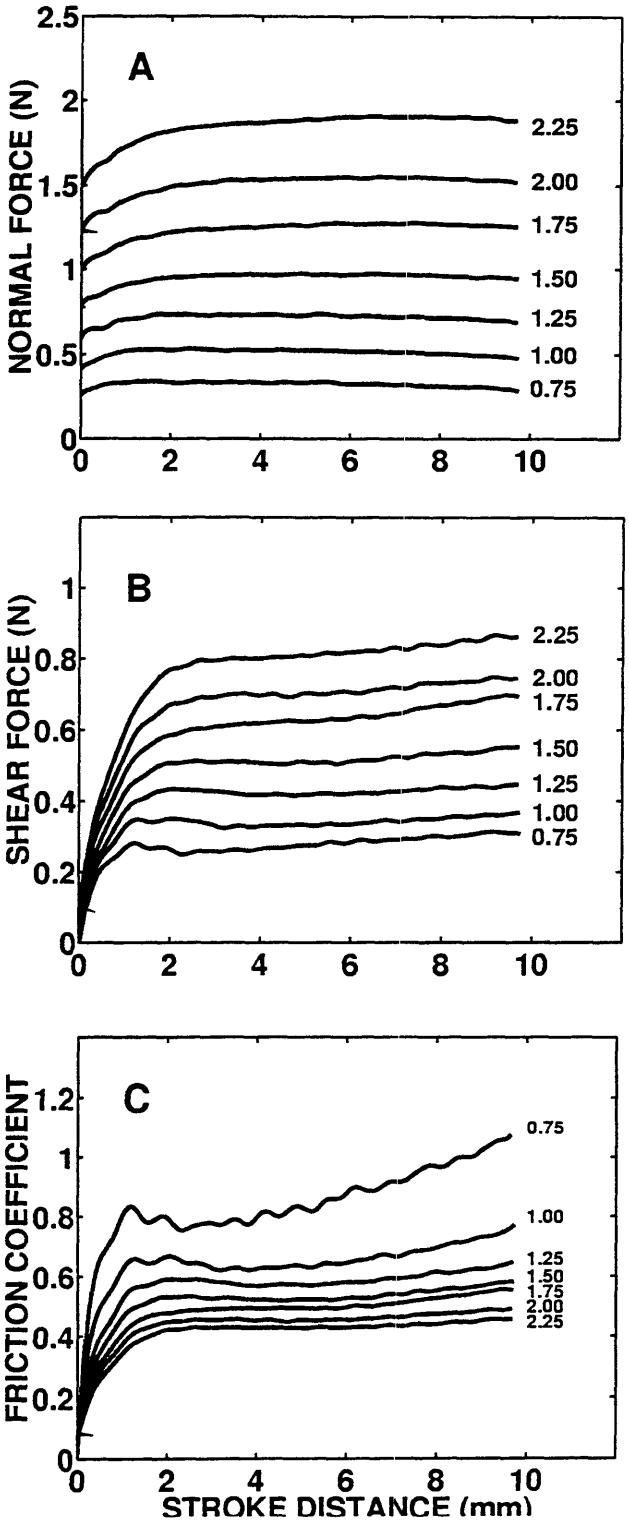

All Depths
Velocity: 16 mm/s
Direction: Forward
Indentor: Glass
Subject: 4

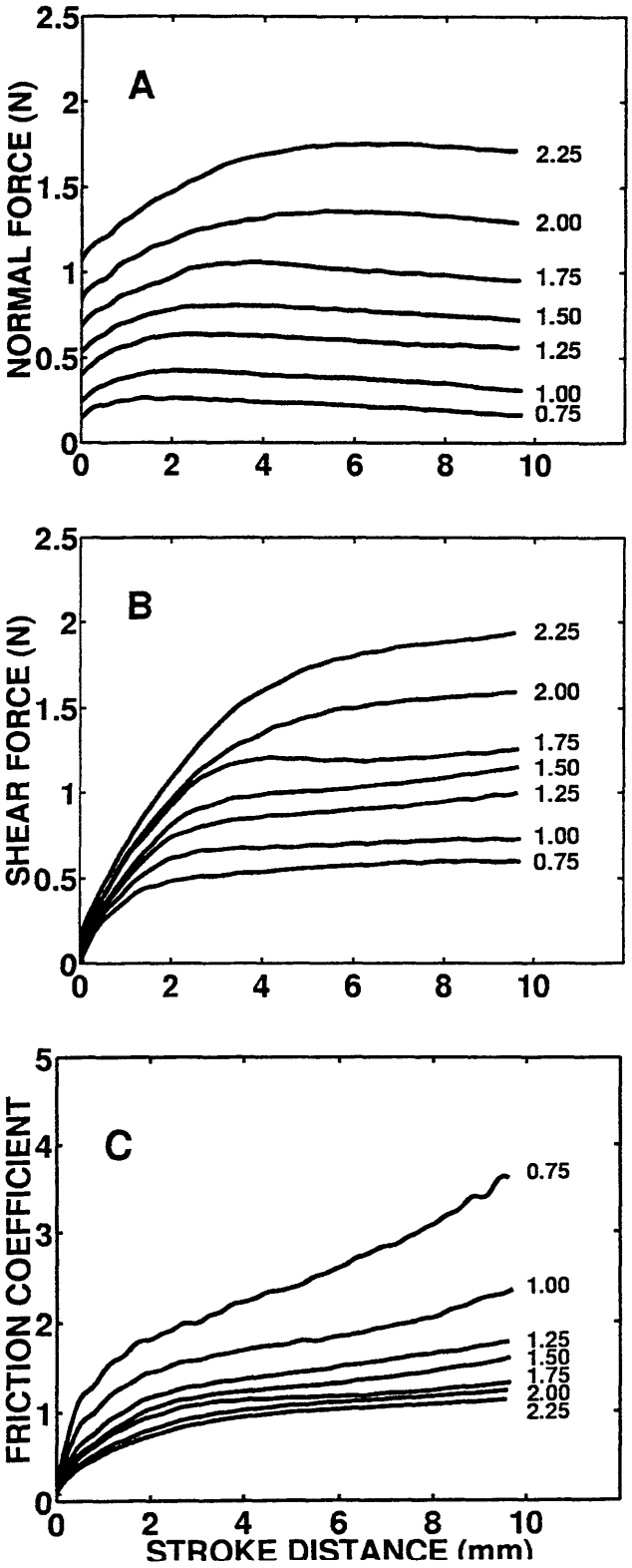

All Depths
Velocity: 16 mm/s
Direction: Forward
Indentor: Glass
Subject: 5

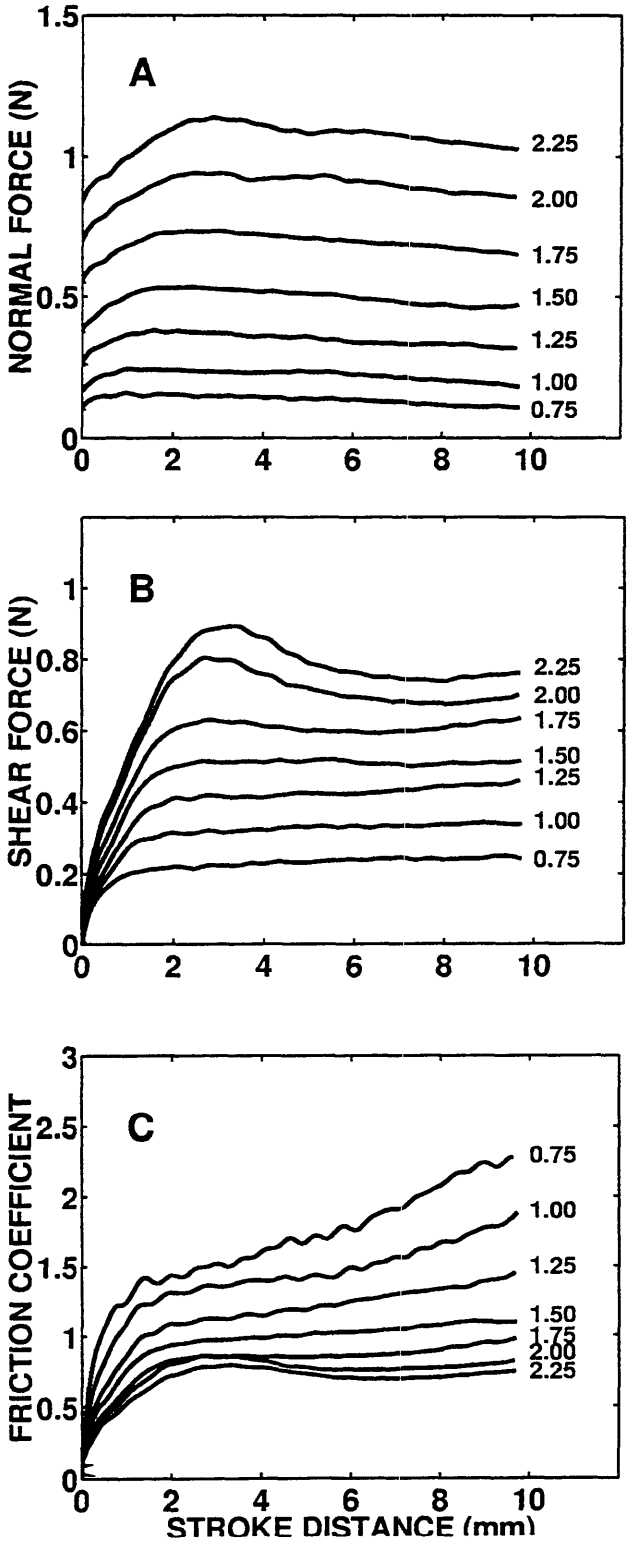

All Velocities
Depth: 2 mm
Direction: Forward
Indentor: Glass
Subject: 2

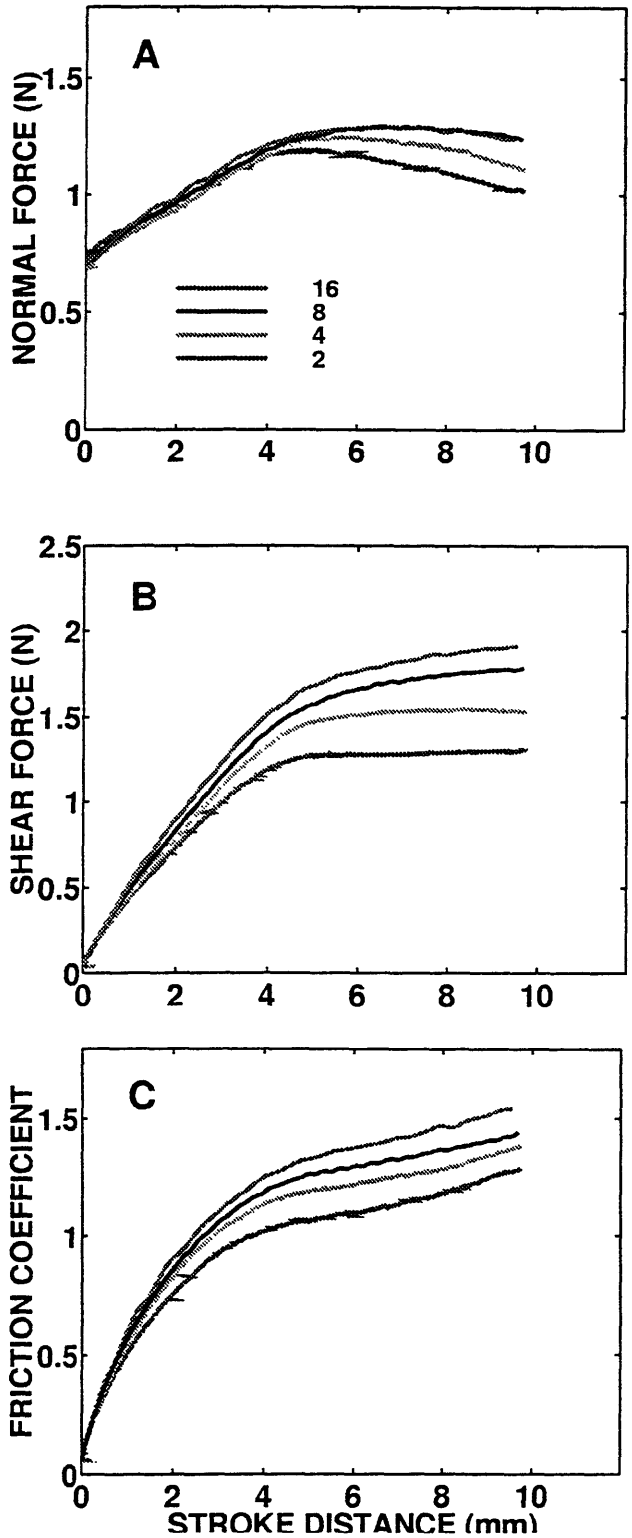

All Velocities
Depth: 2 mm
Direction: Forward
Indentor: Glass
Subject: 3

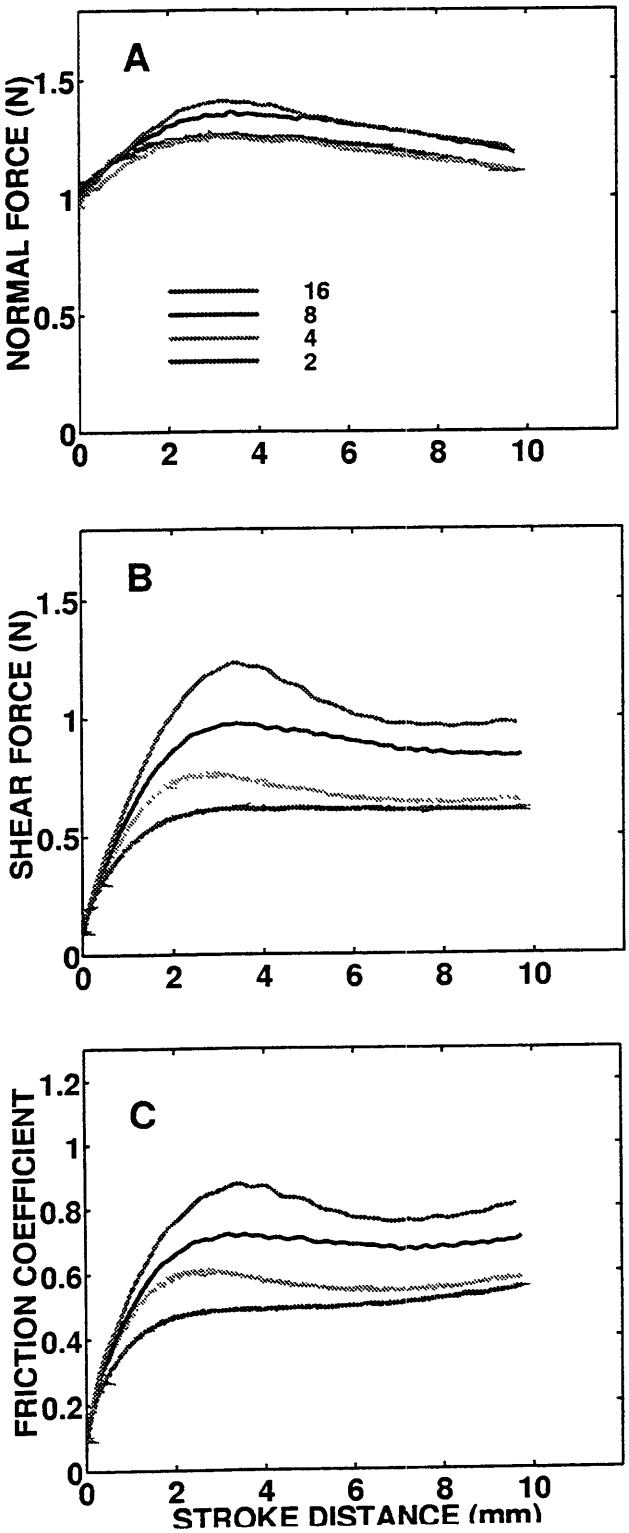

All Velocities
Depth: 2 mm
Direction: Forward
Indentor: Glass
Subject: 5

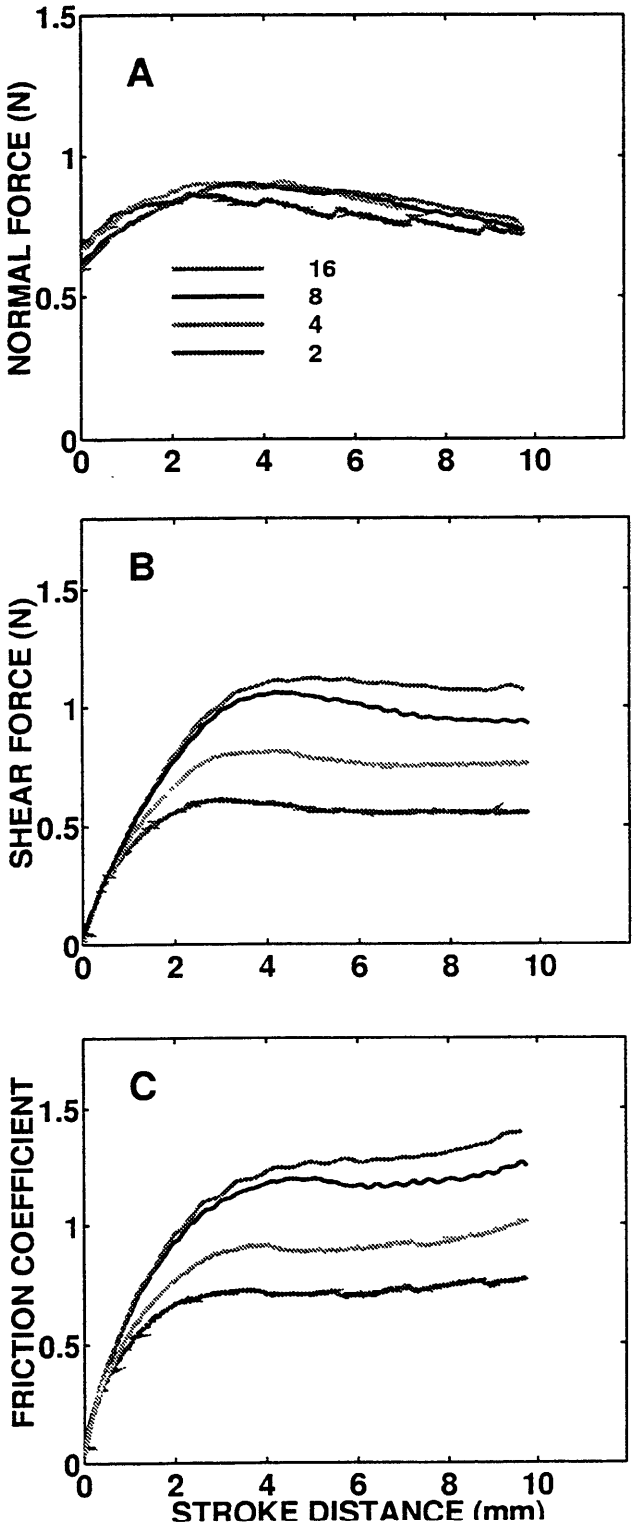

All Depths
Velocity: 4 mm/s
Direction: Backward
Indentor: Glass
Subject: 1

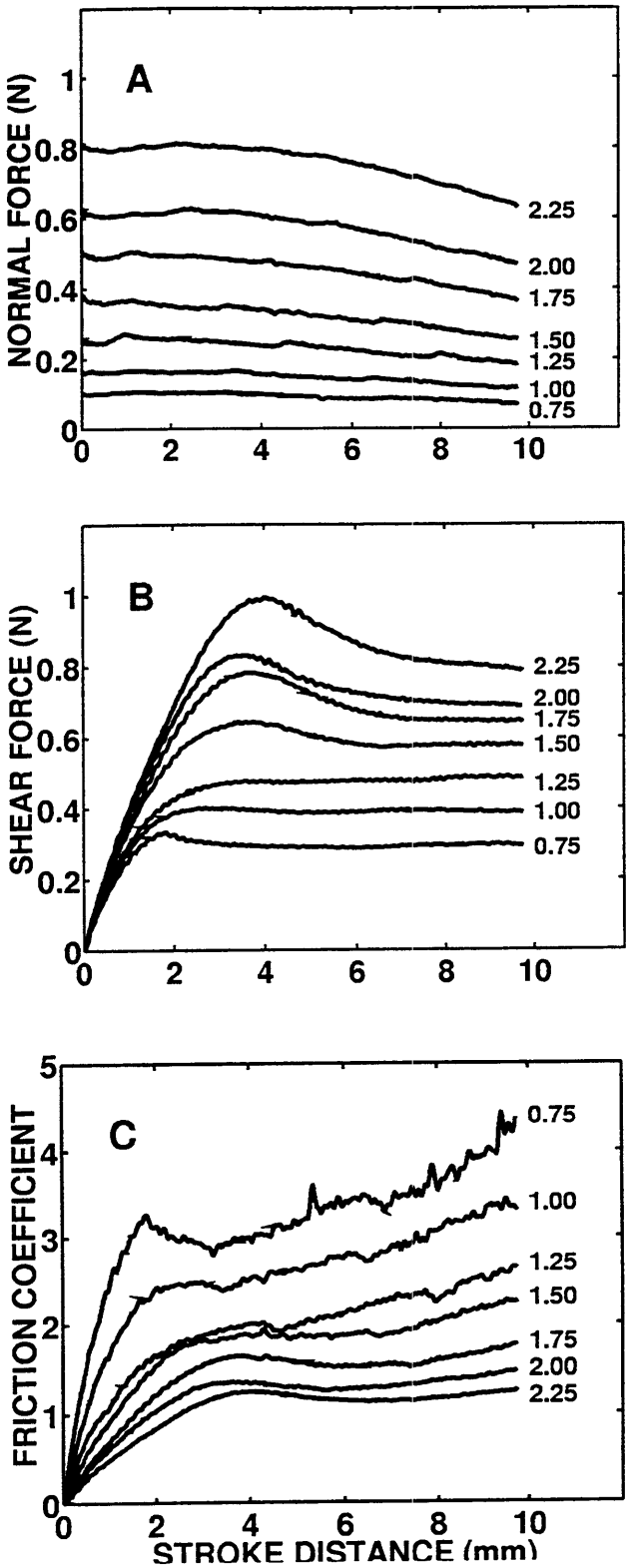

All Depths
Velocity: 4 mm/s
Direction: Backward
Indentor: Glass
Subject: 2

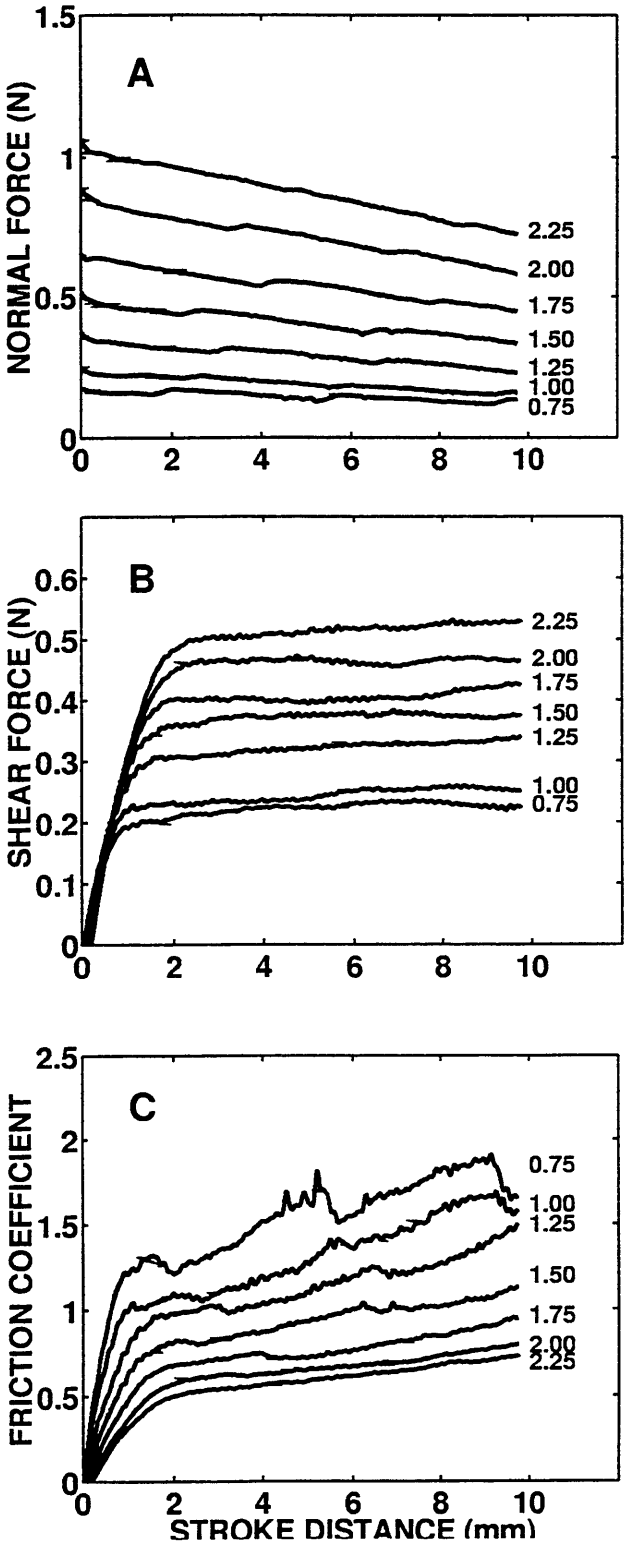

All Depths
Velocity: 4 mm/s
Direction: Backward
Indentor: Glass
Subject: 3

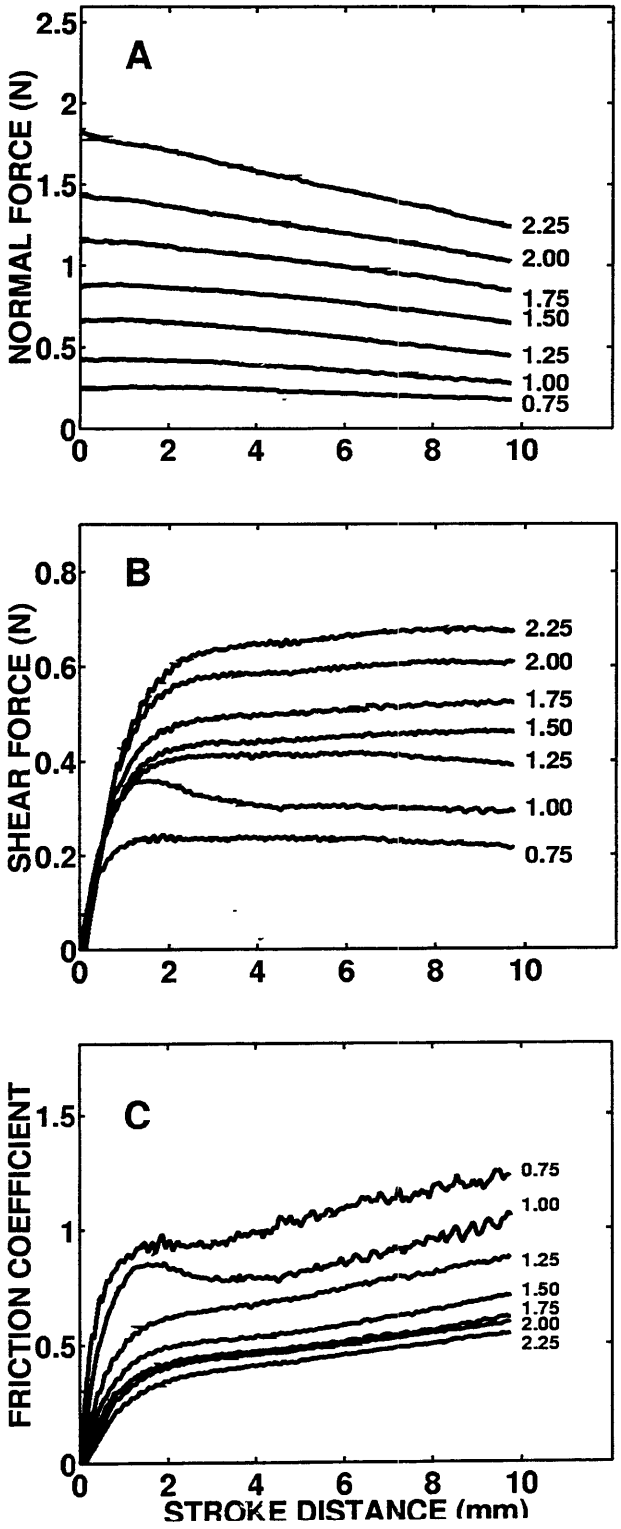

All Depths
Velocity: 4 mm/s
Direction: Backward
Indentor: Glass
Subject: 4

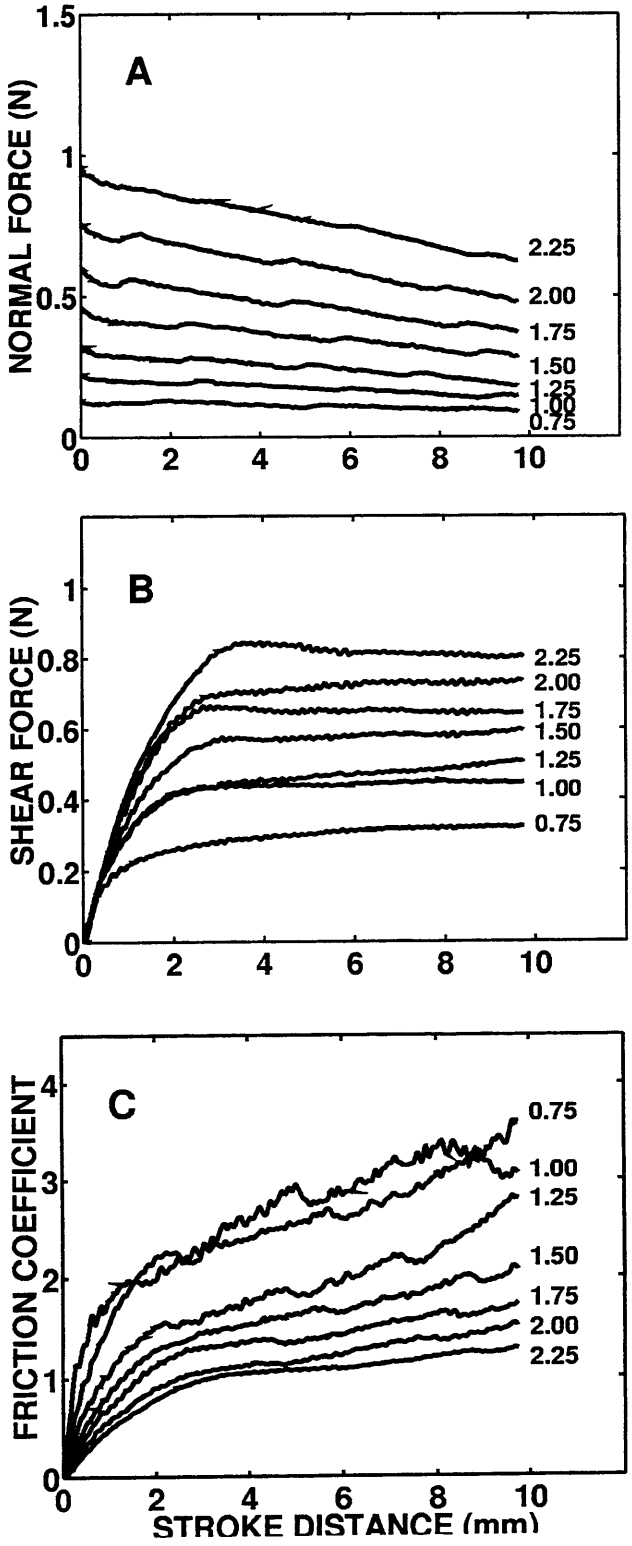

All Velocities
Depth: 2 mm
Direction: Backward
Indentor: Glass
Subject: 1

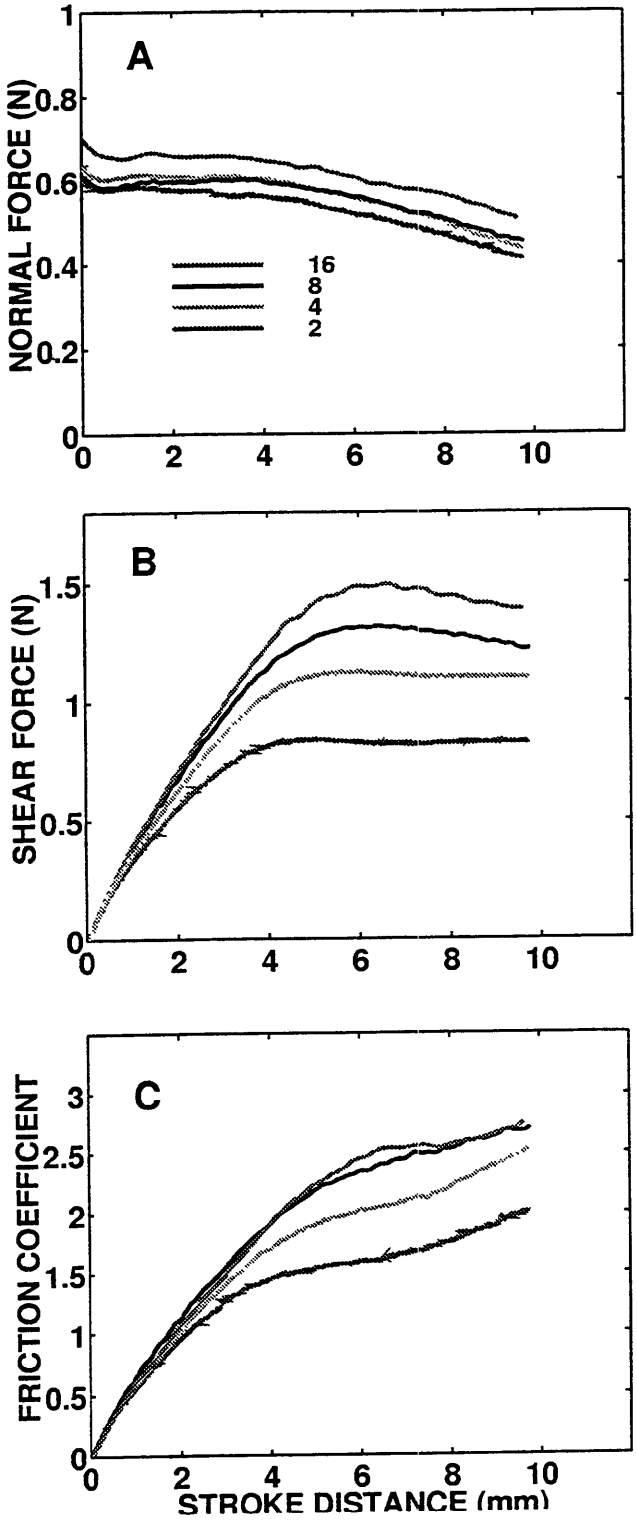

All Velocities
Depth: 2 mm
Direction: Backward
Indentor: Glass
Subject: 2

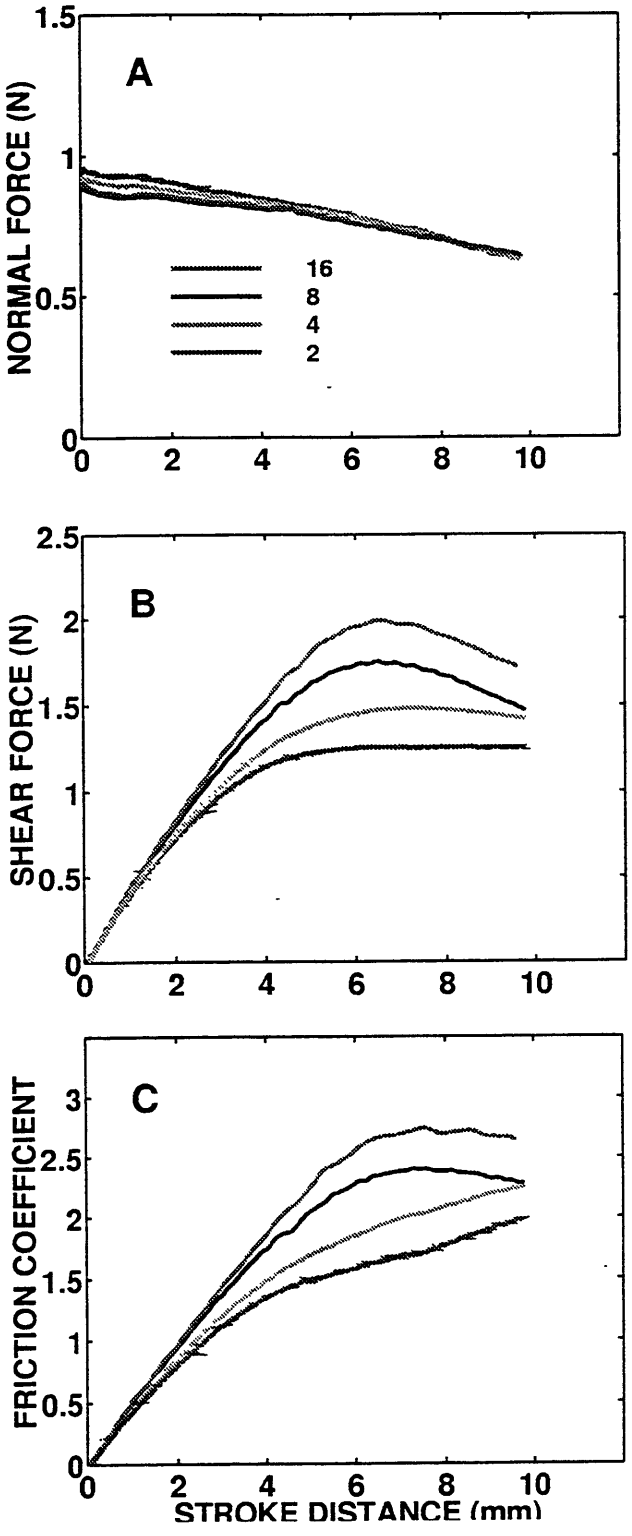

All Velocities
Depth: 2 mm
Direction: Backward
Indentor: Glass
Subject: 3

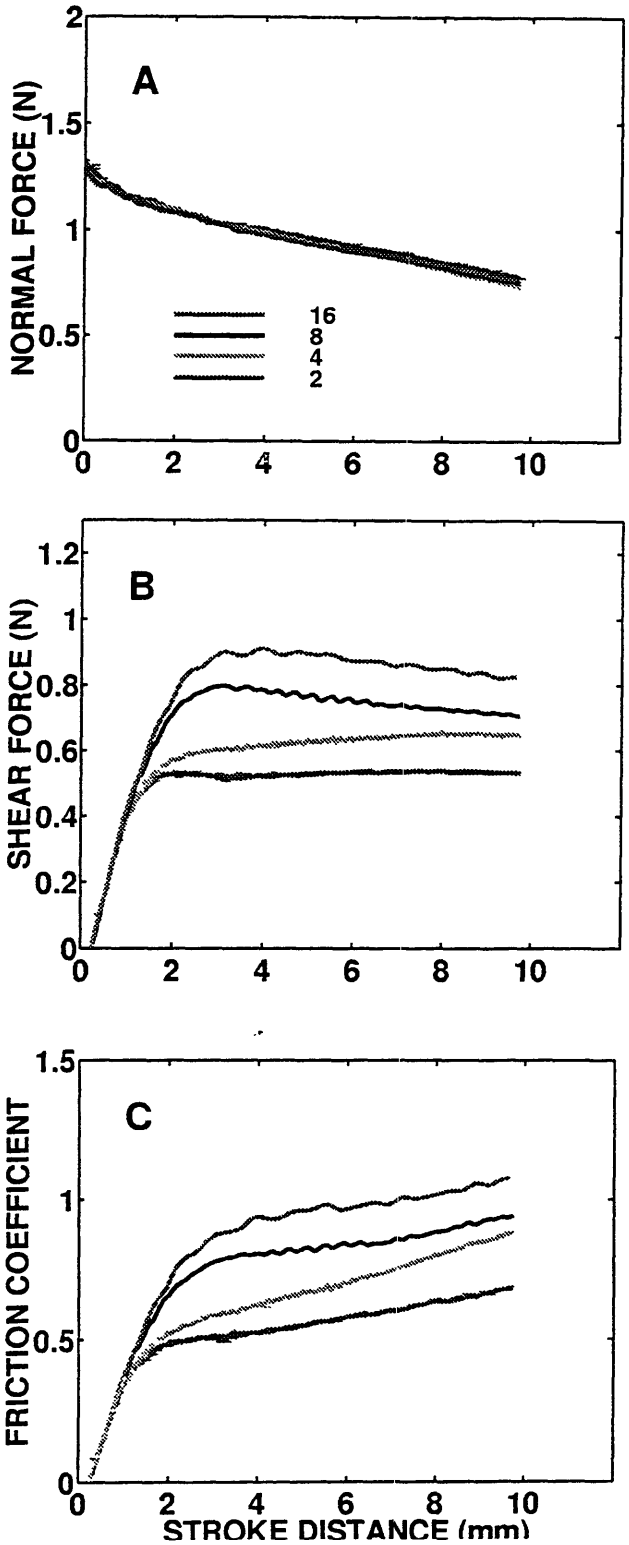

All Velocities
Depth: 2 mm
Direction: Backward
Indentor: Glass
Subject: 5

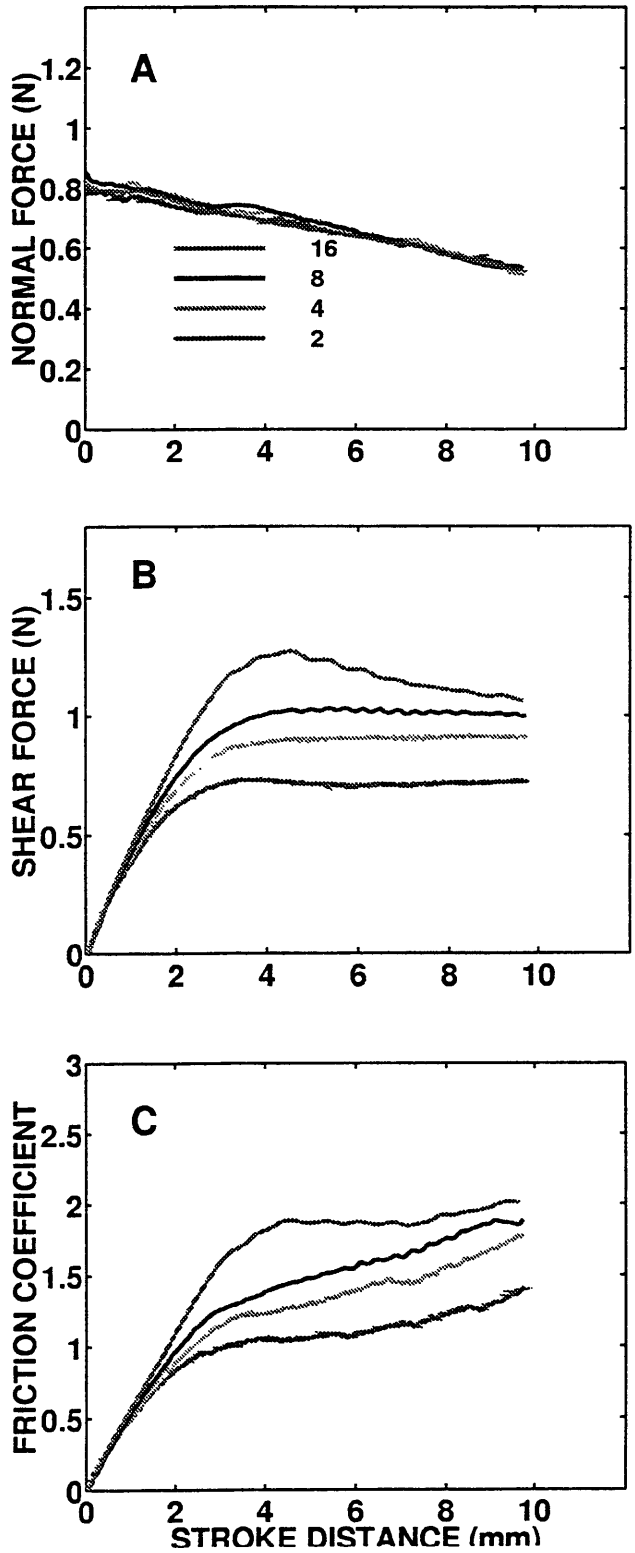

All Depths
Velocity: 4 mm/s
Direction: Forward
Indentor: Polycarbonate
Subject: 1

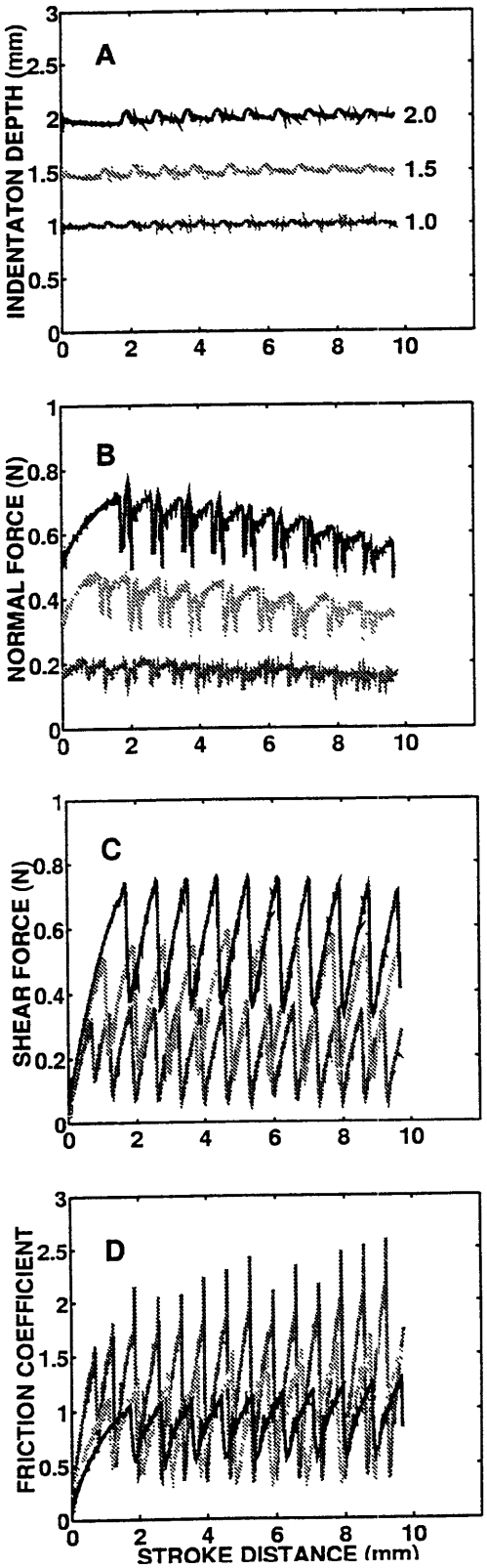

All Depths
Velocity: 4 mm/s
Direction: Forward
Indentor: Polycarbonate
Subject: 2

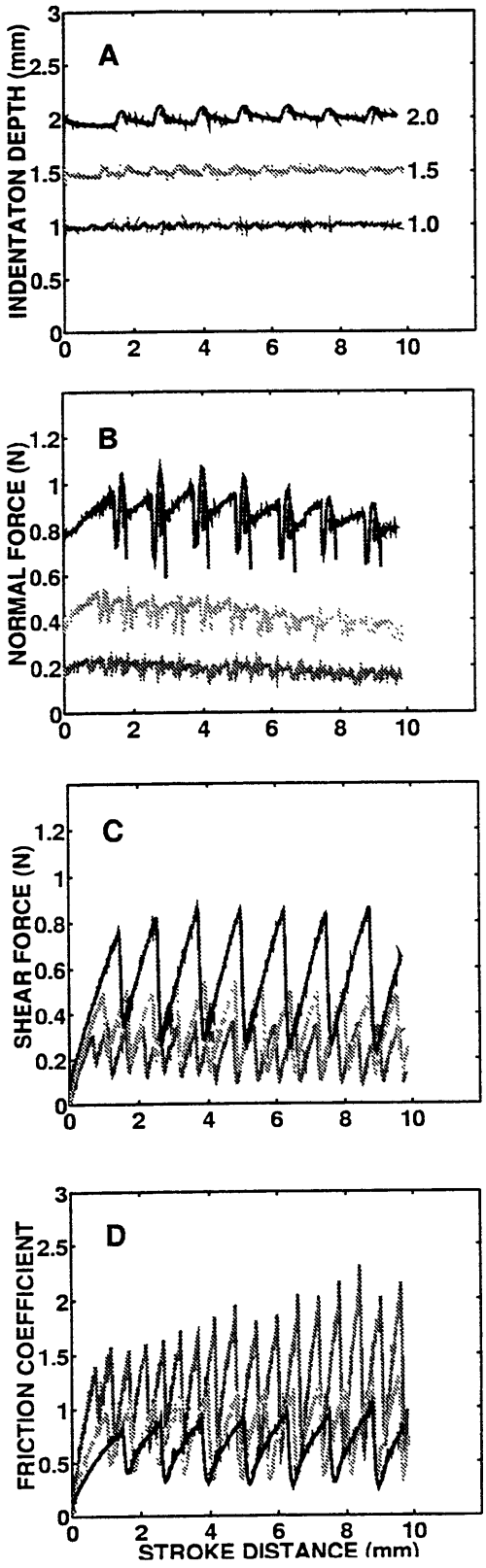

All Depths
Velocity: 4 mm/s
Direction: Forward
Indentor: Polycarbonate
Subject: 3

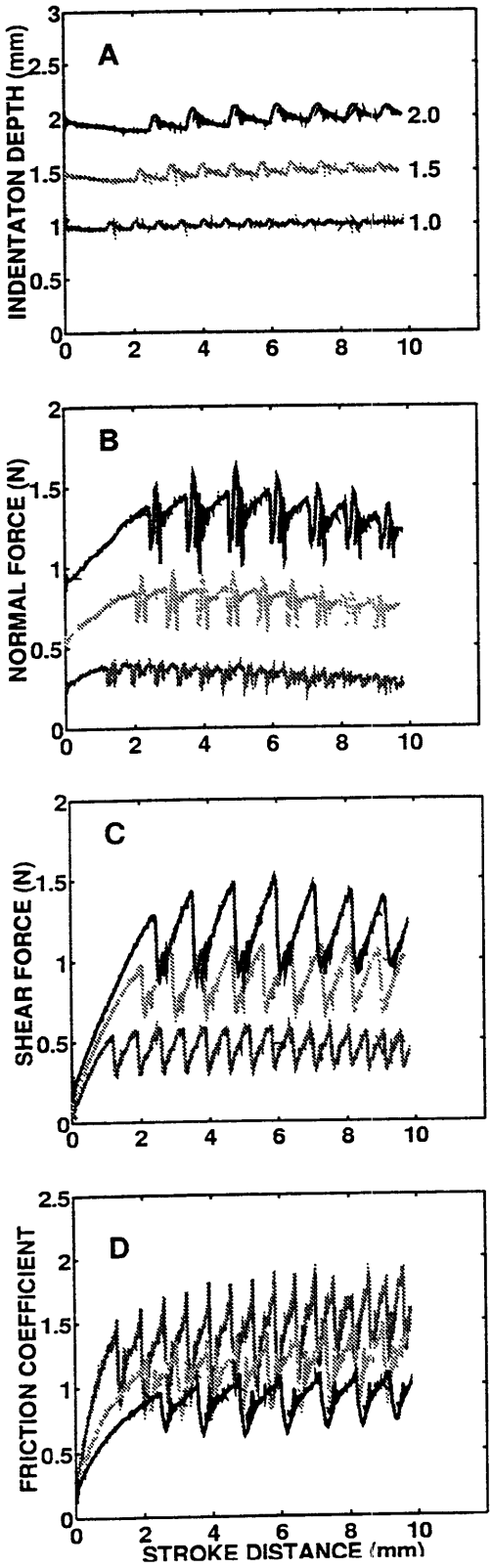

All Depths
Velocity: 4 mm/s
Direction: Forward
Indentor: Polycarbonate
Subject: 4

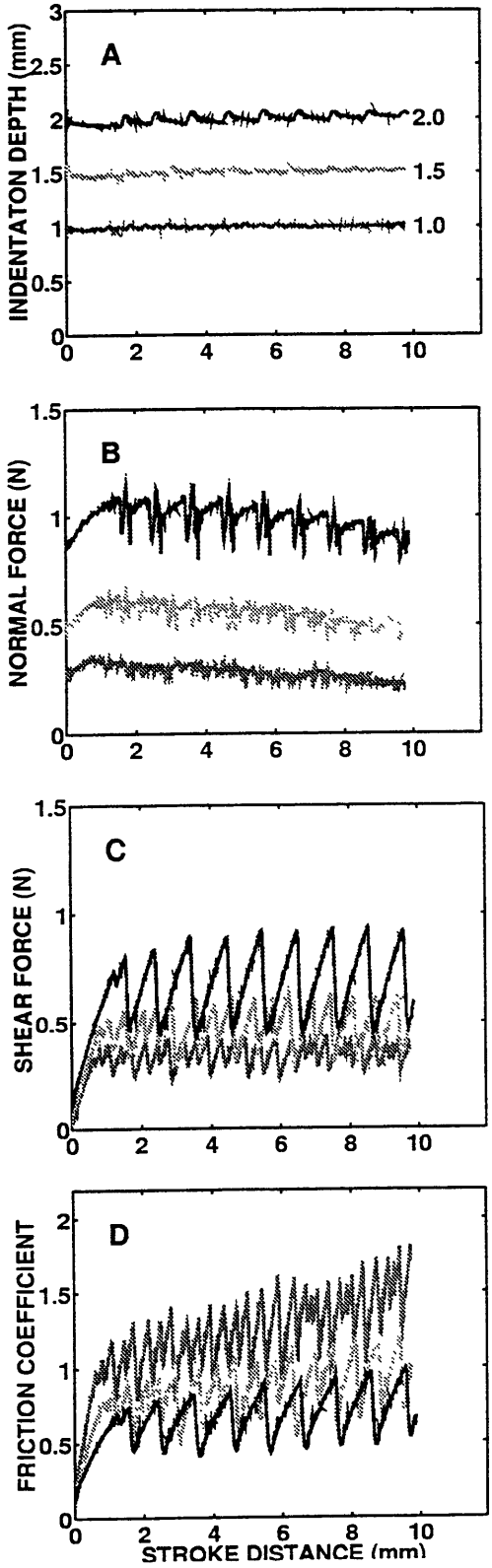

All Depths
Velocity: 4 mm/s
Direction: Forward
Indentor: Polycarbonate
Subject: 5

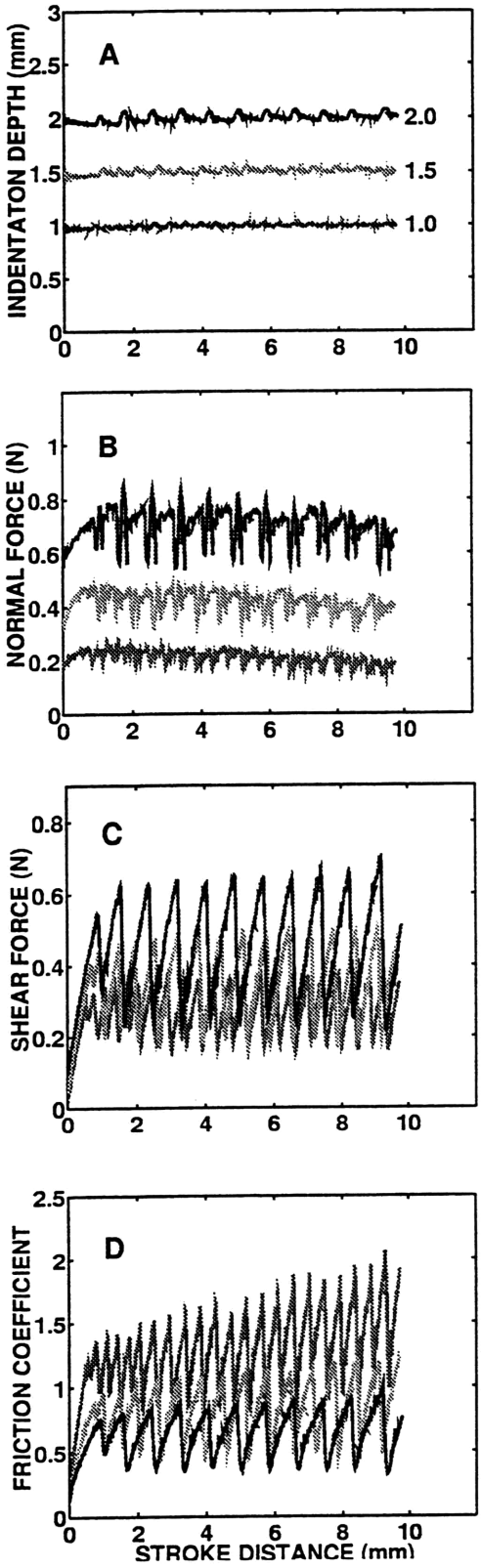

All Velocities
Depth: 2 mm
Direction: Forward
Indentor: Polycarbonate
Subject: 2

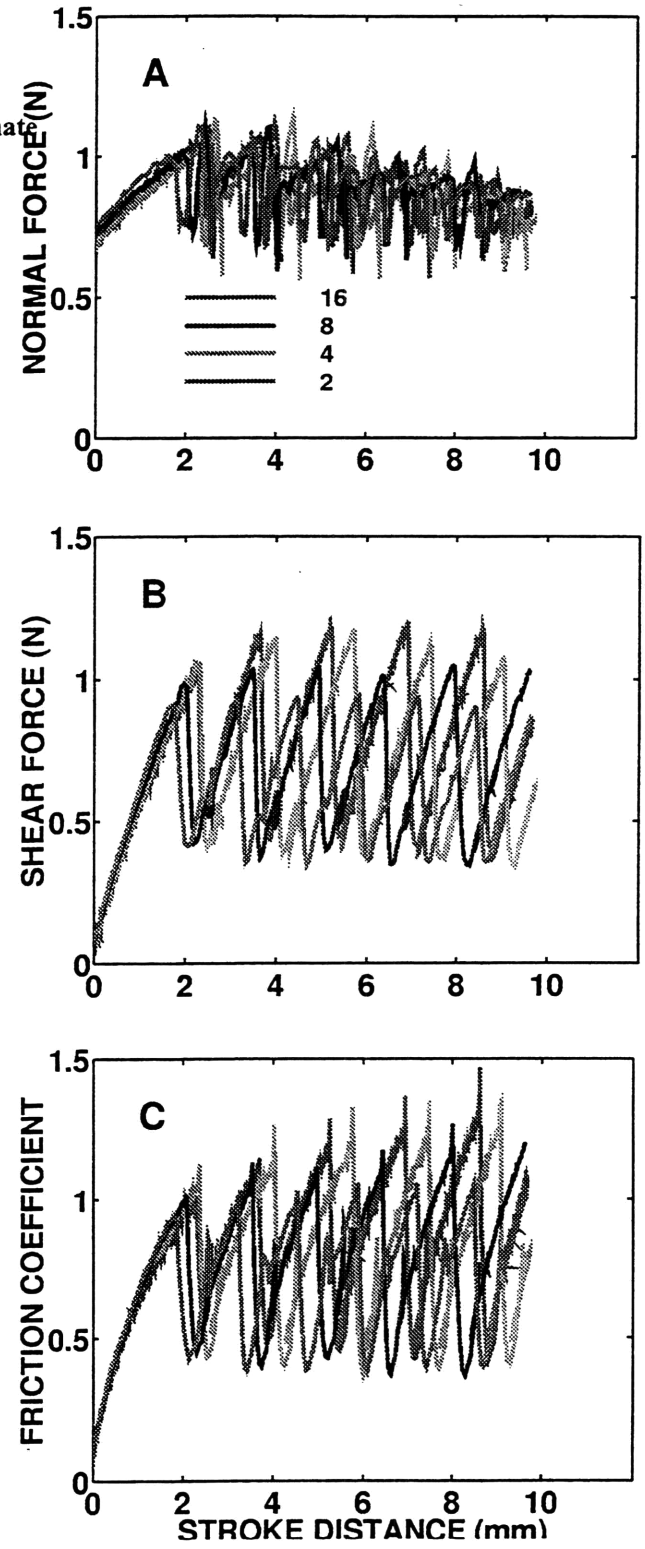

All Velocities
Depth: 2 mm
Direction: Forward
Indentor: Polycarbonate
Subject: 3

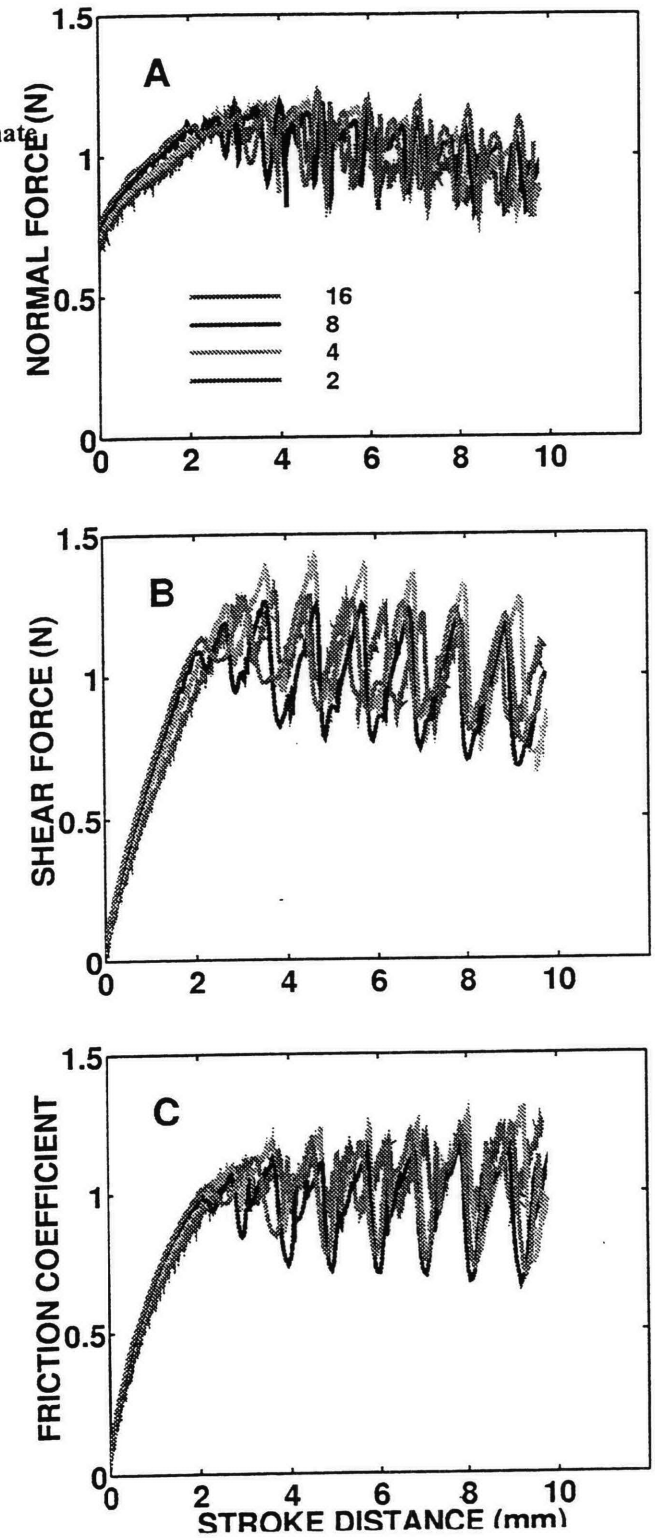

All Velocities
Depth: 2 mm
Direction: Forward
Indentor: Polycarbonate
Subject: 4

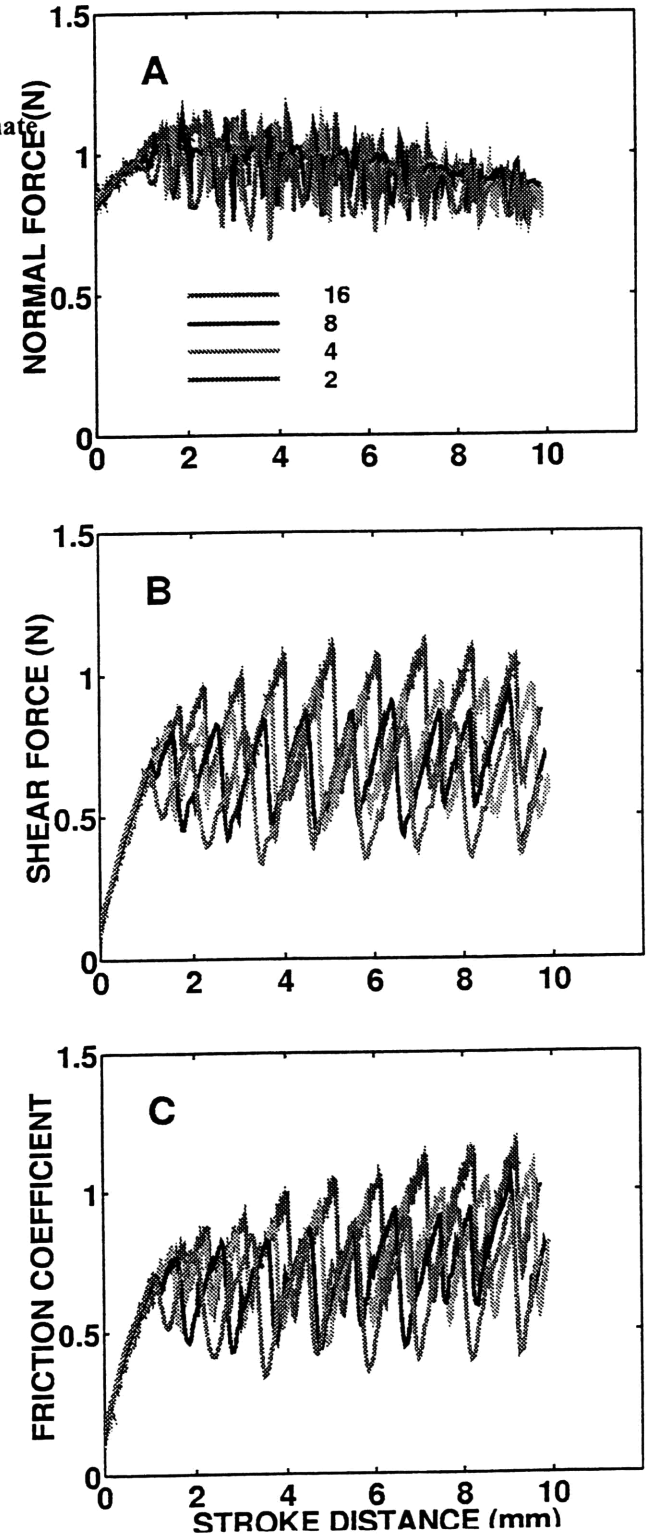

All Velocities
Depth: 2 mm
Direction: Forward
Indentor: Polycarbonate
Subject: 5

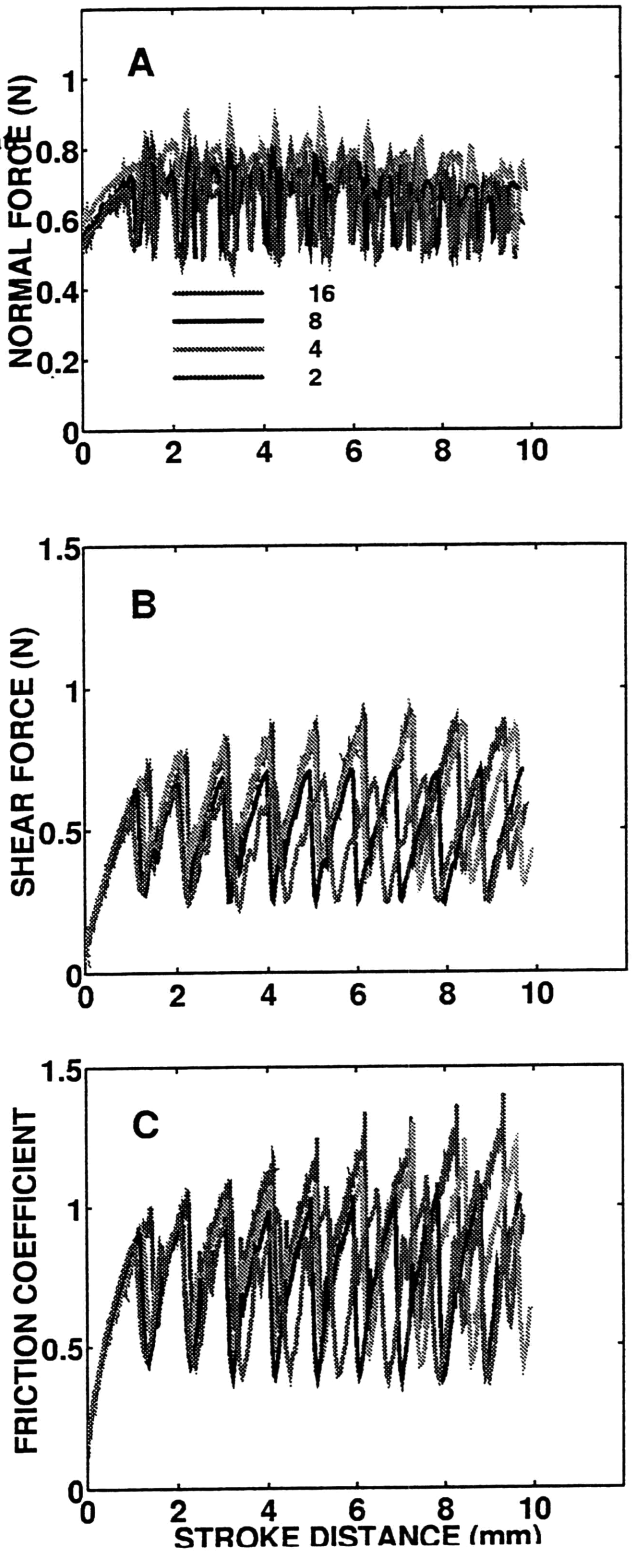

All Depths
Velocities: 4 mm/s
Direction: Forward
Indentor: Acrylic
Subject: 1

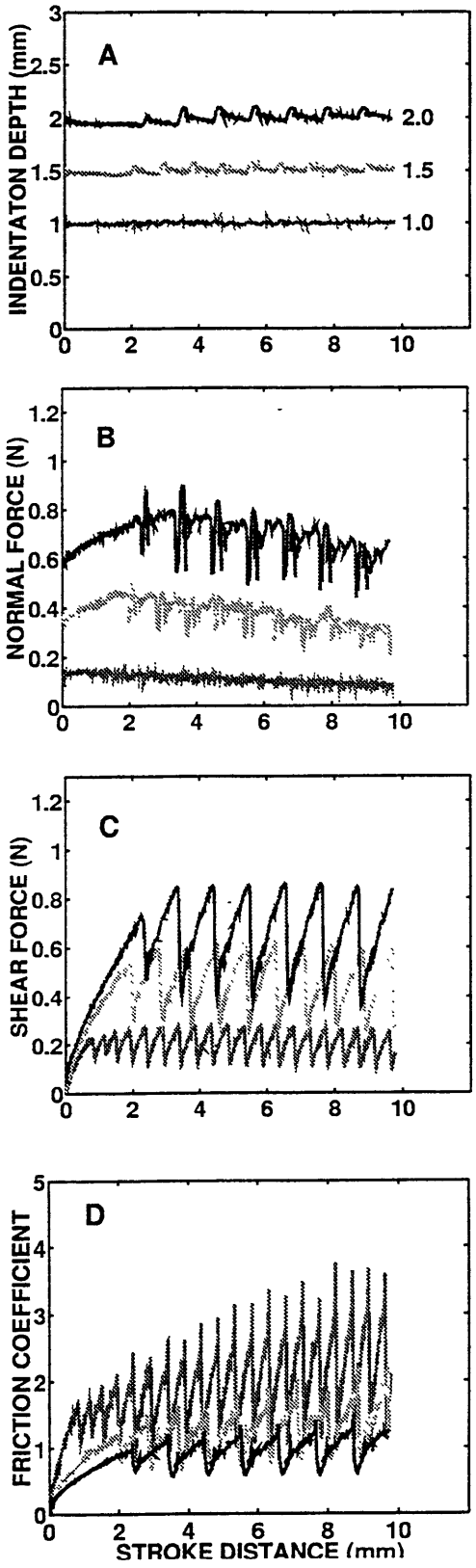

All Depths
Velocities: 4 mm/s
Direction: Forward
Indentor: Acrylic
Subject: 2

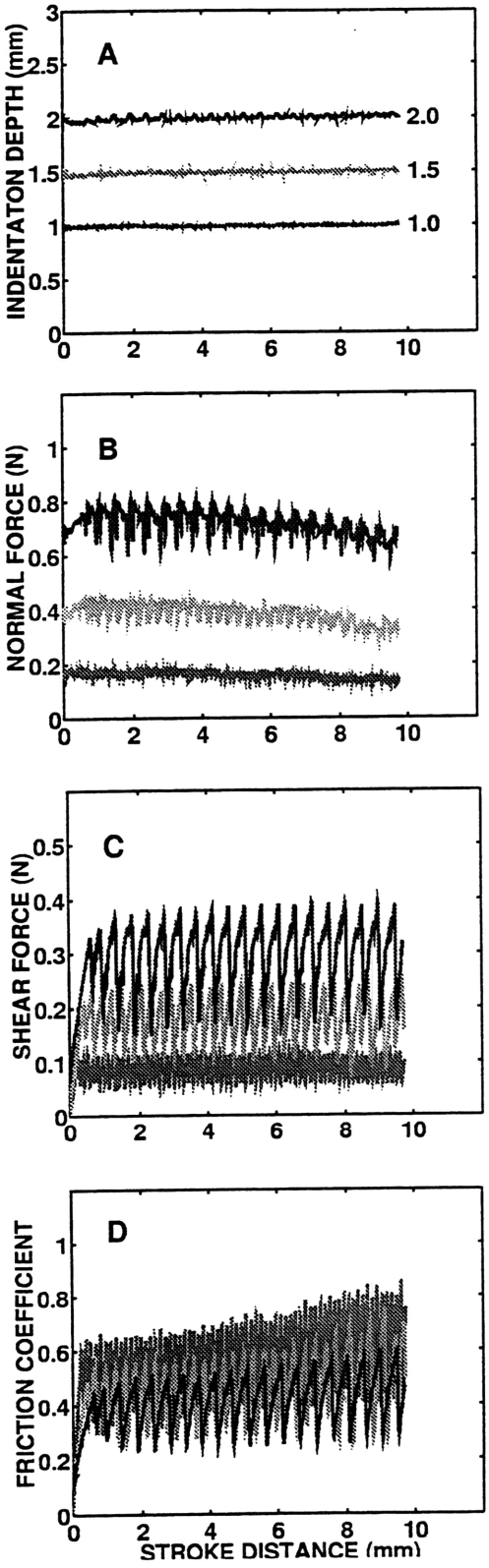

All Depths
Velocities: 4 mm/s
Direction: Forward
Indentor: Acrylic
Subject: 4

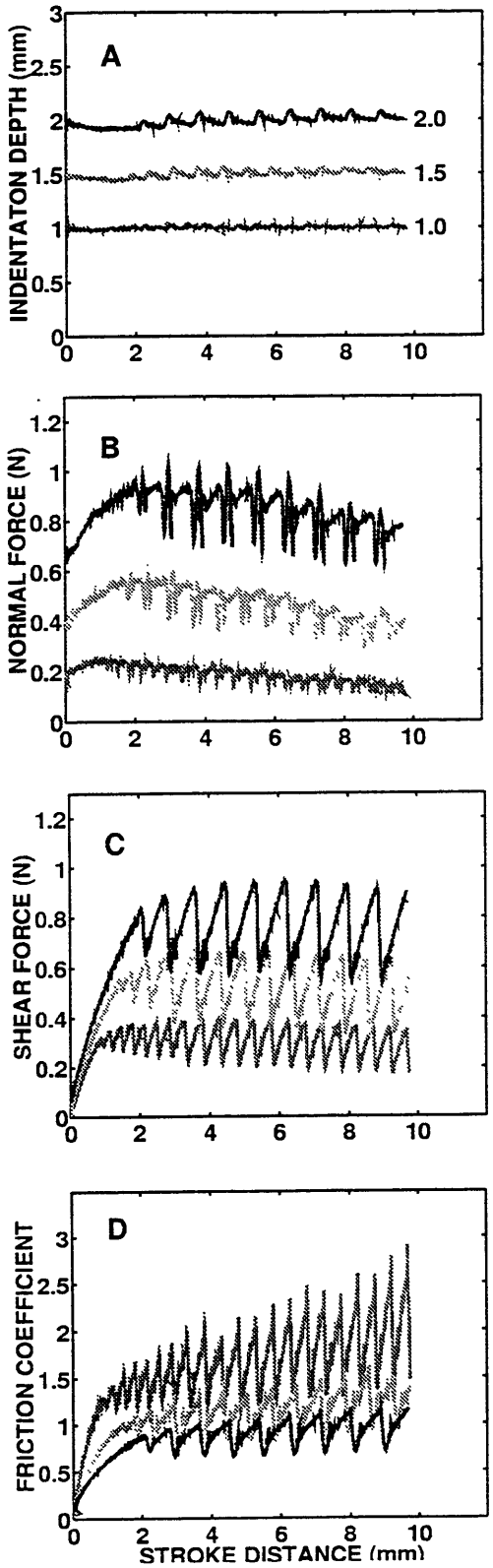

All Depths
Velocities: 4 mm/s
Direction: Forward
Indentor: Acrylic
Subject: 5

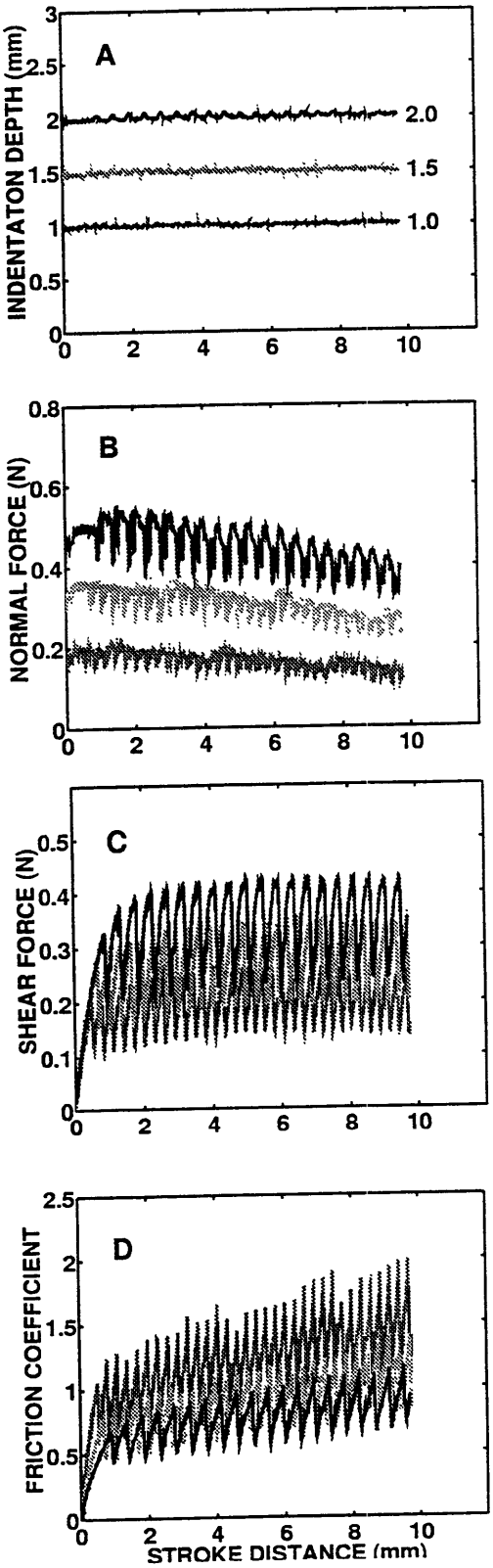

References

Srinivasan, M. A. (1989) Surface deflection of primate fingertip under line load. *J. Biomechanics* **22,** 343-349.

Srinivasan, M. A., Gulati, R. J., and Dandekar, K. (1992) In vivo compressibility of the human fingertip. In *Advances in Bioengineering Winter Annual Meeting of the American Society of Mechanical Engineers.* **22,** 573-576.

Gulati, R. J. and Srinivasan, M. A. (1995) Human fingerpad under indentation I: static and dynamic force response. In *Proceedings of the 1995 Bioengineering Conference.* ASME. **29,** 261-262.

Srinivasan, M. A., Whitehouse, J. M., and LaMotte, R. H. (1990) Tactile detection of slip: surface microgeometry and peripheral neural codes. *J. Neurophysiology* **63,** 1323-1332.

Malker, B. (1991) *Occupational disease and occupational accidents 1989.* Official Statistics of Sweden National Board of Occupational Safety and Health, Stockholm, Sweden, 1991.

Buchholz, B., Frederick, L. J., and Armstrong, T. J. (1988) An investigation of human palmar skin friction and the effects of materials, pinch force and moisture. *Ergonomics* **31,** 317-325.

Bobjer, O., Johansson S.-E., and Sergue P. (1993) Friction between hand and handle. Effects of oil and lard on textured and non-textured surfaces; perception of discomfort. *Applied Ergonomics* **24,** 190-202.

Han, H.-Y., Shimada, A., and Kawamura, S. (1996) Analysis of friction on human fingers and design of artificial fingers. In *Proceedings of the 1996 IEEE International Conference on Robotics and Automation.* Minneapolis, Minnesota. 3061-3066.

Thomine, J. M. (1981) The Skin of the hand. The Hand. Vol. 1, Ed. R. Tubiana, W. B. Saunders & Co.

Yamada, H. and Evans, F. G. (1970) Strength of biological materials. Robert Krieger Publishing Company, New York.

Dandekar, K. and Srinivasan, M. A. (1996) Role of mechanics in tactile sensing of shape. RLE TR-604, Massachusetts Institute of Technology.

Pawluk, D. T. V. and Howe, R. D. (1997) Mechanical Impedance and Energy Dissipation in the Human Fingerpad. In *Proceedings of the 1997 Bioengineering Conference.* ASME. **35,** 591-592.

Bowden, F. P. and Tabor, D. (1986) *The Friction and Lubrication of Solids.* Clarendon, Oxford.

Suh, N. P. (1986) *Tribophysics.* Prentice-Hall, New Jersey.

Blau, P. J. (1995) *Friction Science and Technology.* Marcel Dekker, New York.

Buckley, D. F. (1981) *Surface Effects in Adhesion, Friction, Wear, and Lubrication.* Elsevier, New York.

Howe, R. (1992) A force-reflecting teleoperated hand system for the study of tactile sensing in precision manipulation. In *Proceedings of the 1992 IEEE International Conference on Robotics and Automation.* Nice, France. 1321-2326.

Gulati, R. J. and Srinivasan, M. A. (1997) Determination of mechanical properties of the human fingerpad, in vivo, using a tactile stimulator. RLE TR-605, Massachusetts Institute of Technology.

Franklin, G. F., Powell, J. D., Workman, M. L. (1990) Digital Control of Dynamic Systems. 2nd ed. Addison-Wesley Publishing Company, Inc.

Chen, J.-S. (1996) Human haptic interaction with soft objects: discriminability, force control, and contact visualization. Ph.D. thesis, Massachusetts Institute of Technology.

Fung, Y. C. (1993) *Biomechanics: Mechanical Properties of Living Tissues, 2nd ed.* Springer-Verlag, New York.

Gonzalez, R. C. and R. E. Woods. (1992) Digital image processing. Addison-Wesley Publishing Company.

Johnson, K. L. (1985) *Contact Mechanics.* Cambridge University Press, Cambridge.

Schallamach, A. (1952) The load dependence of rubber friction. *The Proceedings of the Physical Society*, **B, 65,** 657-661.

Roth, F. L., Driscoll, R. L., and Holt, W. L. (1942) Frictional properties of rubber. *J. Research of the National Bureau of Standards* **28** 439-462.

Grosch, K. A. (1963) Relation between friction and viscoelastic properties of rubber. *Proceedings of Royal Society of London* **A, 274,** 21-39.

Schallamach, A. (1971) How does rubber slide? *Wear* **17,** 301-312.

Rorrer, R. A. L., Eiss, N. S., Jr., and De Togni, R. S. (1992) Measurement of frictional stick-slip transitions for various elastomeric materials sliding against hard counterfaces. In *Wear and Friction of Elastomers,* eds R. Denton and M. K. Keshavan, pp. 50-64. ASTM, Philadelphia.